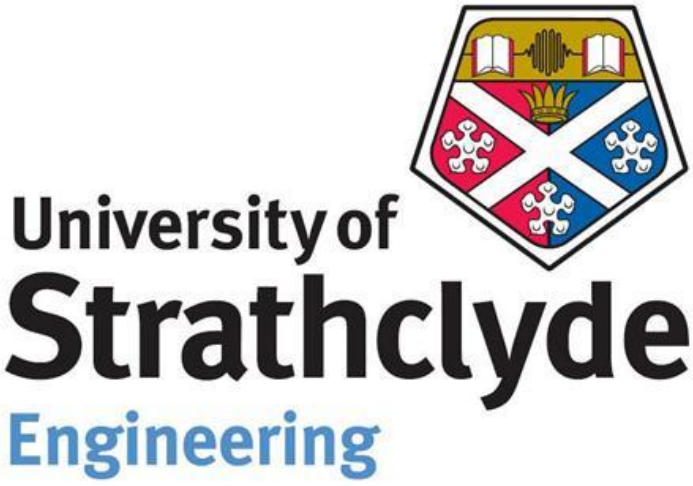

A STUDY OF THE RESIDUAL STRESSES IN DISSIMILAR MATERIAL BRAZED JOINTS

by

Niall Robert Hamilton

Submitted to the Department of Mechanical and Aerospace Engineering

in Partial Fulfilment of the Requirements for the Degree of

DOCTOR OF PHILOSOPHY

IN MECHANICAL AND AEROSPACE ENGINEERING

at the

University of Strathclyde

February 2013

Abstract

At the heart of any procedure for modelling and assessing the design or failure of dissimilar material brazed joints there must be an understanding of the metallurgy and mechanics of the joint. There must also be an understanding of how residual stresses develop due to the joining process. The work presented in this thesis aims to develop this understanding whilst introducing a method, namely thermal autofrettage, of altering the initial residual stress distribution to improve joint performance. Due to differences in material properties, residual stresses develop in dissimilar material brazed joints during the joining process and will affect various failure mechanisms. However, there are several barriers to accurately capturing the stress state in the region of the joint and across the brazed layer using FEA and these are discussed in relation to a metallurgical study of a real dissimilar material brazed joint. It has been shown using a simplified brazed layer material model, the residual stresses predicted by FEA are in reasonable agreement with those measured with X-ray diffraction and can be explained by the relationship in material properties. FEA has also shown that depending on the plastic properties of the brazed layer, thermal autofrettage could be used to alter the initial residual stress distribution to improve the performance of the joint for a number of failure mechanisms. The findings from this research are applicable to dissimilar material brazed joints found in a range of applications; however the references listed are primarily focussed on work in fusion research and development where the use of dissimilar material brazed joints is widespread.

Thesis Supervisor: Dr. J Wood

Supervisor Title: Senior Lecturer

Declaration of authenticity and author's rights

‘This thesis is the result of the author’s original research. It has been composed by the author and has not been previously submitted for examination which has led to the award of a degree.’

Author Signature:

Date:

Supervisor Signature:

Date:

Acknowledgements

Firstly, I would like to express my very great appreciation to Dr. Jim Wood for his continual support, guidance and advice over the past three and a half years. I continue to be inspired by your passion for both the technical and educational aspects of engineering and look forward to keeping in touch with you throughout my career. I would also like to offer my special thanks to my second supervisor, Dr. Alex Galloway, for his invaluable materials advice and support in general.

Thank you to the other members of the Fusion Engineering and Materials Group, namely Mikael Olsson Robbie, Yuxuan Zhang and David Easton, for their continual help and support. I have enjoyed our time working together and I wish you all every success in the future. I would like to offer my thanks to James Kelly for his expert metallurgical advice and training over the past few years. I also wish to acknowledge the work completed by the various undergraduate students in support of this project, namely Tom Peat, Peter Watson, David Wilkie, Katie Fraser and David Cunningham. The work presented in this thesis is better off for your efforts and I wish you every success in your future careers.

My special thanks are extended to the staff of CCFE, in particular to Rob Bamber, Ioannis Katramados and Joe Milnes, for their continual support. The past three and a half years have given me a unique insight into the world of fusion engineering and I am grateful for the opportunity to work in conjunction with CCFE. I am particularly grateful for the selfless help and expert advice given by Dr. Wengzhong Zhu (University of West of Scotland) and Tony Fry (NPL) on various aspects of this project.

I would also like to thank the technical support staff within the department, especially Gerry Johnston, Fiona Sillars, Alex Cairney and Jim Doherty for their support throughout the duration of this project. A big thank you to the guys in the workshop too, namely Tom Farmer, Craig Logan, David Crawford, Fuad Warsame and Neil M^{c}Crindle, for their advice and quality workmanship. I would also like to thank other PhD students, in particular James Ure, Alan Jappy, Fiona Gentles, Susan Reilly and my Space Group friends, with whom I have shared many highs and lows over the past three and half years.

Finally, I wish to thank my family and flatmate Patch for their support and encouragement throughout my studies.

Table of Contents

List of figures

List of tables

List of symbols

c_i	Uncertainty sensitivity coefficient
C_p	Specific heat
d_v	Uncertainty divisor
E	Young's modulus
E*	Effective modulus
f_{ij}	Angular function
H	Height
k	Thermal conductivity / uncertainty coverage factor
K	Stress Intensity
K_{IC}	Fracture Toughness
L	Length
m	Stress singularity parameter / integer
M	Moment
n	Integer
r	Radius
s	Standard deviation
T	Temperature
u	Standard uncertainty
U	Combined uncertainty
x	Cartesian coordinate
y	Cartesian coordinate
z	Cartesian coordinate

α	Coefficient of thermal expansion / Dundurs parameter
β	Dundurs parameter
δ	Thickness
ε	Strain / Emissivity
θ	Angle
λ	Stress singularity parameter
μ	Modulus of rigidity
ν	Poisson's ratio
σ	Stress
σ_{ijo}	Constant stress term
σ_{yield}	Yield Stress
τ	Shear stress
Φ	Angle
Ψ	Angle
ω	Stress singularity parameter

1 An overview of dissimilar material joints in thermonuclear fusion reactors and research aims and objectives

1.1 Introduction

Dissimilar material joints can be found in a range of current and emerging applications such as gas turbines, spacecraft and nuclear power plants. Maximising the performance of such applications often requires structurally sound joints between materials of varying mechanical, chemical and thermal properties. One such emerging application where dissimilar material joints are commonplace is in the first wall and divertor of present day and next step thermonuclear fusion reactors. In this application, the materials facing the plasma have to withstand intense fluxes of charged and neutral particles in addition to incident power densities as high as 20MW/m^2 in some place. Consequently, the materials which are capable of withstanding such harsh environments are limited and diverse. These plasma facing materials must then be joined to the surrounding load carrying structure. For fusion power to be a sustainable source of energy, component reliability is one of the key factors in ensuring the cost of energy produced is competitive with other sources, hence the reliability of such joints whilst operating in the most extreme conditions is critical.

Due to differences in chemical, mechanical and thermal properties, dissimilar material joining presents significant technological challenges. From a mechanics perspective, due to the differences in thermal expansion coefficients and Young's modulus, high secondary discontinuity stresses can occur in the region of the joint as a result of the joining process and during operation. In operation these components are subjected to cyclic high-heat flux and mechanical loads. Loading which is cyclic in nature has been known to cause failure in various different plasma facing components. In addition to this the chemical compatibility of the materials is key to manufacturing structurally sound joints. Wettability of the materials and the formation of brittle intermetallics during bonding have been the focus of much research in the past [1]. In fusion applications in particular, one common technique for joining dissimilar material joint is brazing [2], and it is this method of joining dissimilar materials which will be the predominant focus of this research, however many of the findings will be relevant to other joining technologies.

This introductory chapter:

- Summarises the types of dissimilar material joints found in current and next step thermonuclear fusion reactors.
- Provides a discussion on the nature of residual stresses found in dissimilar material joints and why they are important.
- Provides an overview of brazing as a method of joining dissimilar materials.
- Summarises the failure of dissimilar material brazed joints due to joining and due to operational loads.
- Discusses the challenges in modelling and assessing failure in brazed joints.
- And provides a summary of the aims and objectives of this research.

1.2 An overview of dissimilar material joints in current and next step thermonuclear fusion reactors

The development of fusion power as a commercial source of energy is the holy grail of energy production. Various methods of creating energy from nuclear fusion exist. Methods such as gravitational, magnetic and inertial plasma confinement exist however magnetic confinement is the most developed and is considered a better option for energy production [3]. One of the major engineering challenges in realising fusion power as a commercial source of energy is the housing of a plasma which burns at 150,000,000°C, ten times larger than the temperature at the core of the sun. Clearly no material can withstand such temperatures and current fusion reactors use magnetic fields to control and contain the plasma within a torus shaped reactor known as a tokamak. The technological route towards a fusion reactor is dependent on three tokamak devices: the Joint European Torus (JET) which is currently the largest tokamak in the world, its successor ITER and a demonstration reactor called DEMO [4]. ITER the successor to JET, is a reactor based scale experiment designed to deliver a power output of ten times the power input and demonstrate that it is possible to produce commercial energy from fusion [5]. The next device after ITER is DEMO which is expected to be the first fusion plant to reliably provide electricity to the grid economically. In all current and future generation tokamak fusion devices, the design of the key plasma facing components such as the divertor, limiter and ion cyclotron heating system (ICRH), which are highlighted Figure 1-1, is dependent on the integrity of dissimilar material joints between a range of highly specialised plasma facing materials and the surrounding structure. The design, materials and joining processes for the divertor, limiter and ICRH are briefly discussed in this section.

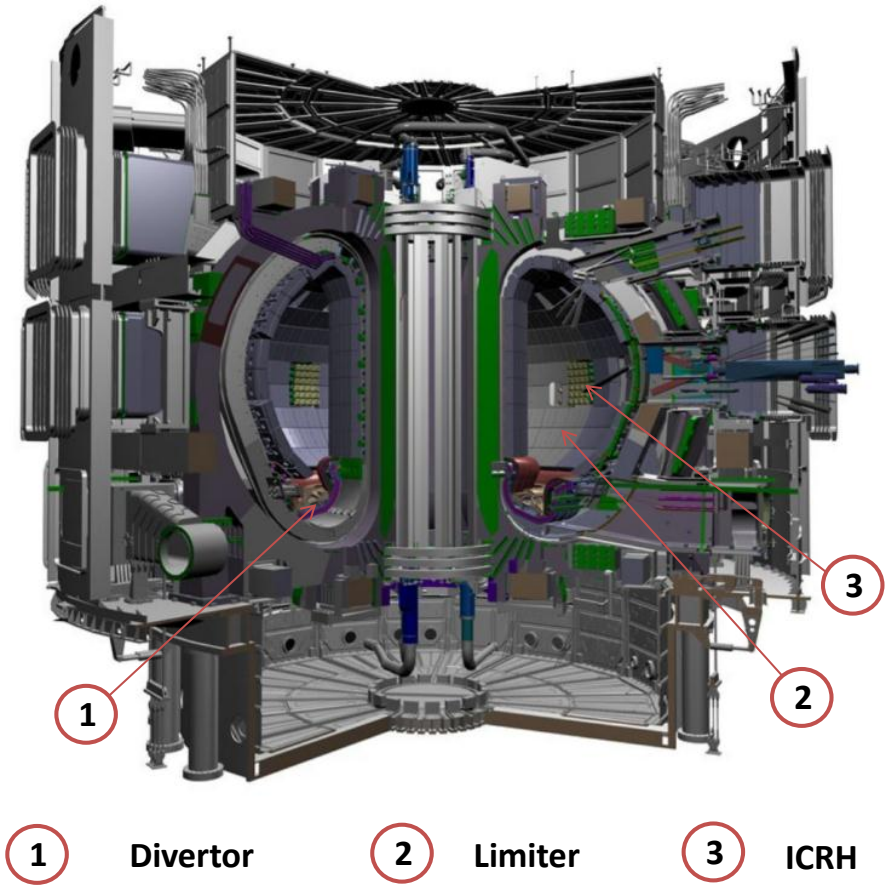

Figure 1-1 – ITER tokamak highlighting key plasma facing components [5]

One of the key components in the tokamak reactor is the divertor (Figure 1-1) which acts as the main interface between the plasma and material surfaces [5]. The function of the divertor is to extract heat, helium ash and other impurities from the plasma. The materials used in the divertor have to survive in extreme conditions. They must be able to withstand intense fluxes of charged and neutral particles in addition to incident power densities as high as $20MW/m^2$ and surface temperatures of up to 3000°C [5]. Consequently the materials that are suitable for use in such applications are limited. For ITER carbon fibre composites (CFCs) and tungsten (W) have been selected as the materials of choice for all plasma facing surfaces due to their high melting point and high thermal conductivity [6] however using W as the sole plasma facing material is currently under consideration. To help cool the materials which face the plasma, the plasma facing material is joined to a heat sink material which has a high thermal conductivity. For ITER a precipitation hardened copper chrome zirconium alloy (CuCrZr) has been selected for the heat sink due to its high thermal conductivity and post-irradiation fracture toughness [6]. For ITER, various plasma

facing components designs have been developed and are shown in Figure 1-2 (W to CuCrZr monoblock design (1), W to CuCrZr flat tile design (2), CFC to CuCrZr monoblock design (3)). These plasma facing components are then assembled into 54 divertor cassettes (part of a cassette is shown in (4) in Figure 1-2). In terms of divertor design for ITER, several joining process have been developed for the plasma facing W or CFC to CuCrZr monoblocks. Diffusion bonding, hot isostatic pressing (HIPing) and brazing have all been developed as potential joining techniques [2]. With upwards of 50,000 CFC monoblocks and 100,000 W tile in current divertor components [6], high component reliability is key.

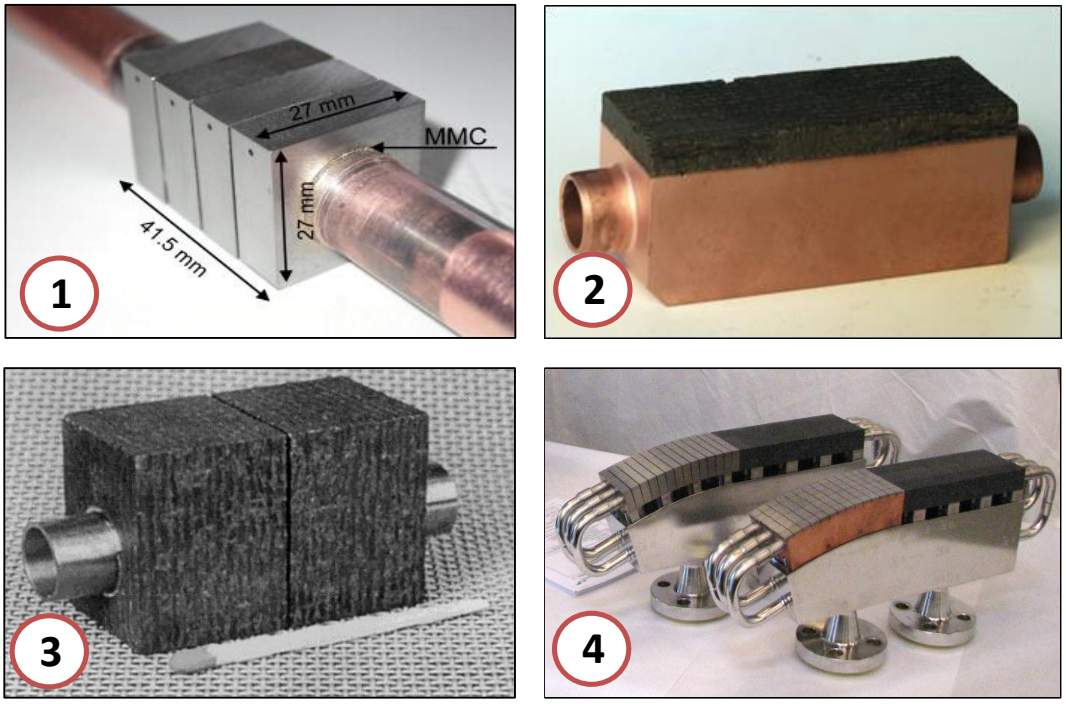

Figure 1-2 – ITER monoblock designs and divertor module

For devices beyond ITER such as DEMO, the conditions in which the plasma facing materials have to survive are even more extreme due to the neutron loads incident on the plasma facing material and the move towards steady state operation. This precludes the use of common materials used in ITER [7]. At present W is regarded as the most suitable material for the divertor in DEMO due to its high melting point, thermal conductivity and strength. However the use of W as a structural material is difficult as it is inherently brittle at low temperatures [8] hence a series of novel divertor designs are being designed and are summarised in [7]. One such design is the helium cooled modular divertor which utilises small cooling fingers with impingement helium jet cooling to withstand the intense heat

and radiation loads [9]. This design relies upon the sound joining of the plasma facing W to an intermediate W alloy which in turn is joined to EUROFER97, a reduced activation ferritic martensitc structural steel developed for use in DEMO [10], as shown in Figure 1-3. Various brazing processes have been developed for joining both the W to W alloy and W alloy to structural steel components [9] [12] and it is estimated that DEMO could have in the region of 500,000 brazed joints between W and steel.

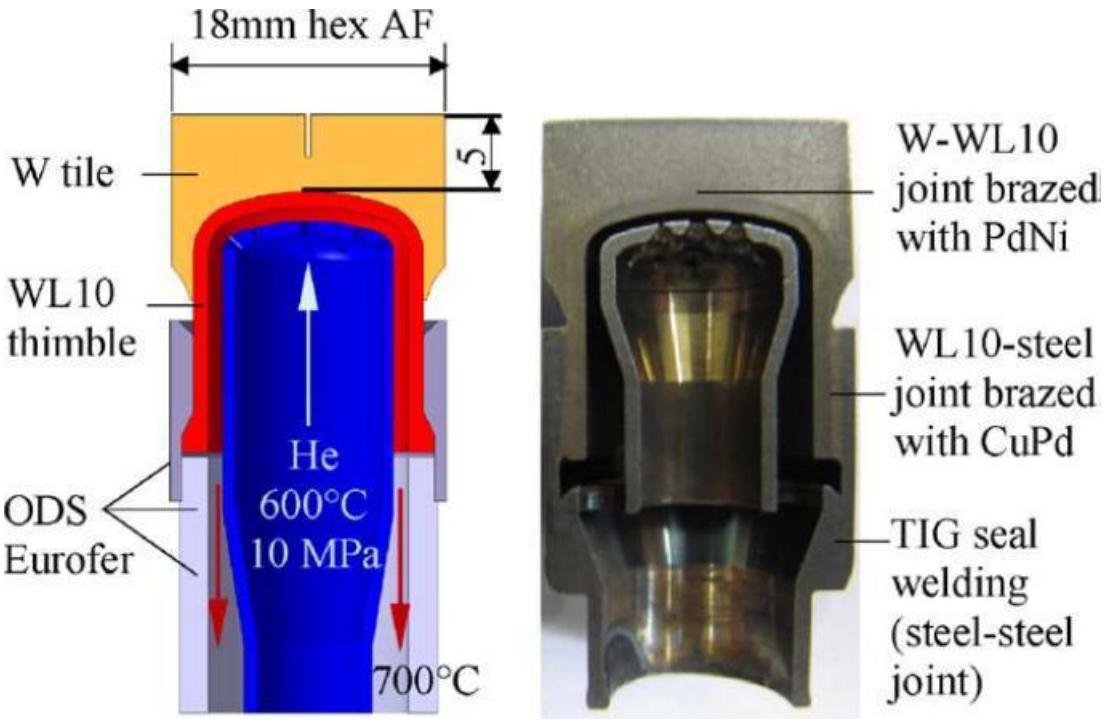

Figure 1-3 - He-cooled thimble proposed for use in DEMO [9]

In addition to the divertor, the limiter and blanket module is another key plasma facing component in tokamak power plants (Figure 1-1). The function of the limiter is to provide shielding to surrounding structure from the plasma in addition to transforming the kinetic energy of the neutrons to heat energy, which in a power plant such as DEMO will be used to generate electrical power [5]. In ITER the design of the limiter uses beryllium as the plasma material due to its low atomic number and good erosion lifetime, however it has a relatively low melting point [2] (which precludes its use in the divertor). The plasma facing beryllium is then joined to a CuCrZr heat sink which is then joined to a 316LN stainless steel as shown in Figure 1-4 [13]. Various different joining technologies have been developed to join beryllium to CuCrZr including HIPing, diffusion bonding and brazing [2].

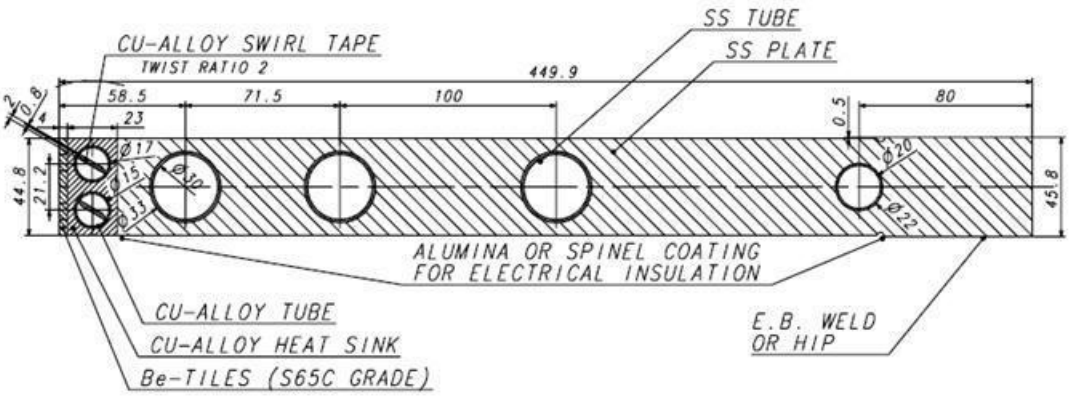

Figure 1-4 - Cross section of ITER limiter [13]

In DEMO, the limiter research is focussed on two main concepts, namely a water cooled lithium lead blanket and a helium cooled pebble bed concept [14] as shown in Figure 1-5. Initial designs of the water cooled lithium lead blanket featured a plasma facing EUROFER steel box containing liquid lithium lead cooled by a bundle of double walled tubes fabricated from EUROFER tubes with a copper (Cu) interlayer (LHS Figure 1-5). A HIPing process has been developed to create these double wall tubes [14]. The helium cooled pebble bed contains a helium cooled plasma facing EUROFER first wall material which is joined by HIPing to a EUROFER stiffening plate which houses a series of breeder and beryllium pebble beds (RHS of Figure 1-5). Research is on-going into the design, materials and joining technologies for each of these designs [15], [16] however it is likely that the final design will require a structurally sound joint between dissimilar materials.

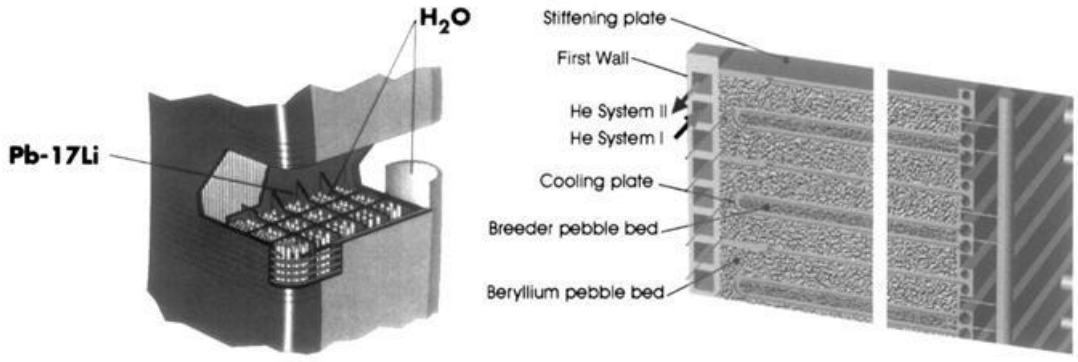

Figure 1-5 - Water cooled lithium lead and helium cooled pebble bed concepts for DEMO blanket [14].

In addition to the dissimilar material joints found in the plasma facing components, such joints are also found in other devices which do not directly face the plasma. One such

example is the ion cyclotron heating system (ICRH) which uses electromagnetic waves to increase the energy of the plasma [17]. In ITER the ICRH is required to transmit 20MW of coupled power to the plasma whilst maintaining plasma confinement. The cross section of the original design is shown in Figure 1-6 and uses two opposed conical ceramics (part no's 3,5) joined simultaneously into a titanium (Ti) alloy structure (part no's 2,6,4) as shown. The ceramic to Ti join is obtained by brazing the Ti to the ceramic [18].

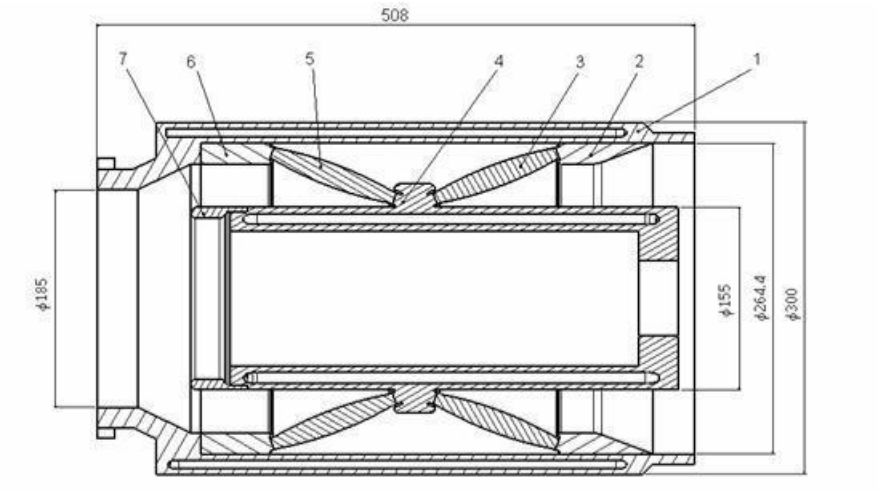

Figure 1-6 - ITER ICRH cross section [18]

As this brief summary clearly shows, the use of dissimilar material joints both in current devices such as ITER and next generation reactors such as DEMO is widespread. Clearly the reliability of current and future fusion devices is dependent on the integrity of dissimilar material joints between a range of highly specialised plasma facing materials and the surrounding structure. Dissimilar material joining presents significant technological challenges and to highlight the problem the thermal and mechanical properties at room temperature for the candidate materials for the ITER and DEMO divertor are listed in Table 1-1 below.

Material	E (GPa)	α (x10^{-6} /°C)	ν	σ_{yield} (MPa)
Pure tungsten [19]	397	4.5	0.279	1385
Beryllium [19]	306	11.3	0.1	252
CuCrZr [19]	128	16.6	0.33	300
316L Stainless [19]	195	15.1	0.3	173
EUROFER97 [20]	206	10.4	0.3	483

Table 1-1 – Summary of room temperature material properties for plasma facing components

This shows there is a considerable difference in both thermal and mechanical properties between the candidate materials. From a mechanics perspective, due to these differences in thermal expansion coefficient, Poisson's ratio and Young's modulus, high secondary discontinuity stresses can occur in the region of the joint as a result of the joining process and operational loads. Furthermore, in operation these components are subjected to cyclic high-heat flux and mechanical loads. Cyclic loading such as this has been known to cause failure in various different components and is summarised in section 1.5.

1.3 The nature of residual stresses in dissimilar material joints

Residual stresses can be defined as "those stresses that remain in a material or body after manufacture and processing in the absence of external forces or thermal gradients." [21]

Residual stresses arise in components during most manufacturing processes which involve plastic deformation and removal of material and can also arise due to non-uniform cooling of a component (e.g. due to quenching). Residual stresses develop in dissimilar material joints during the joining process due to the constraint on free thermal contraction of the parent materials being joined. This occurs due to differences in thermal expansion coefficient and Young's modulus. Temperature can also result in changes in material micro-structure which can also induce residual stresses.

Due to the processing history of a certain material, residual stresses will invariably be present in the parent materials used to fabricate a dissimilar material joint prior to joining with further residual stresses being developed during joining itself. Residual stresses are commonly reduced using stress relief, however due to the nature of the stresses which arise in dissimilar material joints, removing the residual stresses due to joining may not be possible. It does not however preclude stress relieving the parent materials prior to joining

to remove any potential damaging residual stresses due to prior manufacturing processes. The residual stresses developed in dissimilar material joints will be either detrimental or beneficial to performance of the joint in operation depending on whether they are tensile or compressive. These residual stresses will affect various failure mechanisms such as brittle failure and fatigue and this will form the basis of discussion in future chapters of this thesis.

Residual stresses are elastic in nature, although the process that caused them may have involved plastic deformation. They arise from locked-in elastic strain energy in the material's lattice structure. These residual stresses are self-equilibrating i.e the net contribution of tensile and compressive residual stresses across the section must sum to zero.

Residual stresses can be defined as either macro or micro stresses and both may be present in a component at any one time and are often grouped into three different types as defined in [21]. Macro residual stresses (often referred to Type I residual stresses), vary within the body of a component over a range much larger than then grain size of the material. Micro residual stresses, which result due to differences in microstructure, are often classified as either Type II or Type III. Type II residual stresses operate at the grain-size level, Type III at the atomic level.

Micro residual stresses result from the presence of different phases or constituents in a material and can change magnitude and sign over distances comparable to the grain size of the material. Type 2 residual stresses can exist in single-phase materials due to anisotropic behaviour of each grain. They can also develop in multi-phase materials because of the different properties of the various phases. Type 3 residual stresses on the other hand, are micro residual stresses that exist within a grain, essentially as a result of the presence of dislocations and other crystalline defects. The different types of residual stress are shown schematically in Figure 1-7.

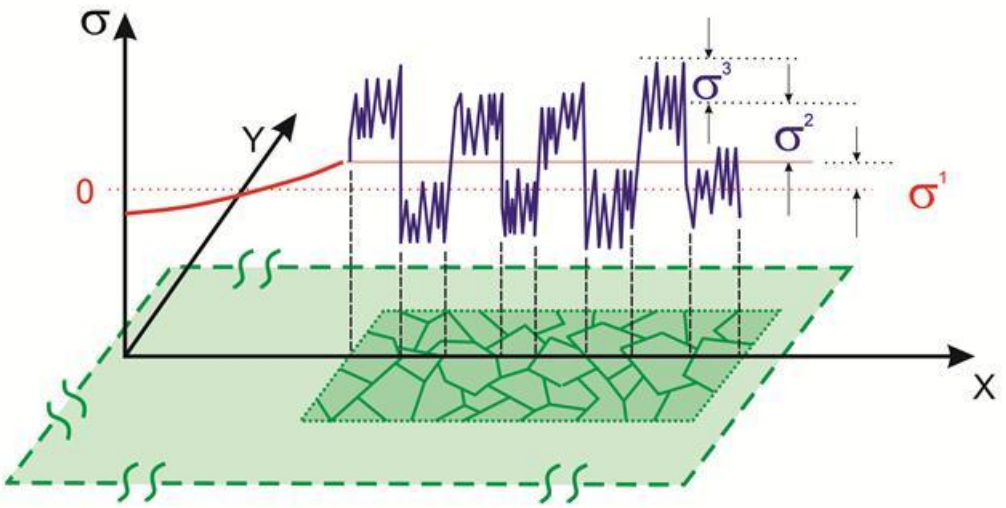

Figure 1-7 - Residual stress categorisation according to scale (modified from [21])

When measuring residual stresses in a material, consideration should be given to the type of residual stress being measured and the sampling volume and resolution of the measurement method. The concept of characteristic volume, which describes the volume over which a given type of residual stress averages to zero, must also be considered. Techniques such as hole drilling, layer removal and X-ray diffraction (XRD) (depending on x-ray spot size) measure residual stresses over large enough volumes such that the Type II and III stresses average zero so that only Type I macro residual stresses can be measured. In the work presented in this thesis, XRD is used to measure residual stress over a spot size of 1mm on materials whose grain size is of region of 10μm, hence the work in this thesis is only concerned with the measurement of Type 1 residual stresses.

1.4 Summary of dissimilar material joining using brazing

As discussed in 1.2, brazing is a joining technique that is widely used to create joints between dissimilar materials in fusion (and other) applications. This section summaries the process of joining two materials using brazing.

Brazing as a means of joining metals instead of using mechanical fastening is perhaps the oldest technique for joining metals and relies on the melting, flow, and solidification of a filler metal to form a leak tight seal [1]. Unlike welding, brazing is a process that only melts the filler metal and not the parts to be joined. The filler metal is then distributed between

the close-fitting parts by capillary action and forms a bond at a molecular level through atomic attraction and diffusion.

Various techniques have been developed to perform brazing using different heat sources such as torches, furnaces, induction heaters and electron beams (all in air, inert gases and in various levels of vacuum). When metals are exposed to air they react with oxygen (oxidation) to form surface oxides which are detrimental to forming structurally sound brazed joints. This oxidation is accelerated at high temperature, hence during brazing it necessary to use a protective flux or a controlled atmosphere such as a vacuum or inert gas to protect the joint during the brazing cycle. In addition pre-cleaning is also required prior to brazing to remove any grease, oil or dirt prior to brazing.

Brazing as a technique for joining dissimilar materials has several advantages and disadvantages over other techniques. One of the key advantages of brazing is that it does not melt the parent materials allowing tighter control over tolerances and in most cases produces a clean joint (however slight changes in composition of the parent materials may occur due to diffusion of brazed elements and will be discussed further in chapter 2). It is also robust as it can be used to join dissimilar materials with large differences in properties, in fact almost every metallic and ceramic material can be joined by brazing [1]. Brazing can also be used join thin components that cannot be welded. However, components that have been brazed have limited operational temperature range due to melting point of the brazing filler. In addition brazed assemblies can have a size limitation on parts being joined as it is difficult to heat large assemblies in a vacuum furnace for example. Joint strength can be very low if good quality joints are not produced (for example due to poor wetting or large voids and inclusions) and usually require tightly fitting parts that have been precision machined. Fluxes and fillers can contain toxic components and tend to be expensive in addition to the costs associated with operating a vacuum oven for example.

Two of the key factors in creating a dissimilar material brazed joint are the wetting and capillary flow of the filler parent material and are summarised in Figure 1-8. A detailed discussion on the phenomenon of wetting and capillary flow is deemed beyond the scope of this thesis, however it is worth touching upon the basic requirements of each in terms of dissimilar material brazing.

Wetting is described as the phenomenon whereby a liquid filler metal or flux spreads and adheres in a thin continuous layer on a solid base metal. Consider the droplet of liquid, shown in Figure 1-8. The degree of wetting of this liquid can be quantified in terms of the angle θ as shown (for θ < 90° wetting is said to occur), with the smaller the angle of θ the higher degree of wetting. For brazing, a high degree of wettability is required (i.e. an angle in the range θ = 10 - 45° [1]). This degree of wetting is required to distribute the filler evenly across the interface and hence create an intimate contact between components being joined.

In brazing terms, capillary action can be described as the force by which the filler liquid is distributed between closely fitted surfaces of the joint to be brazed or soldered. In a properly designed joint, the molten filler metal is drawn completely through the joint area creating a joint free of voids or gaps [22]. Capillary filler metal flow is a function of various parameters namely the capillary driving force, density and viscosity and temperature of the molten metal.

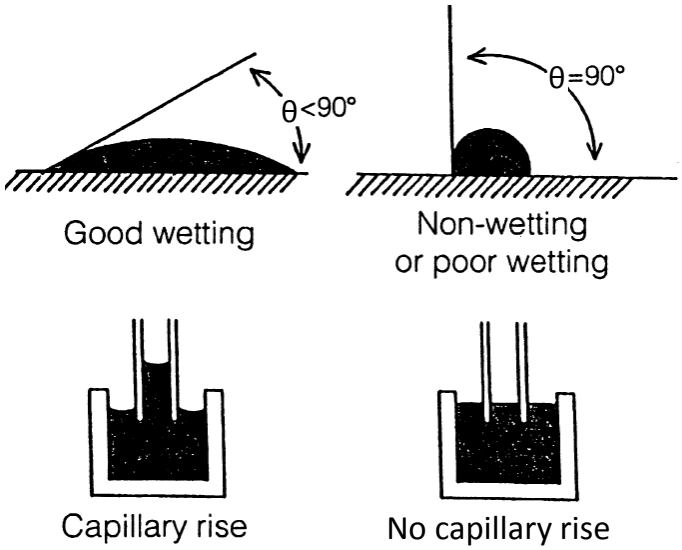

Figure 1-8 – Wetting and capillary action (modified from[22])

The filler materials used in brazing tend to be complex alloys, usually made up from three or more elements depending on the use or application. The selection of the brazing filler is dependent on various considerations. One of the key considerations is the metallurgical compatibility of the filler with the materials being joined such that brittle intermetallic compounds do not form upon brazing. The melting temperature of the filler is another key

consideration. In general minimising the brazing temperature is desirable due to the effects (such as annealing and grain growth) of the heating cycle on the parent material. A lower melting temperature will also reduce the diffusion rate between the braze filler and the parent material. However in some instances service requirements such as joint operating temperature dictate that brazing filler with a high melting temperature be used. In the instances when a minimal brazing temperature is required, fillers with eutectic compositions are frequently used. In addition to their lower melting temperatures, there is no liquid plus solid phase formed during cooling improving the wetting and capillary flow required to form joints between tightly fitting components. In addition to the base filler metal, various alloying elements are often used to lower the melting point of the filler, to facilitate oxide dispersal and improve wettability of the filler on the parent materials. A summary of the base filler metals used for brazing various combinations of parent materials and the effect of each alloying element is deemed outside the scope of this thesis however these are summarised in tables 3.2 and 3.3 in chapter 3 of [1] respectively.

The work presented in this thesis predominantly focuses on understanding the mechanics of dissimilar material joints as opposed to the chemical processes occurring during the joining process, however it is worth touching on some of these issues that can affect joint performance. It is widely known that both porosity due to lack of wetting and the formation of brittle intermetallics are key factors which govern joint performance. Intermetallic phases are compounds containing two or more metallic elements and form due to the complex dissolution and diffusion processes occurring between the braze filler and the parent materials during joining. These phases tend to be brittle with low toughness and result in poor joint strength [1] [23] [24]. These chemical concerns have consequently been the subject of much previous research [25]–[29] to develop brazing processes to form structurally sound joints, however this is not the focus of the work presented in this thesis.

1.5 Failure of dissimilar material joints

1.5.1 Failure during joining

As described in section 1.3 and summarised in Table 1-1, due to differences in thermal expansion coefficient and Young's modulus, high secondary discontinuity residual stresses can occur in the region of the joint as a result of the joining process. This can result in failure of the joint in either in the parent materials or through the interface. Some examples of such cases are given below.

In the field of fusion engineering, Kalin et al [12] developed a brazing process to join W to a ferritic/martensitic steel for use on DEMO components described in section 1.2. During the joining process it was found that cracks initiated in the W a small distance from the brazed layer as shown in Figure 1-9 at some stage during the brazing process. Given the high failure strength of W (ultimate tensile strength of c.800MPa at the brazing temperature and 1400MPa at room temperature [2]) this clearly shows that these joining residual stresses can be large and are significant.

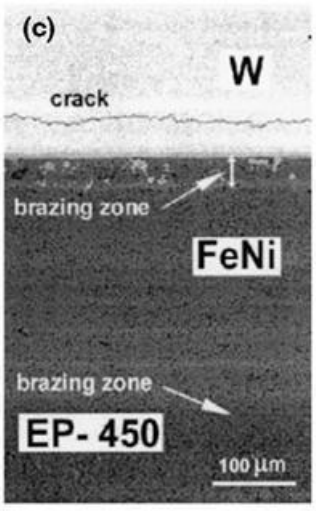

Figure 1-9 – Crack due to joining in W to ferritic/martensitc steel due to joining [12]

There are several examples of similar findings from research into ceramic to steel joining. The Welding Institute [30] found that upon brazing a series of SiC/Alloy600 steel and SiC/304 steel samples failure occurred, either in the ceramic away from or through the interface (Figure 1-10). Similarly, Rohde et al [31], found cracks present in the ceramic close to the interface during cooling in ceramic to steel brazed joints which subsequently initiated failure under mechanical loading.

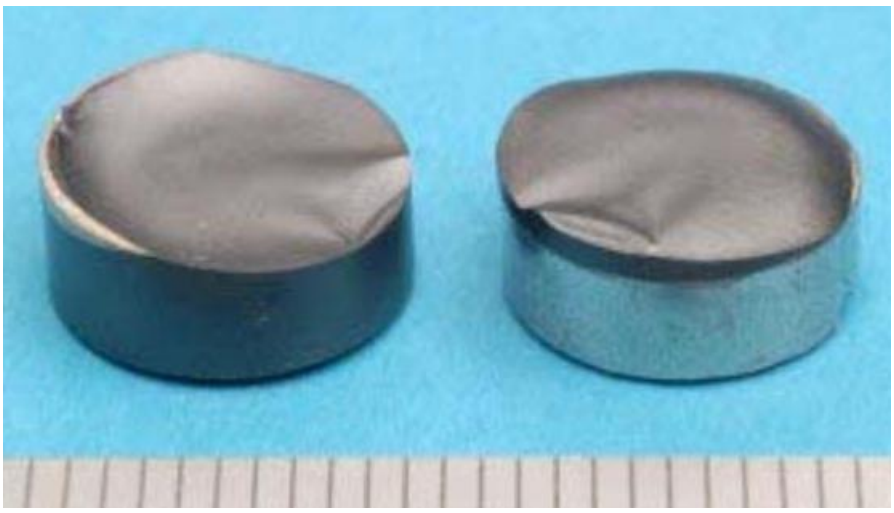

Figure 1-10 - SiC / 304 joints after manufacturing [30]

Clearly, when trying to predict the stress and failure in real dissimilar material joints the thermally induced residual stresses due to joint manufacture can be large and must be taken into account.

1.5.2 Failure due to a mechanically applied load

The strength of dissimilar material joints under a mechanically applied load (both uniaxial tension and shear) has been the topic of much previous research. It has been shown that in certain cases the interface can be strong relative to the parent materials and failure can occur away from the interface in the parent materials. However in certain cases failure can occur in the brazed layer. The following summary highlights previous work relating to the various failure locations of dissimilar and similar material brazed joints under a mechanically applied load.

Blugan et al [32] found that dissimilar material ceramic to steel joints always failed in the ceramic near the joint (Figure 1-11). Blackwell [33] found that a similar material brazed joint between oxygen free high conductivity Cu failed in a purely ductile manner away from the joint at the same level as the parent material. In addition the same study showed that a brazed joint between oxygen free high conductivity Cu to molybdenum joints failed in the Cu away from the interface. In a similar fashion, Brochu et al [23], found that a similar silicon nitride to silicon nitride join failed in the parent materials away from the interface in four point bending. This was also shown by Liu [34] who found similar sintered silicon carbide brazed joints failed in the silicon carbide away from the joint.

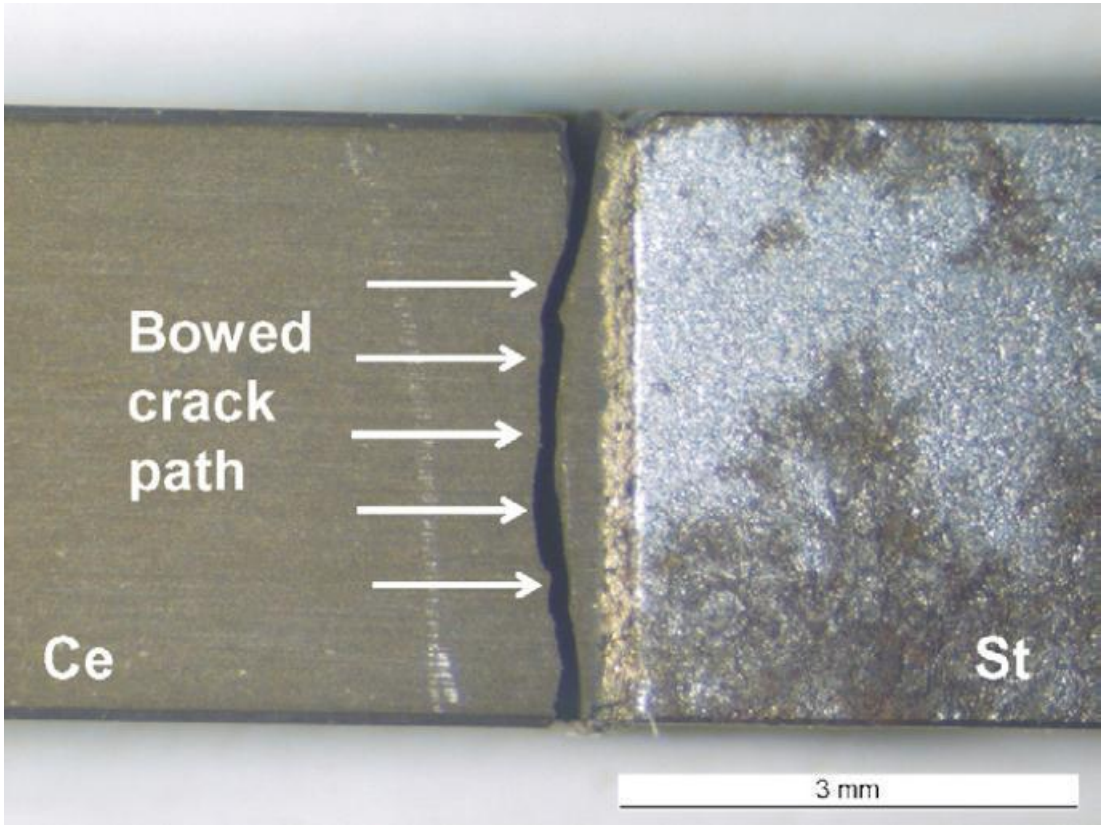

Figure 1-11 – Failure location of ceramic steel joint [32]

However, there are equally examples of both dissimilar and similar material joints failing in the braze layer. Südmeyer [35] found that dissimilar material silicon carbide to steel brazed joints failed in shear through the braze. Blugan [32] also showed that depending on the brazing parameters, failure can occur in the braze layer for ceramic to steel to joints which had previously failed in the ceramic. A similar finding has also been found for a series similar material brazed joints [36] [37].

The reason for these varying failure locations can be attributed to the microstructure of the braze due to the complex chemical reactions occurring during joining in addition to the development of residual stresses due to differences in material properties of both the braze and the parent materials, both of which can be manipulated by varying the joining process parameters. However, clearly if the brazing filler and cycle can be carefully developed then the interface can be strong relative to the parent materials and failure can occur away from the interface in the parent materials.

1.5.3 Failure due to cyclic mechanical or thermal loading

A similar phenomenon is apparent in dissimilar material joints that are subjected to either cyclic thermal or mechanical loading. In these loading scenarios, cracks can initiate and propagate either at the interface or away from the interface in the parent materials as summarised below.

Brossa [38] performed thermal fatigue tests on a series of Cu to W dissimilar material brazed joints. In this case cracking initiated away from the interface in the W. Norajitra [9] performed cyclic high heat flux tests on the W to EUROFER steel thimble shown in Figure 1-3 and found that cracks initiate and propagate through the hexagonal W surface away from the W - W and W - steel brazed joints (Figure 1-12).

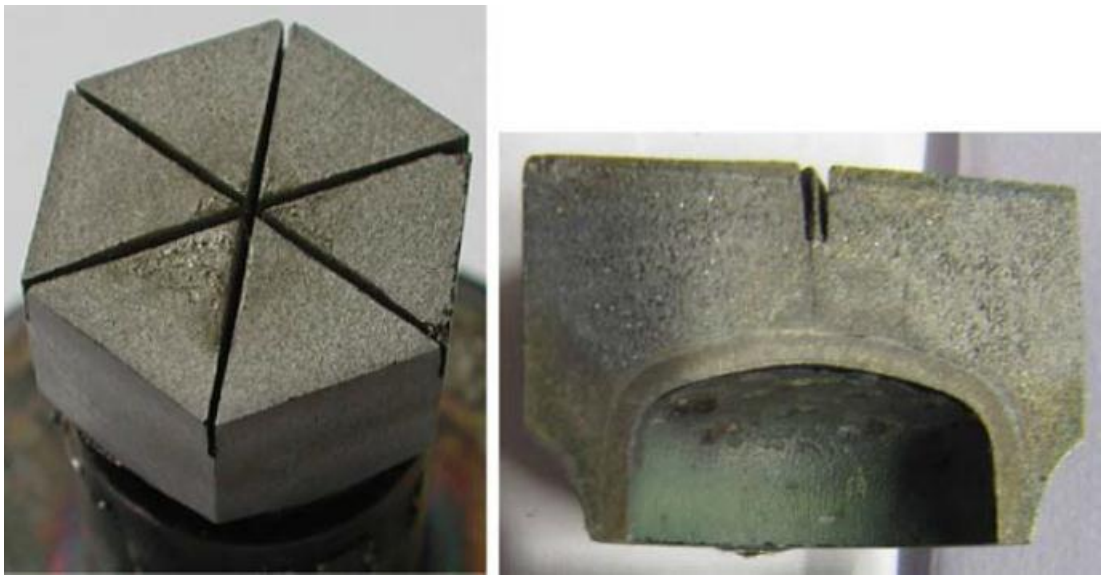

Figure 1-12 – Crack in helium cooled divertor finger module during high heat flux testing [9]

However, Seki [39], performed displacement controlled axial fatigue tests on Cu to W brazed joints and found that cracks initiate and propagate through the brazed layer (Figure 1-13). A similar finding was presented by Horie [40] who also found cracks initiate and propagate through the brazed layer for W to Cu brazed joints in torsion. Similarly, Yao [41], Nishi [42] and Solomon [43] also reported fatigue cracks initiating in and propagating through the brazed layer in a series of dissimilar material brazed joint combinations.

In a similar fashion to the failure locations under mechanical loading, the reason for these varying failure locations can be attributed to the metallurgy of the joint and any porosity or voids and their effect on mechanical properties. However if the brazing filler cycle can be

carefully developed then clearly the interface can be strong relative to the parent materials under cyclic loading mechanical or thermal loading and fatigue cracks can initiate and propagate in the parent materials.

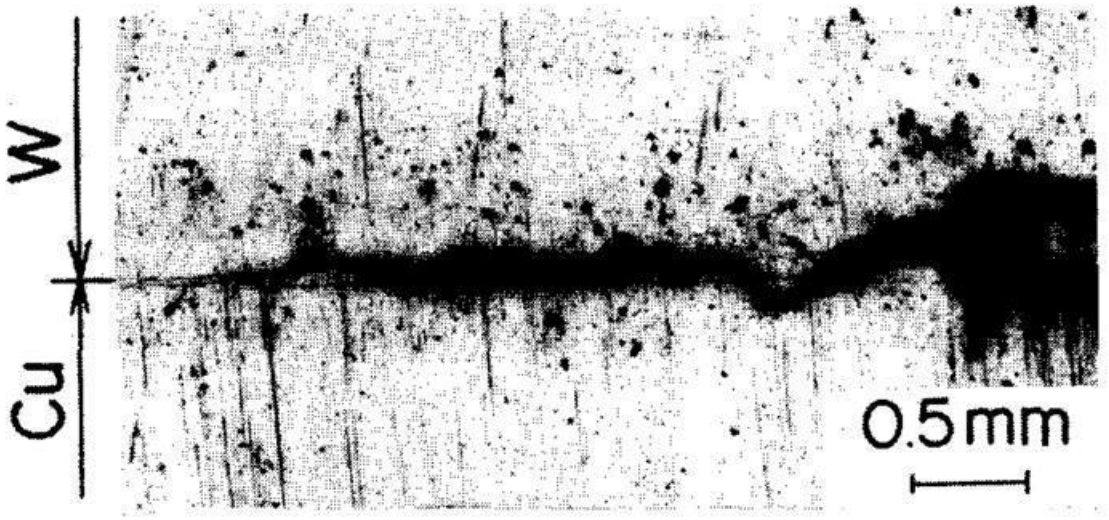

Figure 1-13 - Fatigue crack propagation path in W-Cu braze region [39].

1.6 Challenges in modelling and assessing failure of dissimilar material joints

1.6.1 Residual stresses due to joint manufacture

As described in section 1.5.1 residual stresses due to joining are significant and must be accounted for in any finite element analysis (FEA) or failure assessment procedure for dissimilar material brazed joints. The residual stresses will affect the various failure mechanisms and will be discussed in later sections of this thesis. In addition, given the nature of these stresses, stress relief will be problematic due to the mechanical and thermal properties of the joined materials.

1.6.2 The presence of analytical singularities

Due to the nature of brazed joints, analytical singularities exist in finite element models at the free surface edge of the joint interface, their strength being a function of the degree of dissimilarity between the material properties and any geometric discontinuity that may exist. The stresses obtained at this interface are non-converged and a function of mesh refinement. The existence of these singularities is widely recognized and work has been

done to understand the stress states in such regions and this will be presented and form the basis of an investigation in chapter 3 of this thesis.

1.6.3 Microscale considerations

Due to the relatively small thicknesses of brazed layers (c. 100μm), there are certain challenges associated with including it an FEA model. It follows logic that the mechanical properties of this thin layer will play a key role in the mechanics of the joint hence it is important to model the brazed layer if the stress state in the joint is to be accurately captured. The practice of neglecting the braze layer is effectively assuming that the braze layer and diffusion regions have exactly the same properties (mechanical and thermal) as one of the materials being brazed. Modelling the braze layer as a separate material presents several non-trivial challenges and these issues will be discussed in detail in 2.8 of this thesis.

1.6.4 Lack of defined procedures and material property data

Compared to other joining techniques such as welding, there is a lack of defined and agreed procedures for assessing such joints. In addition there exists the problem of obtaining temperature dependent material property data, not only for the materials being joined, but the brazing alloy too. In the fusion environment this is compounded by the use of exotic materials which can be non-ductile in nature in addition to overcoming the challenges in quantifying the long term effects of fusion levels of irradiation on such materials.

1.7 Summary of aims and objectives

Clearly the use of brazing as a joining technology provides several non-trivial challenges in relation to modelling and failure analysis of dissimilar material joints. However, whilst these challenges exist, at the heart of any procedure for modelling and assessing the design or failure of dissimilar material brazed joints must be a basic understanding of the metallurgy, mechanics and development of residual stresses in the joint and how these will affect the joint in operation.

Consequently, the aim of the work presented in this thesis is threefold:

1. To gain a basic understanding of the metallurgy and mechanics of dissimilar material joints in relation to the modelling and failure of dissimilar material joints.

2. To develop a method for accurately predicting the residual stress state in a real dissimilar material brazed joints.
3. To investigate a method, namely thermal autofrettage, of modifying the residual stress state to improve the performance of dissimilar material joints in operation.

Chapter 2 of this thesis aims to gain an understanding of the metallurgy of dissimilar material brazed joints in relation to finite element modelling and failure analysis of such joints. This is done through a metallurgical study of a Ti/72Ag-28Cu/Cu dissimilar material brazed joint however the findings will be applicable to joints between different parent material combinations and braze fillers. Chapter 3 develops an understanding of the mechanics of, and stress state in, an idealised dissimilar material joint and how different relationships in material properties are likely to influence the stresses developed in the joint.

The aim of chapter 4 is to use FEA to predict the residual stresses due to joining in the Ti/72Ag-28Cu/Cu dissimilar material joint discussed in chapter 2. The residual stresses predicted using FEA are compared to those measured using XRD. Chapter 5 subsequently investigates a post-joining process, namely thermal autofrettage, of modifying the residual stress state due to joining with the aim of improving the performance of the joint in operation. The measured residual stresses using XRD, with and without thermal autofrettage, are compared to those predicted by FEA with a discussion on how changes in the residual stress distribution are likely to affect various failure mechanisms presented. An extensive literature and patent search has not highlighted any research in this area before, hence the concept of thermal autofrettage provides an original contribution to knowledge for dissimilar material brazed joints.

A summary of the findings from this research and a discussion on areas for future work are given in chapter 6.

2 The metallurgy of a titanium to copper joint brazed with a silver based brazing alloy

2.1 Introduction

The experimental work presented throughout this thesis predominantly focuses on dissimilar material brazed joints between copper (Cu) and titanium (Ti) joined using a silver (Ag) based brazing alloy. The brazing alloy used is silver copper eutectic (72Ag-28Cu). This chapter aims to describe the key metallurgical features of the Ti/72Ag-28Cu/Cu joint in relation to the finite element modelling and failure analysis of the joint.

The final microstructure and microstructural evolution of the Ti/72Ag-28Cu/Cu brazed interface is described in relation to microstructure of the as supplied brazing filler. The variations in chemical compositions present within the Ti/72Ag-28Cu/Cu brazed interface are also investigated and the effects of these variations on the mechanical properties (hardness and Young's modulus) are determined using nanoindentation. The findings from this investigation are then used to present a summary of the challenges in modelling the brazed layer and brazing process using FEA, the on-going work that is currently being done to overcome these challenges, and potential dissimilar material joint failure modelling approaches.

2.2 Brazing procedure

The parent materials used in this investigation were Ti grade 2 cylindrical bar and oxygen-free high conductivity (OFHC) Cu C110 of the same geometry. The as supplied parent materials were machined to 14mm diameter by 25mm long. The samples were brazed using 72Ag-28Cu filler which has been used previously to create successful brazed joints between Cu and Ti [36]. The 72Ag-28Cu was in foil form of 0.1mm thick. Table 1 summarises the composition of both Cu and Ti parent materials which have been supplied correct to BS 3839:1978 and ASTM B-348 respectively, and the 72Ag-28Cu brazing alloy which has been supplied correct to EN1044.

Material	Cu	Pb	O_2	Ti	H	C	Fe	Ag
OFHC Cu	99.99	0.0001	0.0004	-	-	-	-	-
Ti grade 2	-	-	0.01	Base	0.02	0.04	0.08	-
72Ag-28Cu	28	-	-	-	-	-	-	72

Table 2-1 - Chemical compositions of materials (%wt)

Brazing took place in a vacuum furnace (5 x 10^{-5} mbar) which was heated at a rate of 10°C/min up to a brazing temperature of 820°C minute with a dwell of 5mins at 750°C. The samples were then allowed to cool in a vacuum overnight to a temperature of c.60°C before being removed and allowed to cool to room temperature in air. Following cooling, the Ti/72Ag-28Cu/Cu samples were cut using an abrasive cutter before experiencing a standard metallographic polishing procedure.

2.3 Microstructural comparison of the braze layer in the as cast and condition and after brazing

The braze filler used in this investigation has a eutectic composition of 72Ag-28Cu. Based on the Ag-Cu phase diagram shown in Figure 2-1, upon cooling through the invariant point at E, one would expect a microstructure to contain layers of the α + β phases that will form simultaneously during the liquid to solid transformation. The actual microstructure of the as supplied 72Ag-28Cu is shown in Figure 2-2. In addition to the expected alternating layers of the α + β, small α dendrites are also present which could be a consequence of non-equilibrium cooling, or the initial composition is either slightly rich in Ag.

The microstructure of a Ti/72Ag-28Cu/Cu brazed joint, as viewed through an optical microscope, is shown in Figure 2-3, with Figure 2-4 showing the SEM backscattered electron image (BEI) of the joint in the region of the Ti interface at a higher magnification. Clearly, various interfacial layers are present within the brazed layer and these are labelled A-F for future reference. It is also clear that the microstructure of the braze filler in the as cast condition and after joining is very different. The difference in microstructures can be attributed to diffusion of elements to and from the braze during the brazing cycle. This diffusion process results in a complex ternary alloy system, the formation of which is explained in the next section of this chapter. In terms of braze quality, it is clear from an optical inspection that there are no obvious voids or inclusions within the braze with good and consistent wetting.

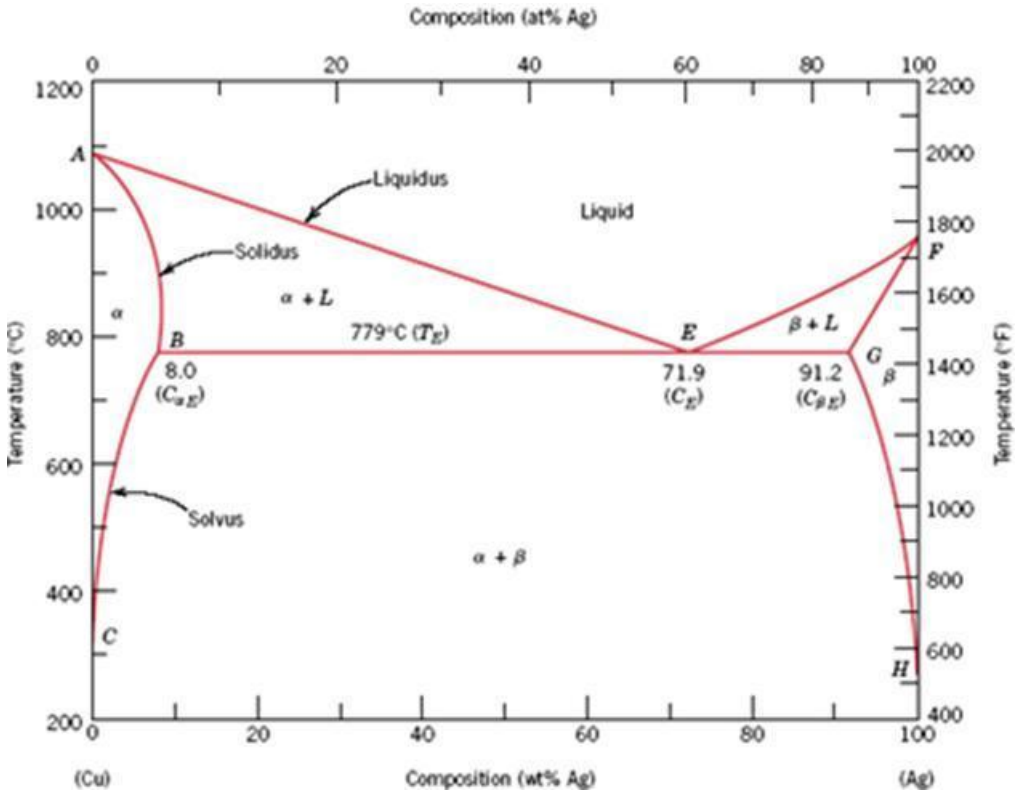

Figure 2-1 – Ag-Cu binary phase diagram [44]

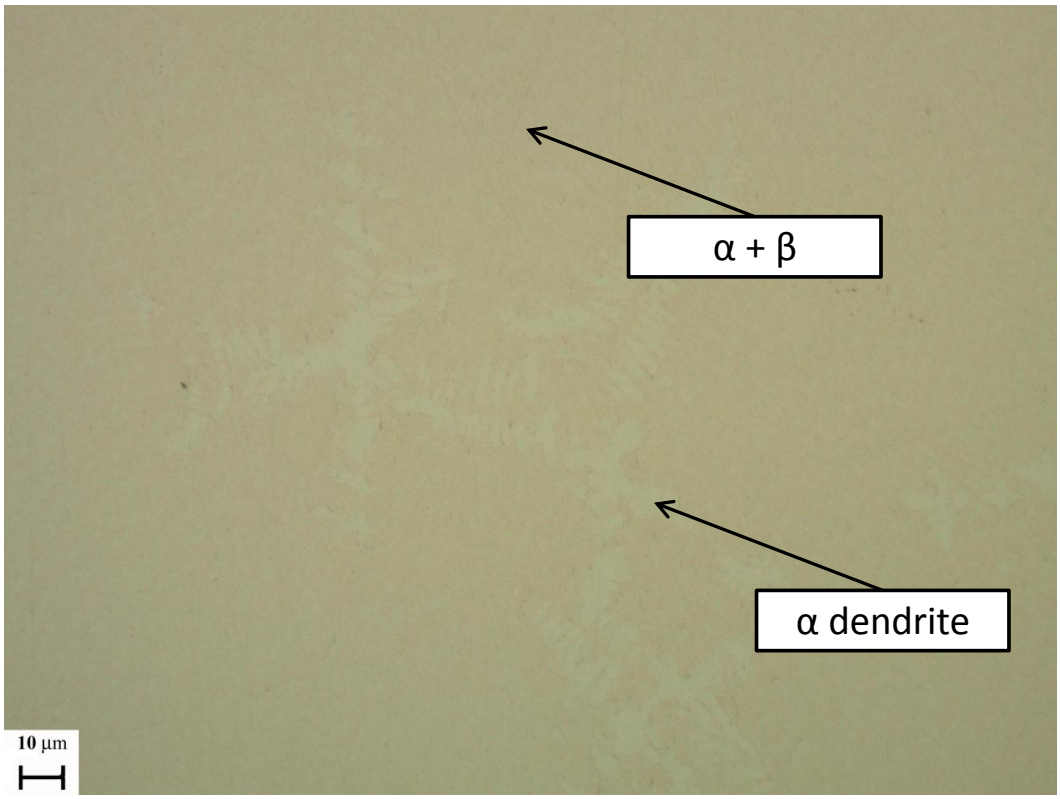

Figure 2-2 – Microstructure of as supplied 72Ag-28Cu

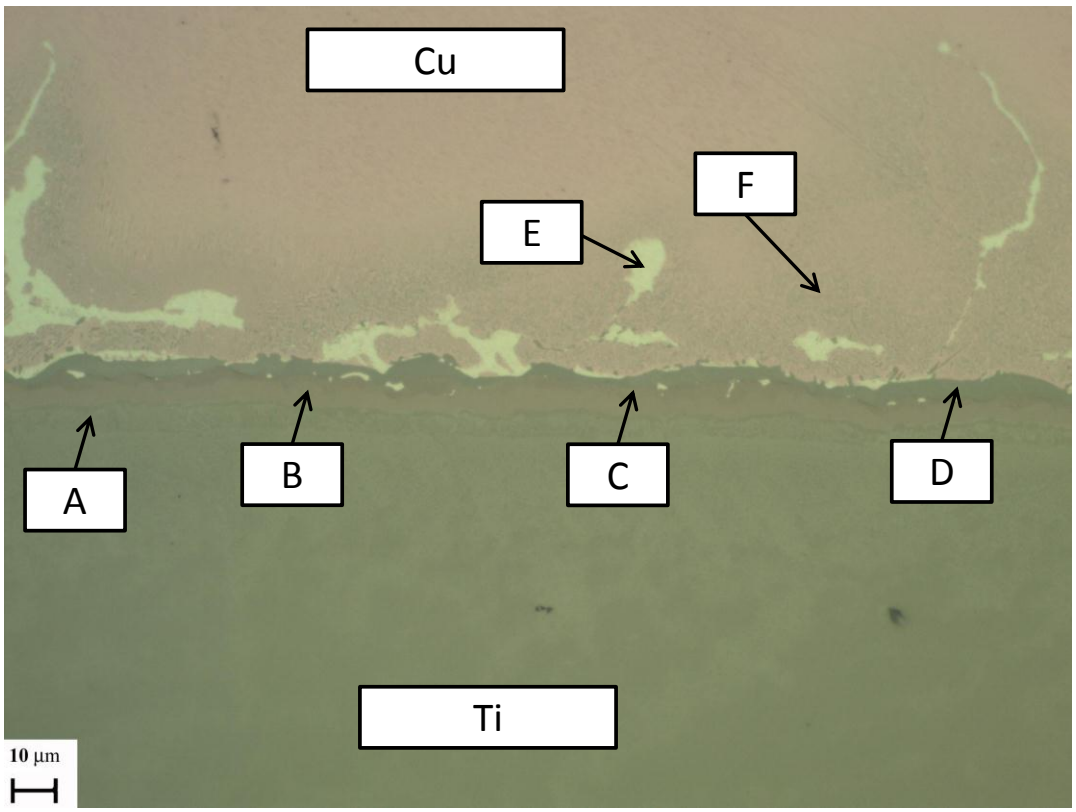

Figure 2-3 - Microstructure of Ti/72Ag-28/Cu brazed interface

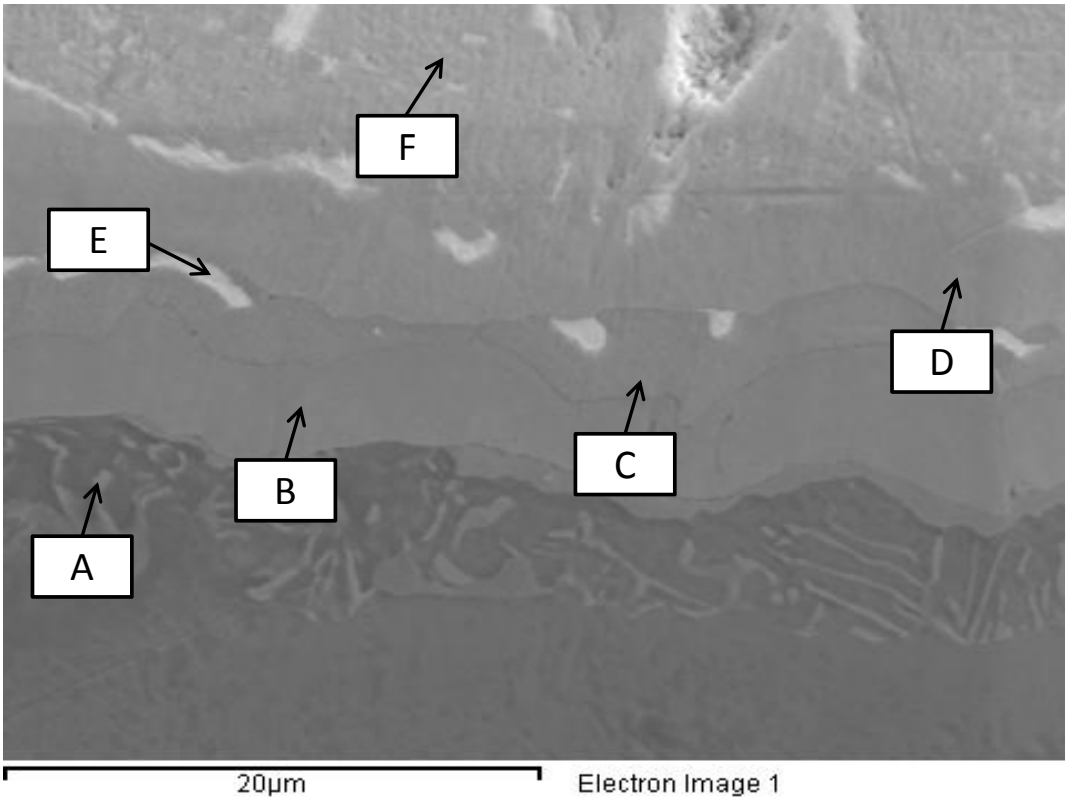

Figure 2-4 – SEM BEI Microstructure of Ti/72Ag-28/Cu brazed joint in region of Ti interface

2.4 Chemical composition and microstructural evolution of braze layer

A quantitative chemical analysis has been performed across the various phases present within the brazed layer to identify the chemical composition of each of the phases shown in Figure 2-3. The chemical composition was analysed using an energy dispersive (EDS) scanning electron microscope (SEM) with an accelerating voltage of 10keV. This allows chemical compositions to be obtained correct to $\pm$ 0.25%. The variation in chemical composition is shown in Figure 2-5 across each of the phases highlighted in Figure 2-3. A summary of the chemical compositions of each of these phases is presented in Table 2-2.

It is apparent from the chemical analysis that there is very little Ag present anywhere in the braze apart from the Ag-rich phase. In addition, given that the braze filler has an initial composition of 72Ag – 28Cu there is clearly diffusion of Ti into the braze and is present in phases, A,B,C,D and F which explains why the microstructure differs to that of the braze filler before joining which has no Ti present. The composition of the phases present within the braze are primarily Cu-Ti intermetallics hence the Cu-Ti binary alloy phase diagram can be used to identify the individual phases in a similar fashion to the work presented in [36]. Based on the results from the chemical analysis each phase is located on the Cu-Ti phase diagram as shown in Figure 2-6. The results from this SEM analysis closely match the results from previous work done in characterising the microstructure Ti/72Ag-28Cu/Cu and Ti/72Ag-28Cu/304 Stainless Steel brazed joints [36] [45].

Phase	Ag (%wt)	Cu (%wt)	Ti (%wt)	Phase
A	1.75	5.21	93.04	Ti rich
B	6.18	50.66	43.16	CuTi
C	3.81	53.22	42.97	Cu_4Ti_3
D	2.96	80.2	16.84	Cu_4Ti
E	94.6	5.4	0	Ag rich
F	6.84	88.71	4.44	Cu rich

Table 2-2 – Chemical composition of phases in the braze

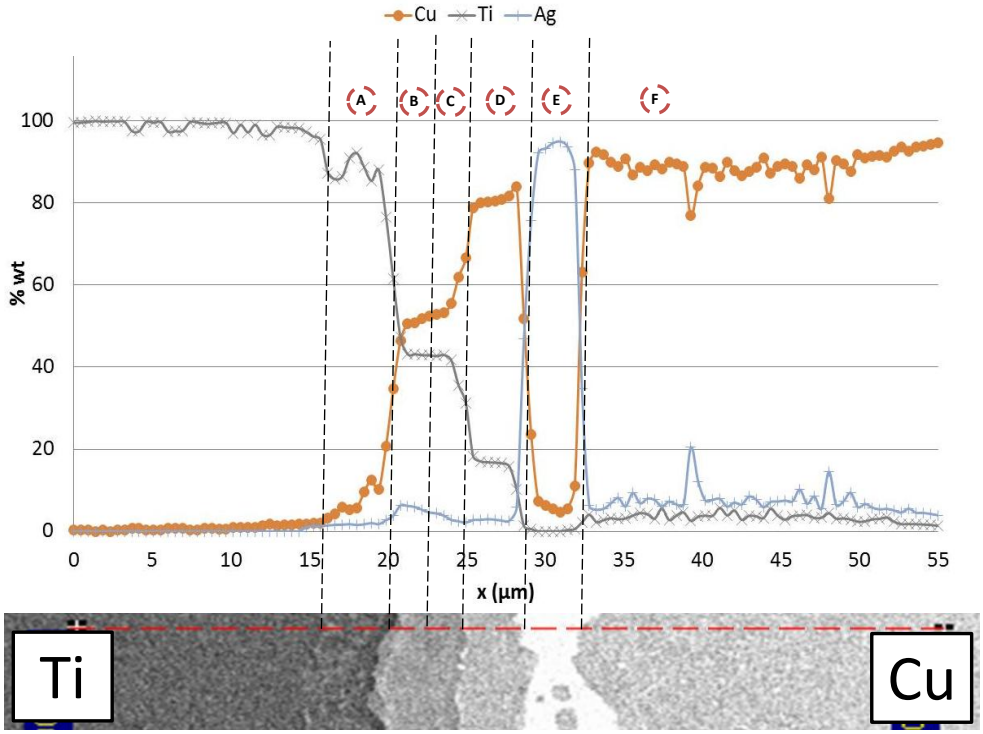

Figure 2-5 - Variation in chemical composition

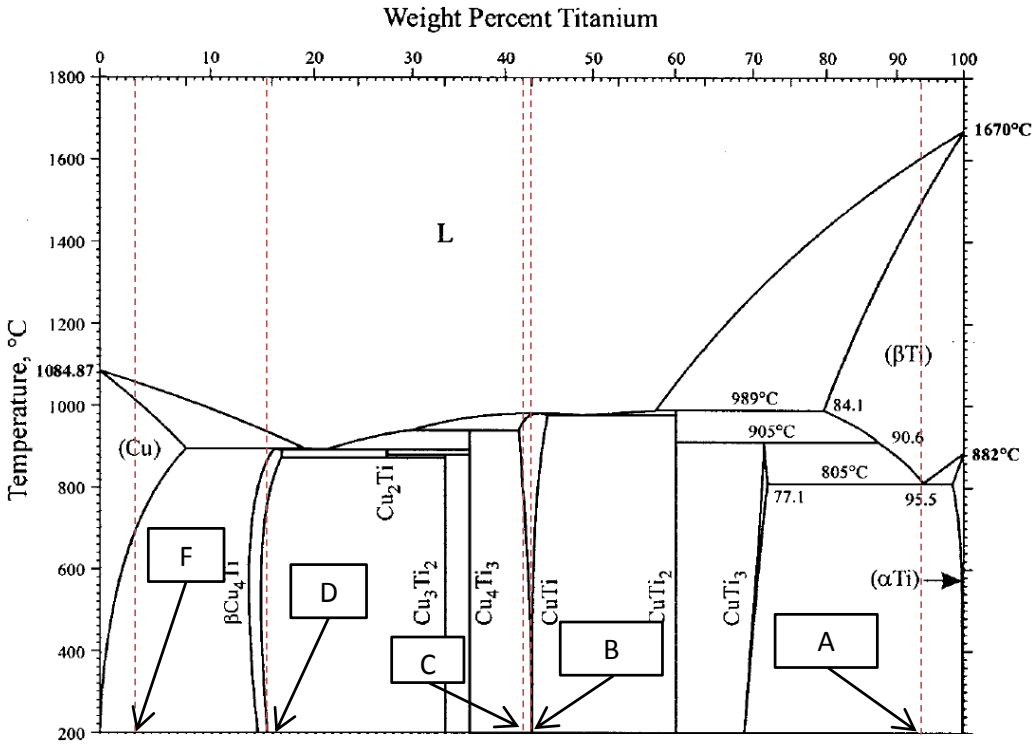

Figure 2-6 - Cu - Ti phase diagram and identification of phases [46]

The microstructural evolution of this interface is complex and is briefly summarised in Figure 2-7 based on a model proposed by Shafiei et al [45] . The Cu-Ti intermetallic compounds can be explained by the diffusion of Ti into the molten braze. Cu has limited solubility in Ti [47], hence only small quantities of Cu are present in phase A at the Ti braze boundary. However the solubility of Ti into Cu is much higher [47] hence large quantities of Ti are found in the various phases present within the braze. Once the filler is melted (step 1) Ti diffuses into the molten filler (steps 2) with the largest concentrations found at the interface of the parent Ti and the molten braze. Eventually a small molten layer saturated in Ti is formed (layer (a) in step 3) which results in the CuTi being precipitated out at the Ti interface (step 4). As the CuTi phase grows (step 5) and the joint begins to cool, the rate of Ti diffusion into the braze is reduced resulting in the formation of the Cu_4Ti_3 with a lower %wt of Ti (step 6). As the temperature reduces further the volume fraction of Cu_4Ti_3 increases (step 7) and eventually Cu_4Ti is formed which contains the lowest %wt of Ti of all the intermetallic phases present (step 8). The formation of these intermetallic phases results in a reduction in %wt of Cu in the remainder of the braze filler which results in Ag-rich regions forming in addition to the Cu-rich region forming (step 9).

Hence, the final 72Ag-28Cu brazed layer contains phases of varying chemical composition and a microstructure which varies considerably to that in the as cast condition. In this case the difference in microstructures can predominantly be attributed to diffusion of Ti into the braze during the brazing cycle.

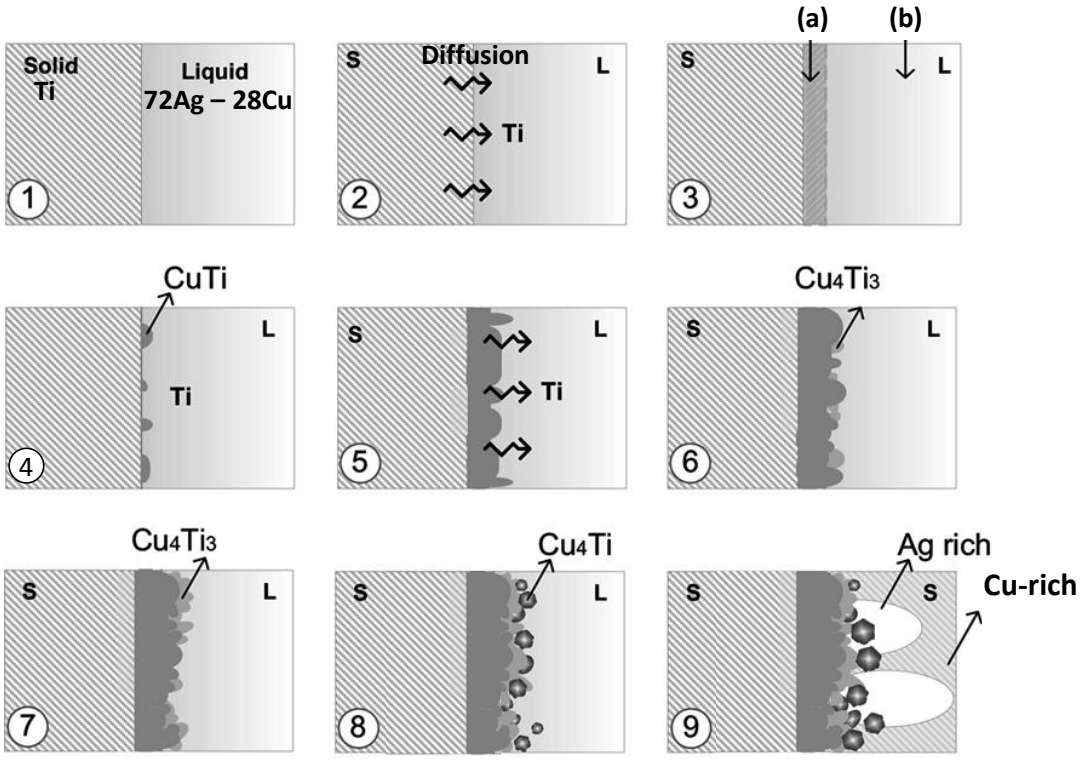

Figure 2-7 - Microstructural evolution of Ti/72Ag-28Cu/Cu braze [45]

2.5 Effect of diffusion on interfacial transition regions

The previous section has shown that, diffusion of elements to and from the braze results in a braze microstructure which is different to the as cast condition and contains phases of varying chemical composition. In addition, due to the mechanism of diffusion (i.e the transport of material by atomic motion) step changes in material compositions between the braze and parent materials, and between the different phases within the braze, will not occur. Instead there will be gradual transition between the individual phases, albeit over a small distance. This diffusion process is present in all brazing and diffusion bonding processes, to a lesser or greater extent, and is a function of the brazing temperature, length of time at the brazing temperature and solubility of the filler and the parent materials [48]. This can be highlighted by considering the atomic structure at the interface in the simple example shown in Figure 2-8.

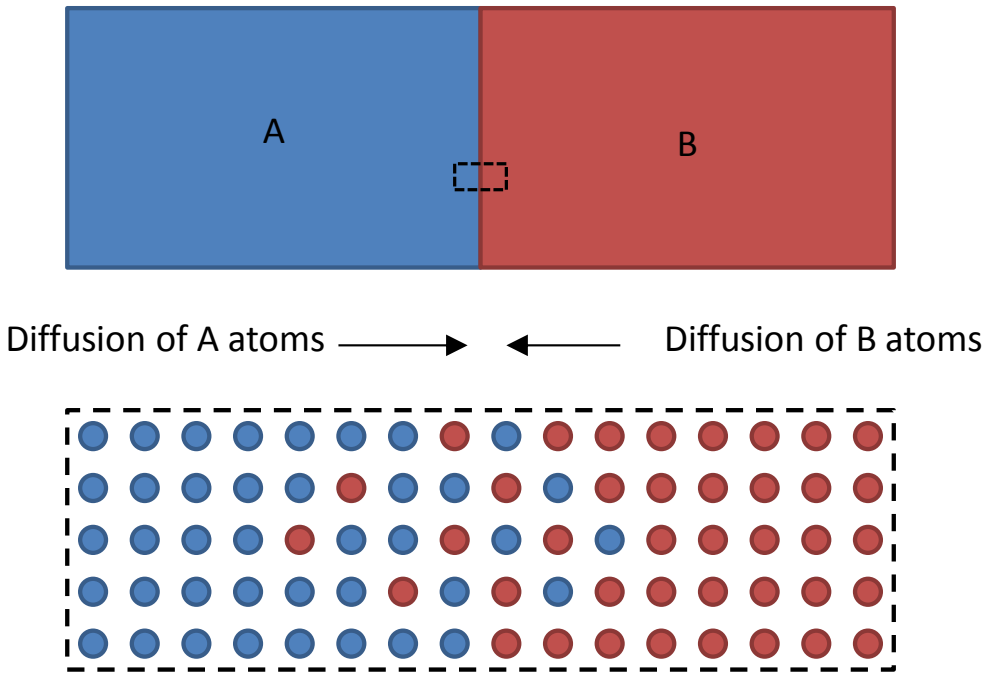

Figure 2-8 – Diffusion at material interface

This can be seen optically at the macro scale in Figure 2-3 as phase F (Cu rich) gradually transitions to the parent Cu material. This is an exaggerated case but a similar grading will occur at a smaller scale between the other phases present within the braze. To highlight this, an additional chemical analysis has been performed across the boundary between phase A (Ti-rich) and phase B (CuTi) the results from which are shown in Figure 2-9. The results clearly show a gradual variation in the chemical composition between phase A (Ti – rich) and phase B (CuTi). This gradual transition is occurring over a very small scale, approximately 3.8µm, in this case but there is no obvious step change in chemical composition. This phenomenon has also been shown to occur in a 316LN stainless steel to CuCrZr joint brazed with a nickel based brazed filler [49].

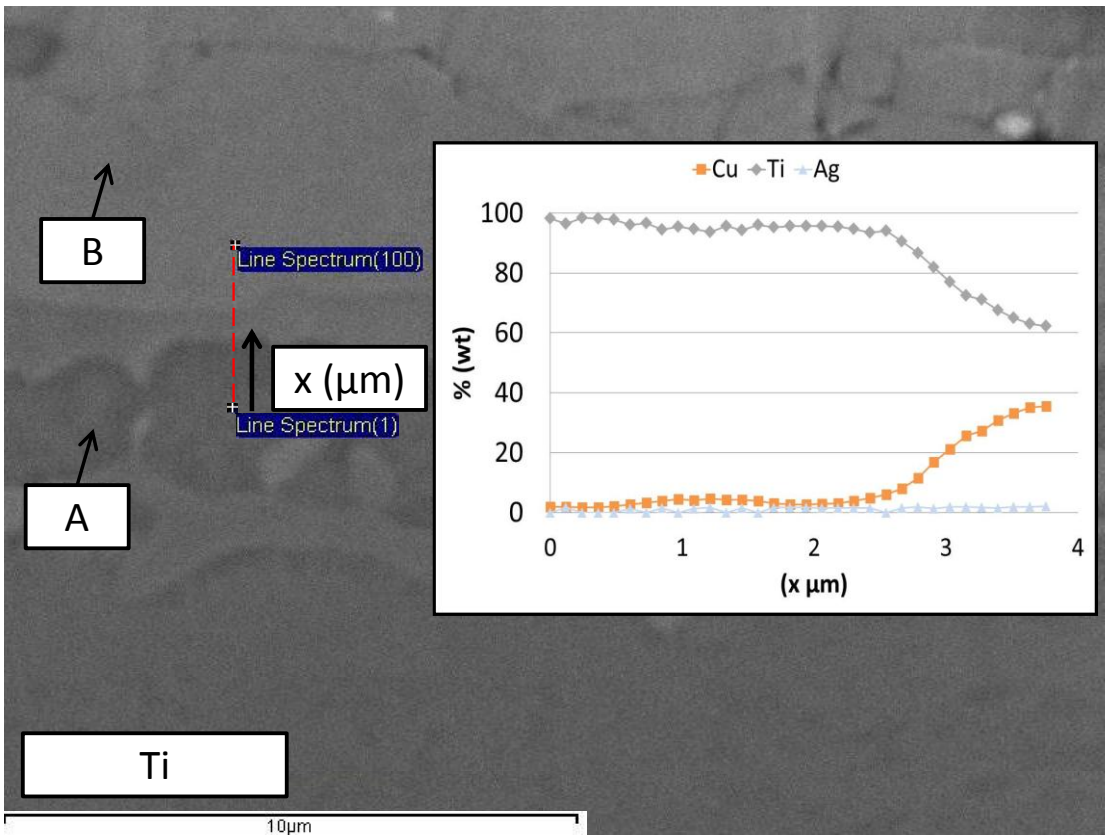

Figure 2-9 – Gradual variation in chemical composition across braze phases

2.6 Variations in mechanical properties across the braze layer

The variations in chemical compositions of each of the phases present within the braze suggests that the material properties will vary considerably across the braze. Consequently, the micro scale mechanical properties of the Ti/72Ag-28Cu/Cu brazed joint have been evaluated using nanoindentation. The purpose of this nano-indentation investigation is to prove (or otherwise) that the differences in chemical composition results in differences in mechanical properties between the individual phases. A series of separate mechanical tests are done on the as supplied 72Ag-28Cu braze filler for use in subsequent FEA and this process is discussed further in chapter 4.

The hardness and Young's modulus distributions have been evaluated on a sample polished across the section of the joint using a G200 nanoindenter. Indents were taken using a Berkovich indentor tip to a measurement depth of 500nm with indent spacing of 4µm with both hardness and Young's modulus being measured using the continuous stiffness measurement method [50].

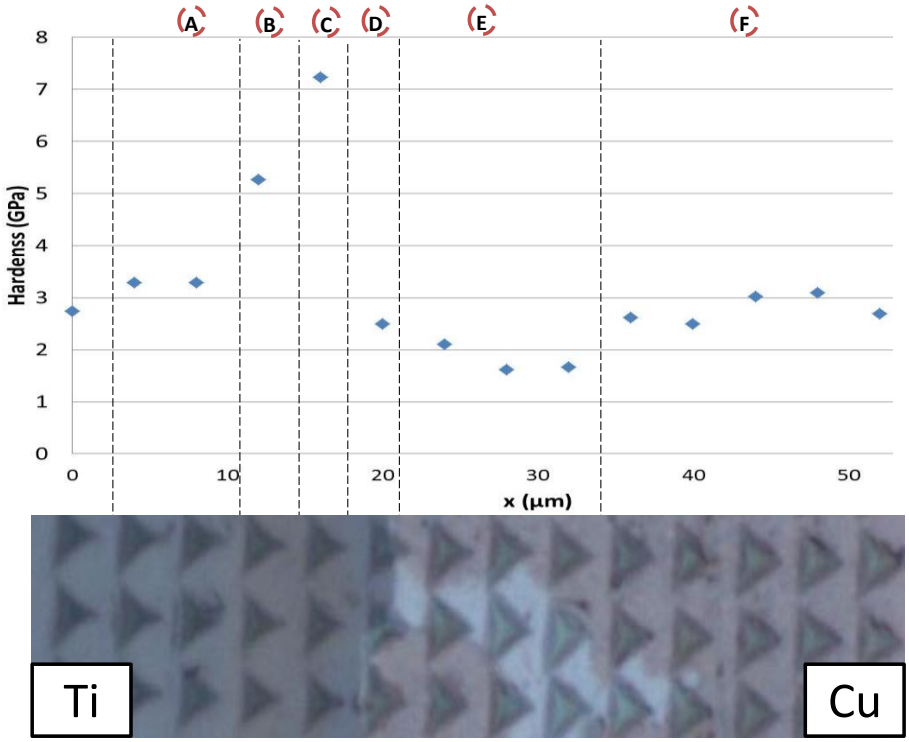

Figure 2-10 and Figure 2-11 show the variations in hardness and Young's modulus across the Ti/72Ag-28Cu/Cu joint, the results are presented for the middle row of indents with the lettering of the phases corresponding to those identified in Figure 2-3. The measured hardness of the Ti, the first point on the graph is 2.74GPa which closely matches values

reported by Mante et al [51].

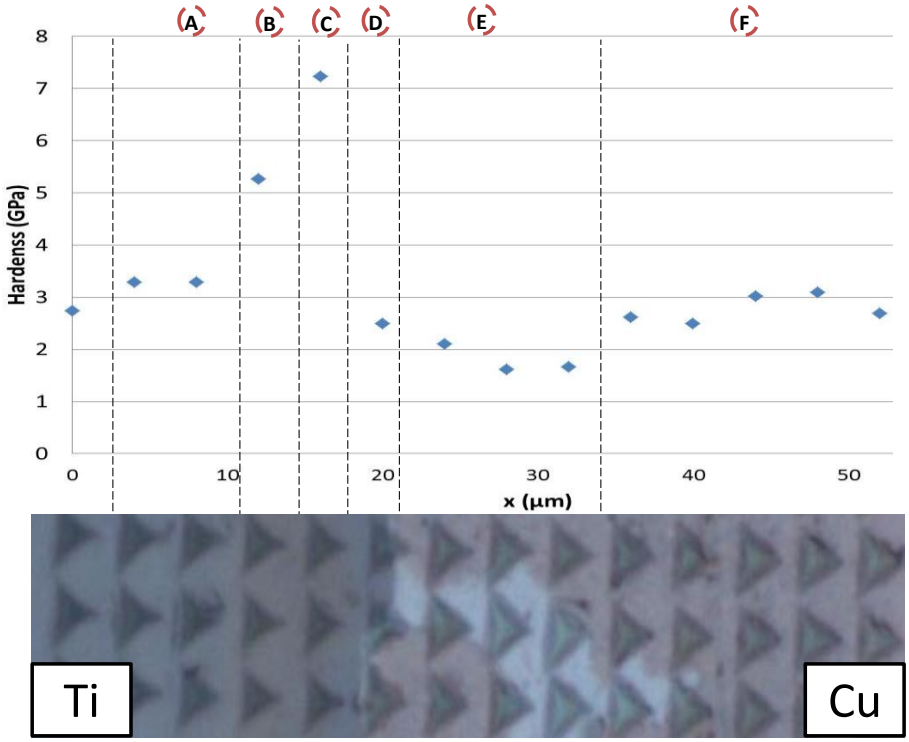

Figure 2-10 clearly shows large variations in hardness within the brazed layer, with phases B (CuTi) and C (Cu_4Ti_3) having the largest hardness. Similarly, the variations in Young's modulus across the Cu/72Ag-28Cu/Ti joint are shown in Figure 2-11, the results are presented for the middle row of indents shown.

The measured Young's modulus of the Ti, the first point on the graph is 125GPa which closely matches values reported for the grade of Ti used in the joint [52]. These results show that that the Young's modulus varies considerably across the braze, with phases B (CuTi) and C (Cu_4Ti_3) clearly having the highest Young's modulus. The Ag-rich phase E has the lowest modulus which is to be expected given the low modulus of pure Ag [52]. The first two indents in phase F (Cu-rich) away from phase E (Ag-rich) region are lower due than the remainder in phase F (Cu-rich) which can be attributed to the surrounding phase E (Ag-rich) below the indents. In general the trends in hardness and Young's modulus correlate well. The scale over which these variations occur is at the same order of magnitude as the thickness of the braze and given the microstructure of the braze such variations are to be expected.

Ashby [53] has shown that the coefficient of thermal expansion and Young's modulus are related by αE = constant suggesting that increase in Young's modulus will result in proportional reduction in coefficient in thermal expansion. This is shown graphically in Figure 2-12. Conversely, fracture toughness has been shown to increase proportionally with Young's modulus as summarised in Figure 2-13 [53]. Hence, the variation in hardness and Young's modulus within the braze layer also suggests large variations in other material properties such as coefficient of thermal expansion and fracture toughness.

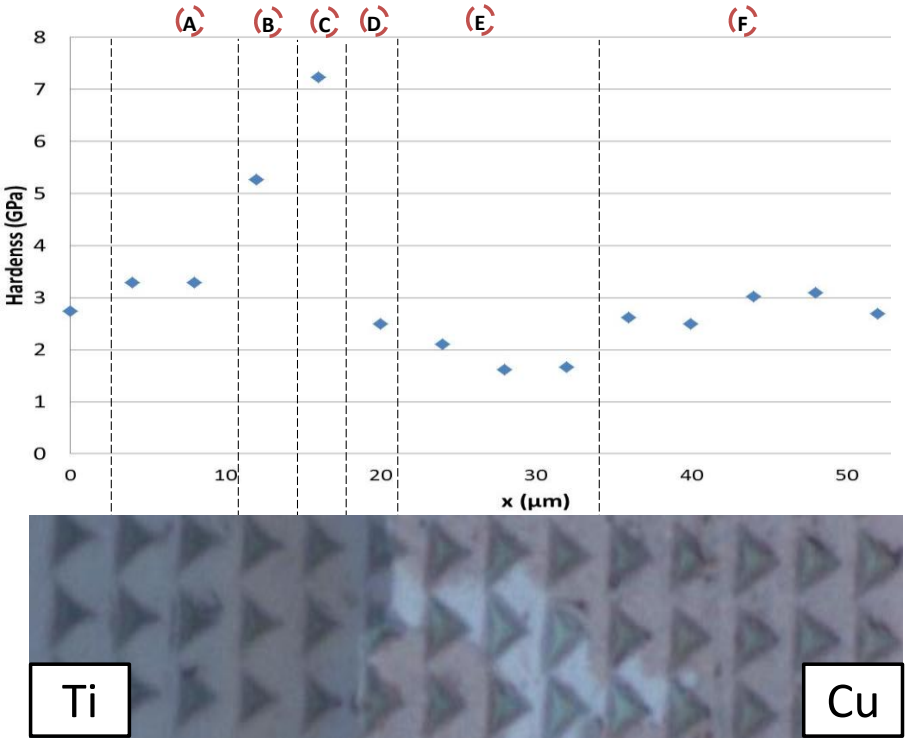

Figure 2-10 - Variations in hardness across Ti/72Ag-28Cu/Cu brazed joint

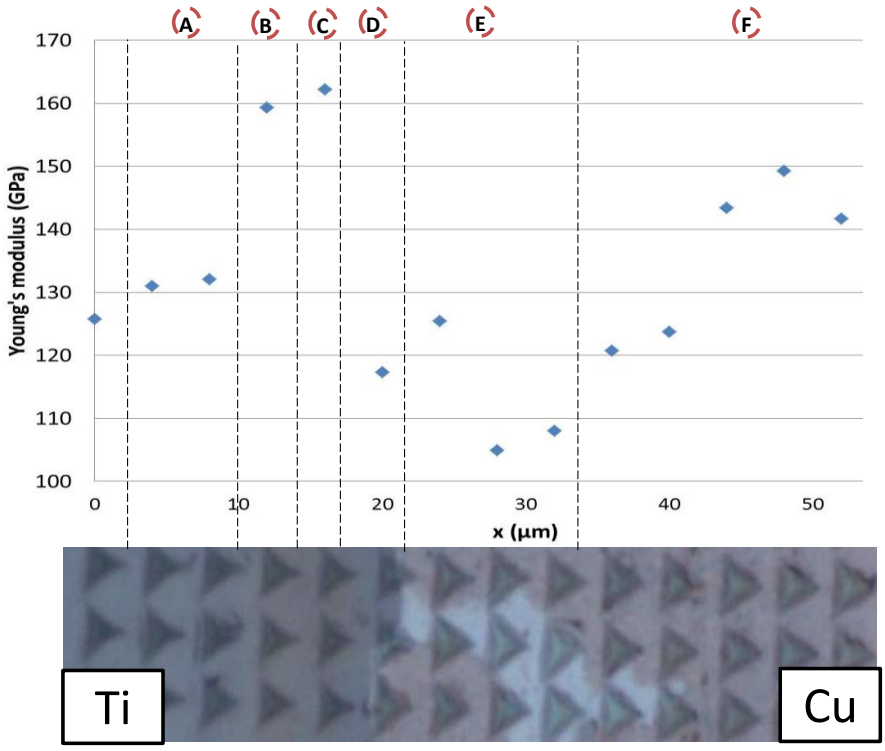

Figure 2-11 - Variations in Young's modulus across Ti/72Ag-28Cu/Cu brazed joint

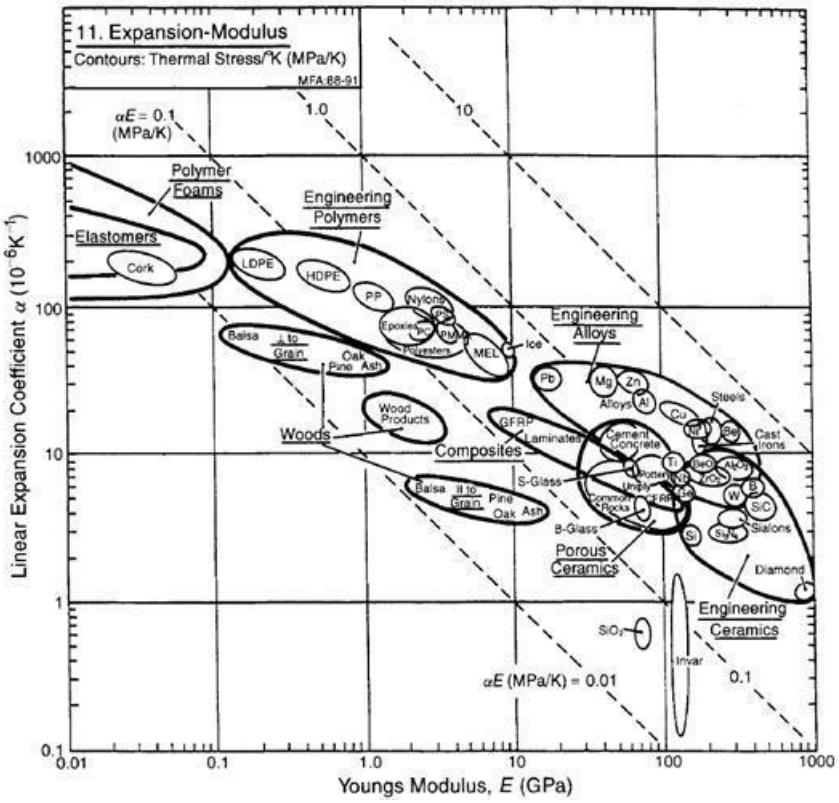

Figure 2-12 - Young's modulus and thermal expansion coefficient relationship [53]

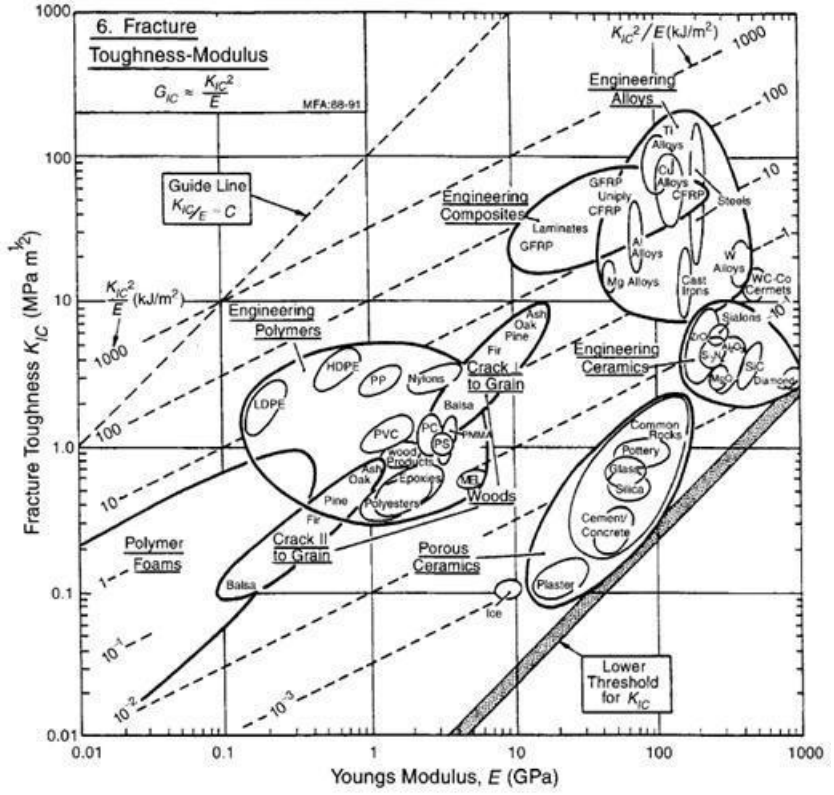

Figure 2-13 - Young's modulus and fracture toughness relationship [53]

2.7 Other findings of interest

The free edge of the Ti/72Ag-28Cu/Cu brazed joint prepared for this investigation is shown in Figure 2-14. A clear meniscus can be seen along the free edge (also present on the other side of the sample however this is not shown) and will provide a stress concentration at the interface. In addition the interface between phase B (CuTi) and phase C (Cu_4Ti_3) has fractured either during preparation or brazing suggesting the interface between these phases has a low toughness. It is likely that the presence of these features will be detrimental to both joint strength and fatigue life. These features could be removed through a post brazing machining or polishing operation. Alternatively an alteration to the brazing process could be made to remove the formation of the intermetallic phase B and C.

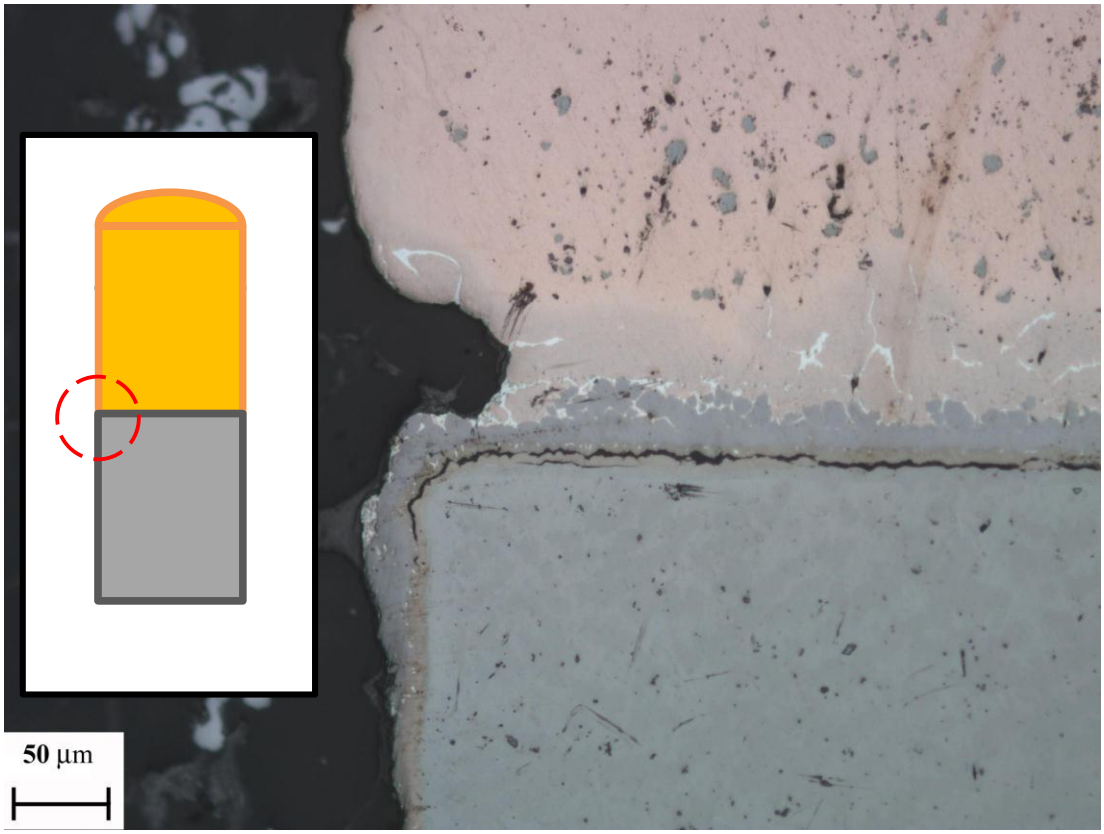

Figure 2-14 - Ti/72Ag-28Cu/Cu joint free edge geometry

2.8 Findings in relation to modelling and failure of brazed joints in general

In terms of finite element modelling of dissimilar material joints, when two dissimilar materials are joined by brazing, a thin braze layer exists at the joint between the two materials. It follows logic that the mechanical properties of this thin layer will play a key role in the mechanics and failure of the joint. If, for example, the braze filler was extremely stiff relative to the parent materials, the degree of constraint at the free edge during cooling from the brazing temperature will be large. If however the stiffness of the material was relatively very low there would be very little constraint on the materials being joined and hence the thermal stresses arising would be significantly different. It is therefore important to capture the effect of the brazed layer if the stress state in the joint is to be accurately captured.

One approach to modelling dissimilar material brazed joints has been to model an abrupt change between both parent materials and to ignore the presence of the braze layer completely [18], [54], [55] as shown on the left hand side of Figure 2-15. The practice of neglecting the braze layer is effectively assuming that the braze layer and diffusion regions have exactly the same properties (mechanical and thermal) as one of the materials being brazed. From a mechanics perspective, this approach fails to account for the effect of the mechanical properties of the braze on the stress state within the joint as well as failing to take into account the presence of large variations in material properties within the braze and any transition zones between the braze and the parent material.

Another modelling approach is to model the braze layer as a separate homogenous material using the as supplied macroscopic material properties of the braze filler[20], [30], [56]–[59]. This assumes an abrupt change in material properties at the interface between both parent materials and the braze filler as shown on the right hand side of Figure 2-15. The approach of modelling the braze layer as a separate material presents several non-trivial challenges. Firstly, due to the relatively small thickness of a brazed layer, extremely small mesh sizes are required if it is to be included in a model. There also exists the problem of obtaining temperature dependent material property data for the brazed layer. Such data is sparse and the material property characterisation will invariably be based on the as supplied brazed filler with the assumption that the material properties of the braze are the

same in the as supplied condition as those after joining. This fails to account for the effect of the diffusion of elements from the parent material into the filler and the subsequent differences in microstructure and hence material properties highlighted in section 2.3. In some instances this approach will be valid, for example when diffusion of elements from the parent material into the braze has a negligible effect on the properties of the braze layer after joining [58].

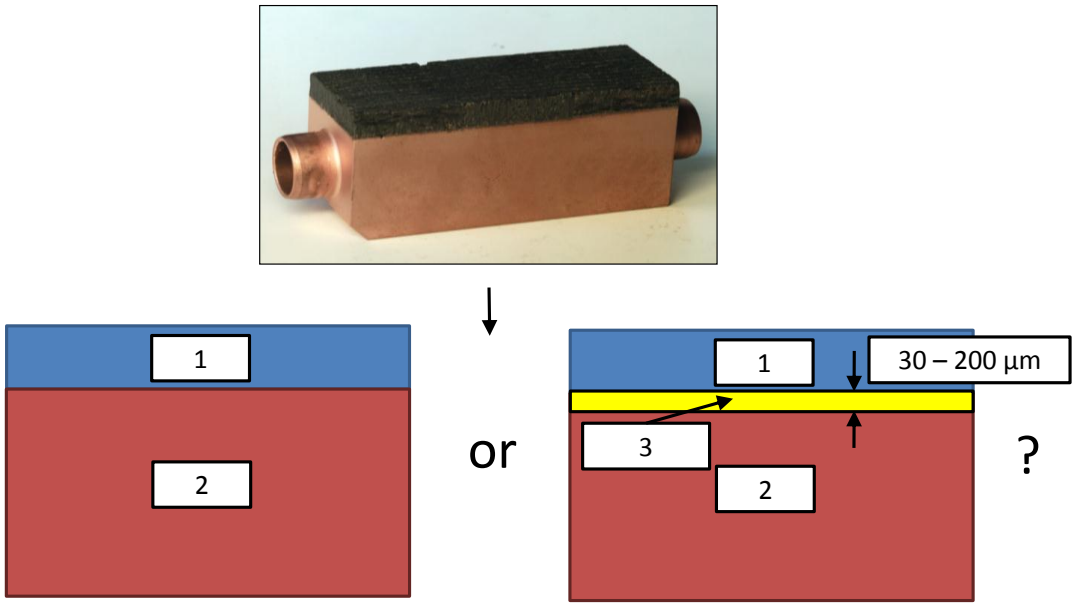

Figure 2-15 – Approximating the brazed layer for FEA

Yet another approach is to model the braze layer as a separate homogenous material taking into account the microstructural changes due to diffusion of elements from the parent materials into the braze layer due to joining [58]. There are various means of achieving this. One way is to cast macroscale samples of the braze layer with a microstructure similar to that found within the braze after joining [58]. An additional approach is to use techniques such as nanoindentation to characterise the mechanical and thermal properties of the brazed layer after brazing and scale these properties up to those commensurate with the scale of the finite element. Both of these techniques are currently the subject of current research to fully characterise the material properties of the brazed layer for use in FEA [60]. Another approach is to use homogenization software such as DIGIMAT-FE [61] to generate representative material properties for complex material microstructures based on the constituents of the individual phases. This technology has predominantly been developed

for use in the composites industry. However, this approach could possibly be adapted for brazing applications.

The practice of both neglecting the brazed layer and modelling the brazed layer as a separate homogenous material fails to take into account the presence of large variations in material properties within the braze and any transition zones between the braze and the parent materials. As a consequence of this abrupt change in properties, converged finite element results will never be obtained at the interface. An idealised brazed joint will therefore fail to model the correct material properties, including fracture toughness and fatigue strength and will also produce large discontinuity stresses at the interface (often a theoretical singularity in the elastic case as described in the next chapter). Clearly, these all must be considered when modelling at such a small scale. In reality, due to these factors discussed, it is unlikely that accurate modelling of the stress state very close to, and across the brazed layer will be possible using these approaches. Moreover when the braze layer is neglected or assumed to have similar properties to one of the joined materials the degree of constraint due to the braze will not be captured and the stress state in the joint not representative. Hence alternative techniques based on experimentally derived test results will be required to predict failure in close proximity to the interface and these are discussed in the future sections.

However, it has been shown in section 1.5 of this thesis that dissimilar material joints can fail very close to the interface in the parent materials and as such in some instances it may not be necessary to fully capture what is happening across the interface. In cases such as this, if a braze layer with representative macroscopic properties is used which applies a representative constraint on the model, converged stresses can be obtained away from the interface which will allow different failure mechanisms to be assessed. In addition, using a simplified approach to model the brazed layer does not preclude its use in design. A simple joint approximation with an abrupt interface between a braze and two dissimilar materials can still be informative in terms of comparing the stress fields away from the interface and comparing different joint designs as long as the degree of constraint due to the braze is accurately represented.

Chapter 4 of this thesis aims to use FEA to predict the residual stress due to joining in a Ti/72Ag-28Cu/Cu brazed joint. This work assumes that the braze layer will have the same material properties before and after brazing hence neglecting the effect of diffusion from

the Ti into the braze. Whilst, for this joint it has been shown that the validity of this approach is questionable, it is better than ignoring its presence completely and highlights the challenges still to be overcome in characterising the brazed layer material properties for use in FEA and any subsequent failure analysis.

2.9 Dissimilar material joint failure modelling approaches

Based on the findings from the work presented in this chapter it is worthwhile reflecting on the potential brazed layer modelling strategies for different failure mechanisms. The appropriate brazed layer modelling strategy will be linked to the specific failure mechanism being considered and these failure mechanisms are discussed in the following sections. In all cases capturing the constraint due to the interface will be important; however detailed stress distributions in the region of the joint may not always be necessary.

Many of the strategies suggested require experimentally derived failure criterion which account for the complex metallurgy of the braze as discussed in this chapter, albeit in a "smeared" manner. This experimental data will only be valid for the materials being joined, the braze filler adopted and the joining process used. Residual stresses due to joint manufacturing cannot be neglected when performing a failure analysis and in general must be accounted for. This section reflects on the level of detail required in any brazed joint model such that the correct stress concentrations are captured for any failure analysis.

2.9.1 Brittle failure

2.9.1.1 Away from the interface

Brittle failure is generally assessed by comparing a maximum principal stress with an allowable value for the parent material. Hence in a dissimilar material brazed joint, this requires the constraint due to the brazed layer to be accurately represented through the use of a simplified braze layer model, in addition to the residual stresses developed during joint manufacture. The mesh refinement would need to be such that it fully captures the local stress concentration due to the interface.

2.9.1.2 Interface failure

When assessing failure at the interface, residual stresses due to joint manufacture must be accounted for in spite of the challenges in predicting the stress state at the interface. These

residual stresses are not accurate at the level fracture will occur when a simplified braze layer is assumed.

Interfacial fracture mechanics methods have been developed to assess decohesion and cracks in dissimilar material interfaces and have been the topic of previous research [62]–[68] and such procedures could be developed for the brittle failure assessment of the interface of dissimilar material brazed joints.

Structural hot-spot stress techniques [69]–[72] are not commonly used to assess interfacial failure in brazed joints, however, they could also be adapted to predict failure at the interface of dissimilar material joints by obtaining a representative stress that is used to compare with an experimentally derived allowable stress.

In addition cohesive zone modelling [73]–[78], which idealises complex fracture mechanisms with a macroscopic cohesive law which relates failure of the interface to its separation have are the topic of current research to assess interfacial failure of brazed joints [79].

At the heart of any procedure to assess brittle failure at the interface, experimentally derived failure criterion is required which inherently accounts for the complex metallurgy of braze discussed in previous sections.

2.9.2 Interface fatigue

In a similar fashion to assessing brittle failure at the interface, when assessing interface fatigue the residual stresses due to joint manufacture must be accounted for.

Techniques such as the use of fatigue strength reduction factors or structural hot-spot stress techniques [69]–[72] could be adapted to assess interfacial fatigue in dissimilar material brazed joints. In addition, interfacial fracture mechanics and a cohesive zone model approaches, the merits of which are discussed in [80], could be adopted. Again, at the heart of any procedure to assess fatigue at the interface, an experimentally derived failure criterion is required which accounts for the complex metallurgy of the braze layer.

2.9.3 Plastic collapse

Plastic collapse only occurs under a primary load and cannot occur due to secondary thermal loading alone. It can of course occur as a result of additional primary loads induced

by buckling caused by secondary thermal loading. Methods for assessing gross plastic deformation of structures generally [81] do not require the modelling of small details such as welds [81]. In addition residual stress fields are invariably not accounted for as they are assumed to be self-equilibrating and do not generally affect the limit state.

In the case of dissimilar material brazed joints, accurately capturing the stress concentration effects due to the interface and stress distribution across the braze is not required. However the effect of the constraint due to the braze on any geometrical field stress or gross stress concentration must be accurately captured and hence a simplified braze layer should be included in any model.

2.9.4 Ratcheting

Modelling ratcheting behaviour generally requires the local stress concentrations to be modelled [81]. Hence in the case of performing a ratcheting analysis on a dissimilar material brazed joint, the local stress concentration due to the braze must be captured and hence a representation of the braze layer must be modelled. The initial ratcheting behaviour will also be influenced by the as-brazed residual stress field and must also be accounted for in such an analysis.

2.9.5 Buckling

The degree of stiffness provided by end fixity due to a brazed joint will generally be important for a buckling analysis concerning attached members or components, hence in these cases obtaining a value for the joint stiffness's through experimentation would be advisable. However accurately capturing the local stress concentration at the interface and across the braze will not generally be required in a global buckling analysis. Modelling post buckling behaviour could involve other failure mechanisms and hence reference should be made to the above sections.

Buckling behaviour could also be influenced by the joining process, if for example the brazing process resulted in a global residual field stress being induced in an assembly and this would have to be accounted for in any buckling assessment.

2.10 Summary

The metallurgical features of a Ti/72Ag-28Cu/Cu dissimilar material brazed joint have been presented. The microstructural evolution of a brazed layer during joining is complex and it has been shown that the microstructure of the brazed layer in a Ti/72Ag-28Cu/Cu joint is completely different to that of the 72Ag-28Cu parent braze material. The variation in microstructure can be attributed to diffusion of elements from the parent material into the molten braze during joining. The phases present within the braze after joining vary in chemical composition and hence mechanical and thermal properties which has been highlighted using nanoindentation. It has also been shown that due to diffusion, step changes in material properties do not exist and instead there is a gradual transition occurring over a very small distance (c 2-3μm).

In terms of FEA, modelling the braze layer presents several non-trivial challenges. Firstly, when two dissimilar materials are joined using brazing, a thin braze layer exists at the joint between the two materials, typically of the order of 20-100μm thick. It follows logic that the mechanical properties of this thin layer will play a key role in the mechanics of the joint and hence its influence must be captured in any finite element model. Characterizing the material properties of the brazed layer on the as supplied state for use in any finite element model will be valid when diffusion of the elements into the braze is negligible. In the case when there is a change in microstructure due to diffusion of elements from the parent materials (such as in the Ti/72Ag-28Cu/Cu joint discussed in this chapter) alternative techniques such as casting samples for material property characterisation which account for the changes in microstructure due to joining or developing nanoindentation techniques to measure the material properties within the braze after joining can be used. Alternatively, sensitivity studies could be employed to ascertain the significance of likely variations in properties.

There are however, several barriers to accurately capturing the stress state in the region of the joint and across the brazed layer, as highlighted by the findings of this metallurgical investigation. At the heart of any procedure to assess failure at the interface, an experimentally derived failure criterion is required which inherently accounts for the complex metallurgy of braze. However this does not preclude using a simplified braze layer with representative material properties in design and assessing failure away from the

interface. The modelling strategy required when assessing failure of dissimilar material brazed joints is dependent on the failure mechanism. In summary and in general:

- When assessing brittle failure away from or at the interface, the constraint due to the braze and residual stresses due to joining must be accounted for hence a representation of the braze layer must be modelled.
- When assessing plastic collapse, accurately capturing the local stress concentration effects due to the interface and stress distribution across the braze is not required. However the effect of the constraint due to the braze on any geometrical field stress or gross stress concentration must be accurately captured and hence a representation of the braze layer must be modelled.
- When assessing ratcheting, the local stress concentration due to the braze must be captured and hence representation of the braze layer must be modelled. The initial ratcheting behaviour will also be influenced by the as-brazed residual stress field and hence must be accounted for in such an analysis.
- When assessing buckling, accurately capturing the local stress concentration at the interface and across the braze will not generally be required. However the degree of stiffness provided by end fixity due to a brazed joint will be important for a buckling analysis concerning attached members or components, hence in these cases obtaining a value for the joint stiffness's through experimentation would be advisable.

3 The mechanics of, and stress state in, a typical join between dissimilar materials

3.1 Introduction

Whilst the performance of dissimilar material brazed joints is dependent on formation of brittle intermetallics and the presence of porosity and flaws [23], [24] , the stresses developed within the joint due to differences in material properties such as coefficient of thermal expansion and Young's modulus will also play a key role in stresses developed within the joint. It is intuitive that the larger the mismatch in material properties the higher the stress concentration at the interface and the more likely the joint is to fail. In addition to differences in material properties, process variables such as brazing temperature, joint geometry and plasticity will all influence the stresses developed within the joint due to joining and any subsequent thermal and mechanical loading.

The aim of this chapter is to develop an understanding of the mechanics and stress state in an idealised dissimilar material joint. This understanding will form the basis for explaining results in future chapters of this thesis. More specifically the aims of this chapter are to:

- Develop a mechanism which explains how the high interface stresses occur due to the constraint on the materials being joined (section 3.2)
- Gain an understanding of dissimilar material joint theory (section 3.3)
- To use FEA to develop an understanding of the key features of the stress state in an idealised dissimilar material joint and how different relationships in material properties will affect this stress distribution (section 3.4)
- To gain an understanding of how plasticity affects the mechanics of the joint and (section 3.5)
- To gain an understanding of how a small interlayer (such as a brazed layer found in brazed joints) and varying joint size affects the stress developed within the joint (section 3.6).

3.2 Constraint mechanism at a dissimilar material interface

In addition to understanding the stress state predicted by elastic theory or FEA, it is useful for engineers to understand the mechanism causing the high stresses in a simple butt joint

between two dissimilar materials with an abrupt interface, namely the constraint on free expansion and contraction of both materials in the region of the joint. The following cases aim to highlight how one might expect the stress field surrounding the interface to look by considering the relative expansion and constraint on expansion of the two materials. It may be stating the obvious, but it is worth noting that under a thermal load, if the coefficients of thermal expansion are identical then there will be no stresses developed in the joint.

Consider the simple 90° dissimilar material joint as shown in Figure 3-1, where $E_1 = E_2$, $\nu_1 = \nu_2$, but $\alpha_1 = 2 \times \alpha_2$. Assuming both materials are initially of equal widths and at a stress free temperature of 1000°C, when the joint is cooled to 20°C the thermal contraction of material 1 will be twice that of material 2. To maintain compatibility of displacements of both materials at the interface a stress state is developed due to the constraint on free expansion which results in high stresses in the region of the joint at the free edge. Assuming plane stress conditions (i.e. σ_z, τ_{yz}, $\tau_{xz} = 0$), the compatibility constraint of the interface has the effect of applying a couple at the interface (M_z) which results in significant interlaminar normal stress (σ_y) being developed perpendicular to the interface. These interlaminar normal stresses perpendicular to the interface are larger in magnitude than the other components which at first may be counter intuitive. The effect of this couple is a step change in the sign of the σ_y across the interface. Given the deformed shape shown in Figure 3-1, material 2 will develop a tensile σ_y during cooling, and material 1 a compressive σ_y during cooling. In this case the greater the difference in CTE, the larger this constraining effect hence the larger the stress perpendicular to the interface. The magnitude of the stresses will also be dependent on the Young's modulus of the materials. For a given differential expansion with stiffer materials, a greater constraint is required to maintain compatibility and hence a more severe local stress state will arise.

In addition to the development of stresses perpendicular to the interface, other stress components will exist due to the compatibility constraint of the interface. The stress state developed at the free edge of a dissimilar material joint interface is similar to that found in composite laminates, the theory of which has been the subject of previous research [82]–[84]. The compatibility constraint at the interface also applies a positive shear stress in the region of the joint at the free edge in both materials. Material 1 also develops a compressive σ_x and material 2 a tensile σ_x away from the free edge [85] as shown in the left hand side of Figure 3-2.

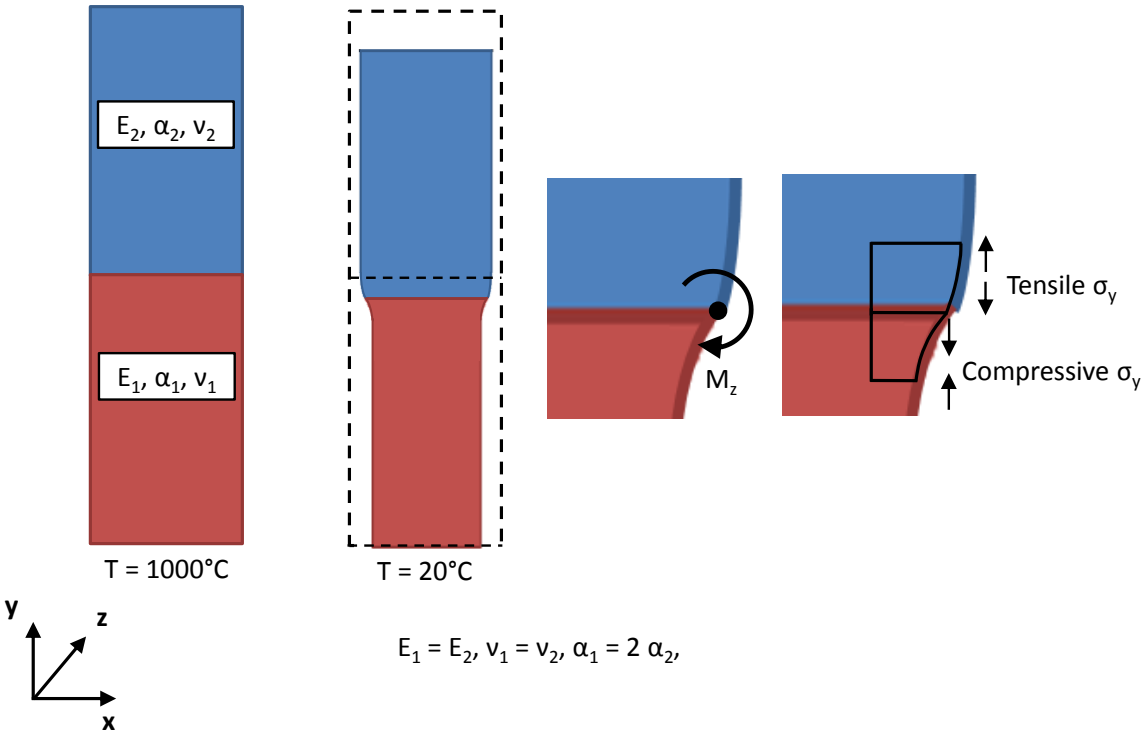

Figure 3-1 – Deformed shape of both materials at interface

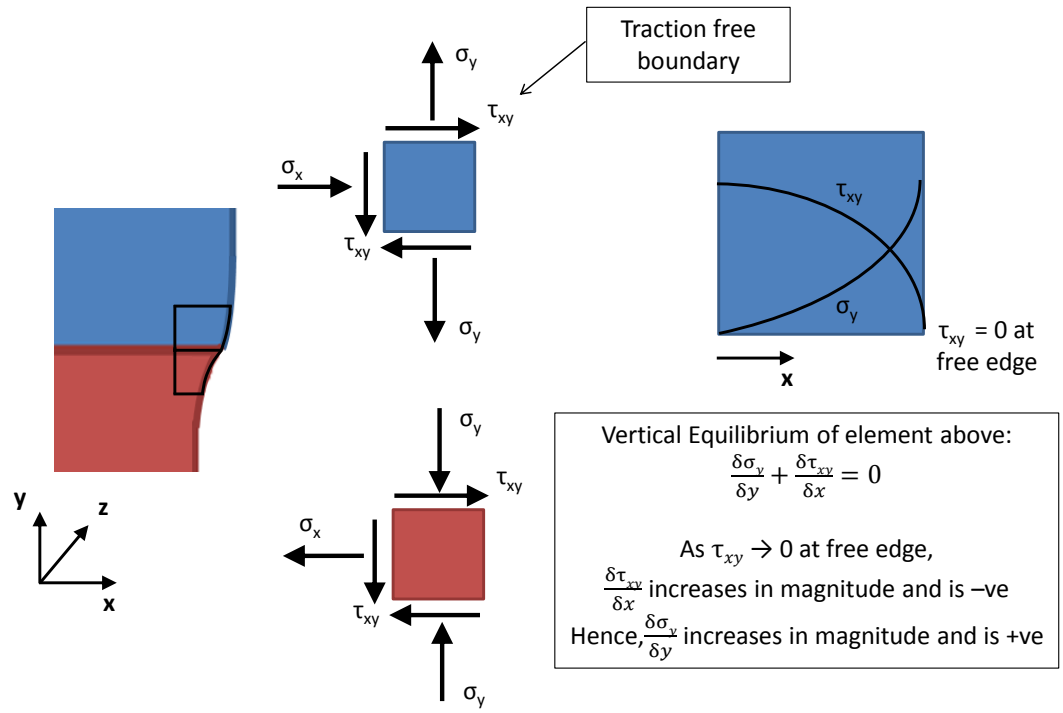

Figure 3-2 – Free body diagram of elements either side of the interface

However this is a simplification of the stresses components acting on each element. As shown in the right hand side of Figure 3-2, due to the presence of a stress free boundary at the free edge, the τ_{xy} (and σ_x) stress component tends to zero through the thickness of the elements. To maintain vertical equilibrium, the interlaminar normal stress σ_y increases to a maximum at the free edge of the component as described in the theory of composite laminates [82]–[84].

The constraint on free expansion can also be used to describe the stress field surrounding the interface under an isothermal uniaxial mechanical load when the materials have equal Poisson's ratios but different Young's modulus. Again it may be stating the obvious, but it is worth noting that under a uniaxial applied mechanical load, if the Young's modulus and Poisson's ratios are identical then there will be no stresses developed in the joint due to the constraint of the interface i.e. it is a homogenous material. However, in the case where there is a difference in Young's modulus e.g $E_1 = 2 \times E_2$, $\nu_1 = \nu_2$, for a given externally applied remote stress perpendicular to the interface σ_∞, ε_y in material 1 will be half of ε_y in material 2 remote from the interface due to the difference in the Young's modulus. In the case where the Poisson's ratios are equal, ε_x in material 1 will be half ε_x in material 2. This case is now analogous to the case described above and the same argument for development of internal stresses holds. Hence, in this case minimising the difference in stiffness will reduce the constraint on expansion and reduce the geometrical stress concentration due to the interface.

3.3 Theory describing the stress field in a simple butt joint between dissimilar elastic materials

As mentioned in section 1.6.2, analytical singularities can exist in finite element models at the free edge of the joint interface, their strength being a function of the degree of dissimilarity between the material properties and any geometric discontinuity that may exist. The existence of these singularities has been the subject of previous research and this section aims to summarize the theory developed to describe the stress field in a simple butt joint between dissimilar elastic materials. Consider the 90° butt joint geometry in Figure 3-3, assuming the materials have been joined such that a layer of varying material properties between both materials does not exist and both materials have linear elastic material properties, the free edge stress field near at the interface can be described as [86]:

$$\sigma_{ij}(r,\theta) = \frac{K}{\left(\frac{r}{L}\right)^{\omega}} f_{ij}(\theta) + \sigma_{ij0}(\theta)$$ ***Equation 3-1***

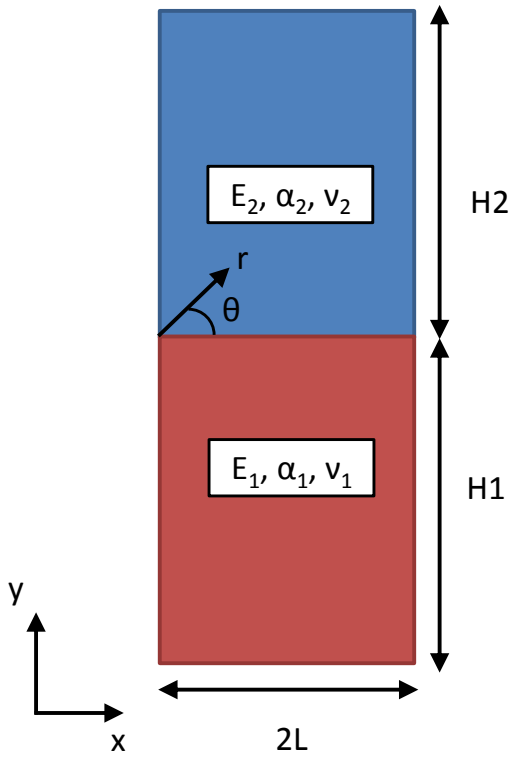

Figure 3-3 - Simple butt joint between dissimilar elastic materials

where r and θ are polar coordinates having their origin at the material interface and L is the characteristic length as per Figure 3-3. In reality it is likely that a thin layer with varying material properties will exist at the joint as shown in the previous chapter, hence 2 interfaces will occur in reality. The parameters ω and σ_{ij0} are solely dependent on the properties of the materials being joined whilst K and σ_{ij0} are dependent on both the material properties and loading type. A brief description of each of these terms and their significance is given below.

3.3.1 The Stress Singularity Exponent, ω

The stress singularity ω exponent, is dependent on the Dundurs [87] parameters (α, β), which in turn are dependent on the elastic properties (Young's moduli E_1 and E_2, and Poisson's ratios ν_1 and ν_2) of both materials, and the angles of the joined material [88]. The

singularity exponent is not dependent on the coefficients of thermal expansion (CTEs) of both materials and is independent of joint dimensions H and L in figure 1 for a 90° butt joint. For a 90° butt joint, according to Bogy [89], [90], the stress singularity parameter, ω, can be obtained by solving the following equation:

$$\lambda^2(\lambda^2-1)\alpha^2 + 2\lambda^2\left[sin^2\left(\frac{\pi\lambda}{2}\right) - \lambda^2\right]\alpha\beta + [sin^2\left(\frac{\pi\lambda}{2}\right) - \lambda^2]^2\beta^2 + sin^2\left(\frac{\pi\lambda}{2}\right)cos^2\left(\frac{\pi\lambda}{2}\right) = 0 \qquad \textit{Equation 3-2}$$

And

$$\lambda = 1 - \omega \qquad \textit{Equation 3-3}$$

Where the Dundurs parameters α, β are given by [91]:

$$\alpha = \frac{m_2 - km_1}{m_2 + km_1} \qquad \textit{Equation 3-4}$$

$$\beta = \frac{(m_2 - 2) - k(m_1 - 2)}{m_2 + km_1} \qquad \textit{Equation 3-5}$$

Where

$$k = \frac{\mu_2}{\mu_1} \qquad \textit{Equation 3-6}$$

$$m_i = \frac{4}{1 + \upsilon_i} \quad \text{for plane stress} \qquad \textit{Equation 3-7}$$

$$m_i = 4(1 - 4\upsilon_i) \quad \text{for plane strain} \qquad \textit{Equation 3-8}$$

where ν_i is the Poisons ratio of material i. μ is the shear modulus related to Young's modulus E and Poisson's ratio ν by:

$$\mu = \frac{E}{2(1+\upsilon)} \qquad \textit{Equation 3-9}$$

For the majority of realistic material combinations [88], ω is positive therefore a stress singularity exists and the theoretical stress at the interface is infinite. When $\nu_1 = \nu_2$, the stress singularity exponent increases with increasing difference in moduli [86]. Therefore for any change in stiffness the theoretical elastic stress at the interface is infinite under an infinitesimally small mechanical or thermal load in both materials. As well as there being a metric for the strength of singularity that exists between two linear elastic dissimilar materials, it has also been shown [91], [92] that the sign of the singular stress at interface can be either negative or positive. A figure describing the sign of the singular stress field has been published by You [92], however this only holds for cooling from an assumed stress free temperature. This is useful for establishing the sign of the residual singular stress fields due to manufacturing. This diagram can also be modified for bulk heating assuming both materials are initially at room temperature [91]. Figure 3-4 shows the original diagram for cooling from an assumed stress free state, Figure 3-5 for heating.

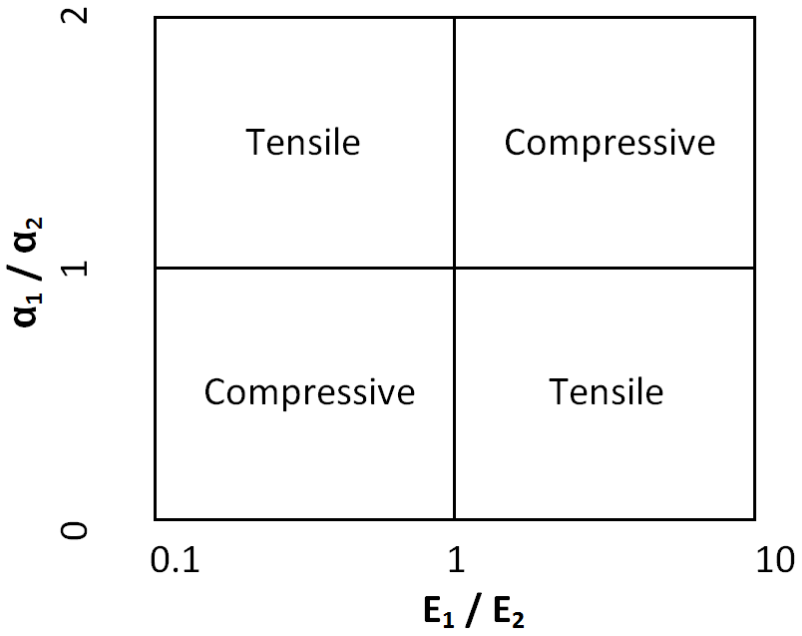

Figure 3-4 - Sign of singular stress field due to bulk cooling

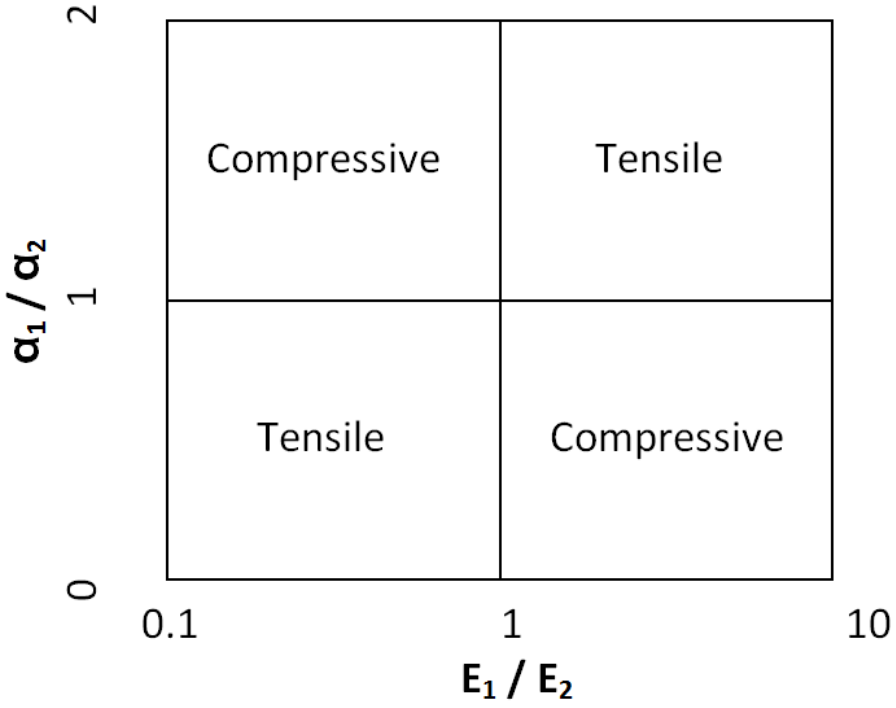

Figure 3-5 - Sign of singular stress field due to bulk heating

3.3.2 The Stress Intensity Factor, K

K is defined as the stress intensity factor, but is different to the stress intensity factor used in fracture mechanics as it has units of stress [91]. It is dependent on the elastic properties of the materials, the loading scenario (either thermal or mechanical loading) and shape of the joint, however is independent of joint dimensions [86]. As pointed out by You [92], the stress intensity is a single scalar value and is a common parameter for all stress components in the singular stress field of a perfectly bonded interface.

For certain ratios of L/H, the stress intensity factor can be determined analytically. In all other cases FEA is required. It has been shown [86] that for H1/L ≥ 2 and H2/L ≥ 2, the stress intensity factor is given as:

$$-\frac{K}{\sigma_\infty} = 1 - 2.89\omega + 11.4\omega^2 - 51.9\omega^3 + 135.7\omega^4 - 135.8\omega^5 \qquad \textit{Equation 3-10}$$

where σ_∞ is an externally applied tensile load perpendicular to the interface. For thermal loading this relationship still holds, however σ_∞ in Equation 3-10 must be replaced with σ_0

in Equation 3-13. For all the cases in this paper, the geometry investigated has H1/L ≥ 2 and H2/L ≥ 2 hence the stress intensity factor can be determined using Equation 3-10.

In order to determine K using FEA, $\sigma_{ij}(r,\theta)$ must be obtained from FEA. The following equation can then be plotted:

$$log\left[\frac{\sigma_{ij}(r,\theta)-\sigma_{ij0}(\theta)}{f_{ij}(\theta)}\right]=-\omega.log\left(\frac{r}{L}\right)+logK \qquad \textbf{Equation 3-11}$$

Which is the equation of a straight line of a slope with gradient m = –ω, and the y intercept c = logK. In this case, both ω and K can be compared to the analytical models to ensure the results agree. In addition plotting Equation 3-11 will allow the zone of influence of the singularity to be determined. When Equation 3-11 has a negative gradient, the stress distribution is behaving in a singular fashion, however a certain distance away from the interface, the singularity will not have an effect and Equation 3-11 will no longer have a negative gradient.

3.3.3 The Angular Function, $f_{ij}(\theta)$

The formulas for the angular functions are omitted in this paper due to their complexity, however they can be found in ref [91]. It is worth noting that the angular function is only dependent on the angle of the joint, Young's modulus and Poisson's ratio. It is not a function of CTE and is not singular.

3.3.4 The Constant Stress Term, σ_{ij0}

The constant stress term, σ_{ij0}, is given by:

$$\sigma_{r0}=\frac{\sigma_0}{2}(1-\cos 2\theta) \qquad \textbf{Equation 3-12 a}$$

$$\sigma_{\theta 0}=\frac{\sigma_0}{2}(1+\cos 2\theta) \qquad \textbf{Equation 3 12 b}$$

$$\tau_{r\theta 0}=\frac{\sigma_0}{2}(1+\cos 2\theta) \qquad \textbf{Equation 3 12 c}$$

Where

$$\sigma_0 = \Delta\alpha . \Delta E^* . \Delta T \qquad \textit{Equation 3-13}$$

And

$$\Delta\alpha = \alpha_1(1+\upsilon_1) - \alpha_2(1+\upsilon_2) \qquad \textit{Equation 3-14}$$

$$\Delta E^* = \left[\frac{1}{E_1^*} - \frac{1}{E_2^*}\right]^{-1} \qquad \textit{Equation 3-15}$$

And

$$E_i^* = \frac{E_i}{\upsilon_i} \quad \text{for plane stress} \qquad \textit{Equation 3-16}$$

$$E_i^* = \frac{E_i}{\upsilon_i(1+\upsilon_i)} \quad for\ plane\ strain \qquad \textit{Equation 3-17}$$

The constant stress term for mechanical loading is zero [86] but is very important for thermal only loading as it is this term which accounts for differences in CTE and is finite.

3.4 The stress state in an elastic dissimilar material joint as predicted by FEA

3.4.1 Key features of dissimilar material joint stress field

As discussed in chapter 2, to fully capture the stress state in a real dissimilar material brazed joint, the brazed layer and joining process must be accounted for [49]. However a simple joint approximation with an abrupt interface between two dissimilar materials can still be informative. In this cases it has been used to gain an understanding of the key features of the stress field in the region of a dissimilar material interface and the relationships in material properties driving the development of large stresses and hence failure in the joint.

In addition to the theory described in the previous section, the stress state at the interface of an abrupt change in material properties using FEA has been the topic of much previous research [88], [91], [92]; however it is pertinent to understand the key features of the stress state that will form of the basis of future discussion. As explained section in 3.2, due to

differences in thermal expansion coefficient, Young's modulus and Poisson's ratio, large stresses can develop in dissimilar material joints under thermal and mechanical loading particularly along any free edge in the region of the interface. To highlight the key features of the stress field, results from a simple plane stress FEA model between two dissimilar elastic materials with an abrupt interface have been used.

A plane stress FEA model of a 90° dissimilar material butt joint has been created in ANSYS 12.1 and is shown schematically in Figure 3-6. The entire geometry is prescribed an initial temperature of 500°C and a final temperature of 0°C. It is assumed the temperature distribution varies uniformly from 500°C to 0°C hence any variation in temperature throughout the specimen is neglected. The dimensions of the joint arbitrarily chosen to be L = 25mm and H_1=H_2=100mm with symmetry boundary conditions applied along the centre of the joint. A displacement constraint along the bottom surface is also applied as shown in Figure 3-6. The model has been meshed using plane stress PLANE42 4 noded quadrilateral elements. To fully capture the singular stress field a highly refined mesh has been used. In this instance an element size of 0.25mm has been used which corresponds to 100 elements through the thickness of the model and 400 elements vertically. The material properties have been arbitrarily chosen and are summarised in Figure 3-6 with both materials assumed to be perfectly elastic. The free edge stress distribution from the elastic FEA is shown in Figure 3-7.

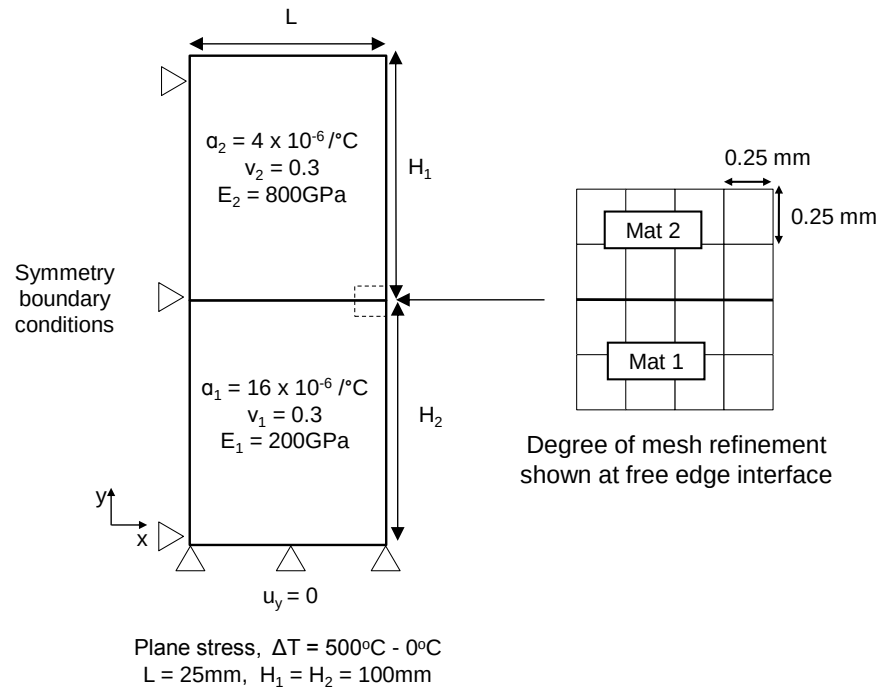

Figure 3-6 – Model schematic and mesh at free edge.

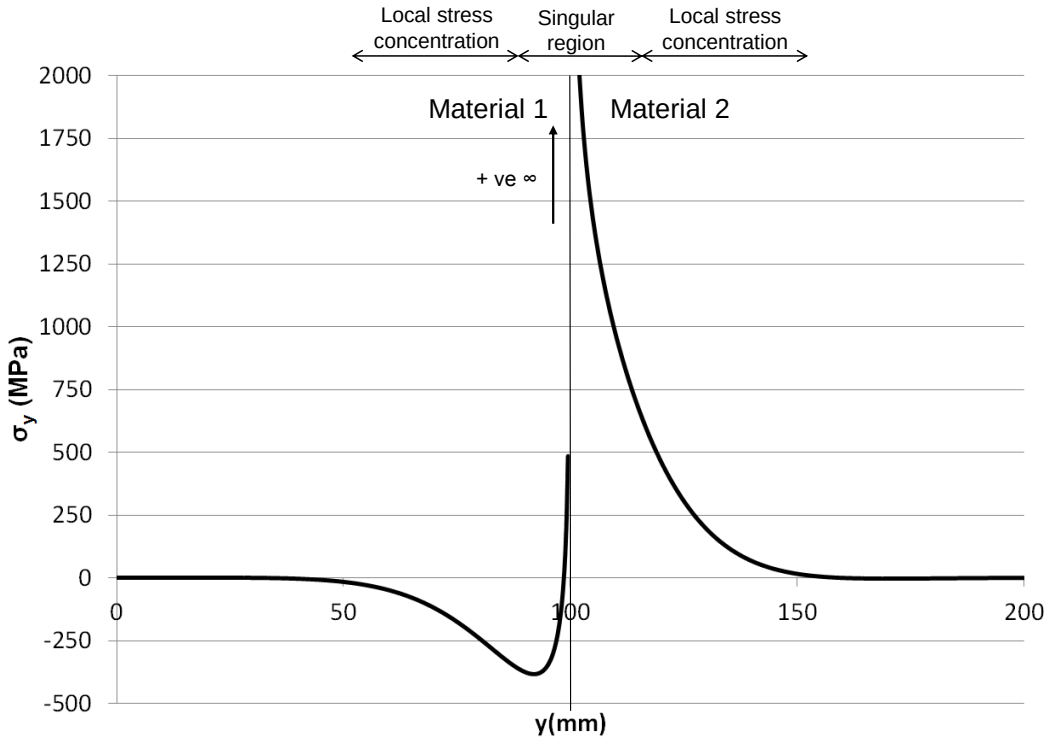

Figure 3-7 - Free edge stress perpendicular to the interface in a simple dissimilar material joint during cooling

Firstly, due to this particular relationship of elastic properties (E_1, E_2, v_1, v_2) an analytical singularity exists at the interface, hence as the interface is approached the stresses in both materials tend, in this instance, to positive infinity along the free edge is as to be expected from Figure 3-4.

However, the singularity only has an effect in the proximity of the interface. Outwith this region there is what can be a termed a local stress concentration, i.e the stress concentration due to the interface that is not influenced by the singularity. This can be illustrated in the context of the stress distribution in material 2 in Figure 3-7. Remote form the interface there is a region of compressive stress along the free edge (c. y = 50mm to y = 90mm), however as the interface is approached this stress distribution begins to tend to positive infinity as the singularity at the interface begins to dominate the stress distribution.

The trends in local stress concentration can be explained using the constraint mechanism developed in Section 3.2. In the example used in Figure 3-7, the deformed shape and hence the forces acting on the elements either side of the interface are as described in Figure 3-1. Hence the moment (M_z) due to the compatibility constraint results in material 1 having a compressive local stress concentration with material 2 having a tensile local stress concentration.

3.4.2 Zone of influence of singularity

To determine the zone of influence of the singularity Equation 3-11 is plotted for the free edge results shown in Figure 3-7, the results from this shown in Figure 3-8. In order to do this the theoretical parameters described in the Equation 3-11 must be calculated. These are summarised in the following table, based on the theory presented in section 3.3. As H1/L = H2/L = 100/25 = 4 the stress intensity factor for thermal loading can be estimated using Equation 3-10.

Parameter	Value
Dundurs parameter, α	0.6
Dundurs parameter, β	0.21
Stress singularity exponent, ω	0.085
Angular function, f_r (θ = 90)	1.369
Angular function, f_r (θ = -90)	0.956
Stress intensity factor, K (MPa)	4326
The Constant Stress Term, σ_{r0}	-5330

Table 3-1 – Theoretical parameters

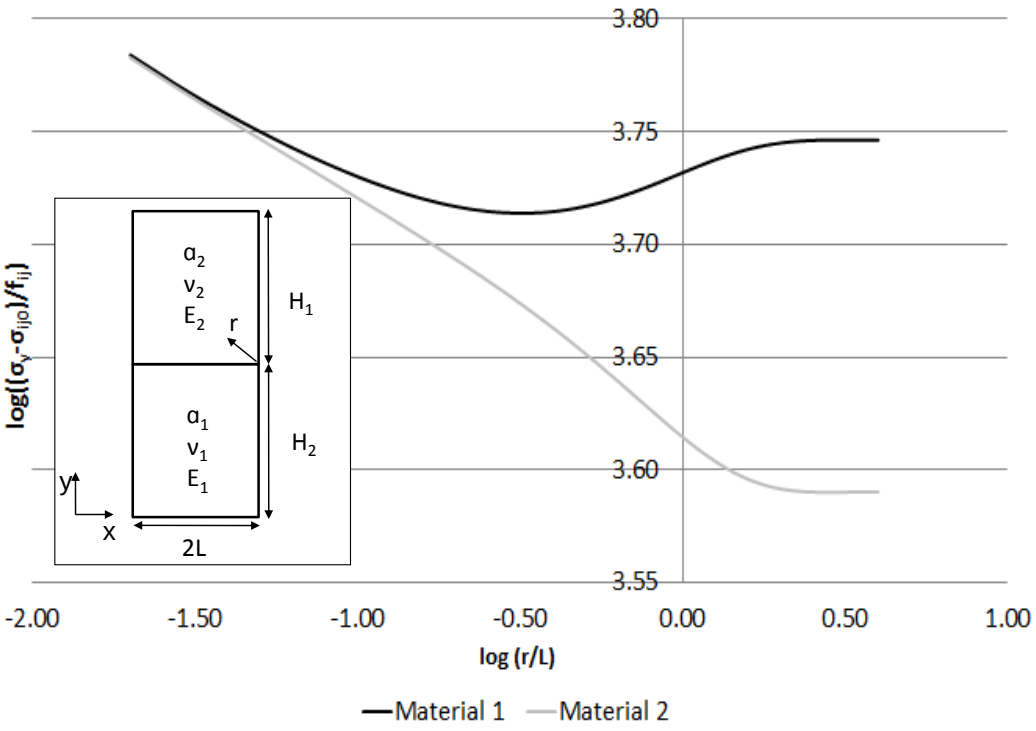

Figure 3-8 – Equation 3-11 plotted along free edge

When the stress along the free edge is behaving in a singular fashion, i.e. σ_y varies with $(r/L)^{-\omega}$, the graph of Equation 3-11 should have a negative gradient. When the gradient is not negative (i.e 0 or +ve) there results are not behaving in a singular fashion. For material 1 which occurs at a log(r/L) of approximately -0.5 and in material 2 this occurs at log(r/L) of + 0.45. The initial gradient of both of these lines is equal to the stress singularity exponent (not shown in Figure 3-8).

3.4.3 The effect of properties on singularity strength and local stress concentration

To investigate the effect of material properties on the strength of singularity and local stress concentration due to the interface a series of cases have been analysed using both linear elastic dissimilar material joint theory and the. The FEA model setup, geometry and mesh are identical to the FEA model used in Section 3.4.1, the only difference being the properties of both materials. The cases analysed are summarised in Table 3-2 for cooling from an assumed stress free temperature of 500°C, with the free edge stress perpendicular to the interface distributions as predicted by FEA are shown in Figure 3-9. These relationships in material properties may not necessarily be representative of real material property combinations but are still informative in terms of understating the mechanics of at the joint.

Case No	E_1 (GPa)	E_2 (GPa)	ν_1	ν_2	α_1 ($x10^{-6}$)	α_2 ($x10^{-6}$)	ω	σ_{r0} (MPa)	K (MPa)
1	400	100	0.3	0.3	4	16	0.085	-2667	2163
2	400	100	0.3	0.3	4	8	0.085	-889	721
3	200	100	0.3	0.3	4	16	5.413×10^{-7}	-4000	4000

Table 3-2 – Summary of cases analysed and theoretical parameters

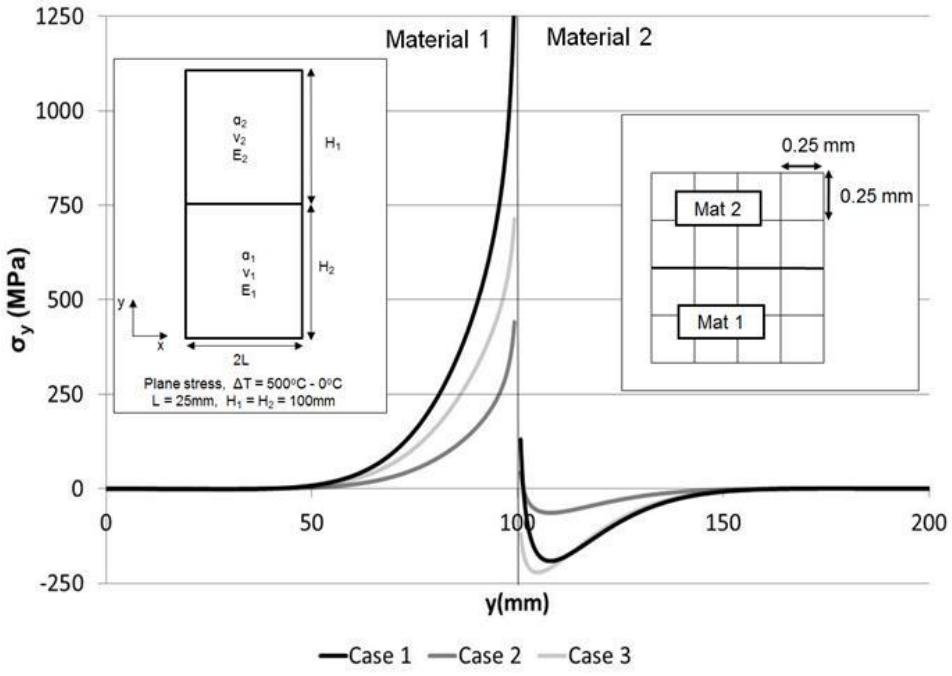

Figure 3-9 - Free edge stress distributions for cases summarised in Table 3-2.

The strength of the stress singularity exponent, ω, is dependent solely on the geometry of the joint, the Young's modulus and Poisson's ratio of the joined materials. It is independent of the coefficients of thermal expansion of the joined materials. When the Poisson's ratio of the materials joined are similar, the stress singularity exponent increases with increasing difference in effective moduli as described in [86]. Based on the relationships in material properties, in each of the cases in Table 3-2 ($E_1/E_2>1$, $\alpha_1/\alpha_2<1$) a tensile singularity would be expected which is clearly shown in Figure 3-9.

In cases 1 and 2, the difference in Young's modulus of both materials is constant (hence singularity strength is the same), however there is greater difference in coefficient of thermal expansion in case 1. This results in a larger constraint due to the compatibility constraint and hence larger a local stress concentration away from the interface e.g. at y =80mm and 120mm).

In cases 1 and 3, the coefficients of thermal expansion are the same, however material 1 has a lower stiffness in case 3 than in case 1. In this case the singularity strengths are different; however the thermal strains due to heating will be the same. In material 2, outside the zone of the singularity, the stress perpendicular to the interface due to the constraint mechanism is similar in both cases as material 2 has constant Young's modulus (e.g at y = 120mm). However in material 1, the Young's modulus is larger in case 1, hence the degree of constraint and hence local stress concentration is larger (e.g. at y = 120mm).

This simple example, as well as giving an insight into the elastic stress state, shows that local stress concentration effects can be fully explained using the constraint mechanism described in section 3.2. In addition to these large tensile stresses perpendicular to the interface along the free edge there are other significant stress components, however the largest stress component is perpendicular to the free edge.

3.4.4 Mechanical vs. thermally induced stress fields

The stress state in dissimilar material joints under a mechanical only load has the same characteristics in terms of a local stress concentration and a singularity as under thermal load. Figure 3-10 shows the free edge stress distribution case 1 with a uniaxial applied tensile stress of σ_∞ = 200MPa applied at room temperature ignoring the effects of cooling from a stress free temperature.

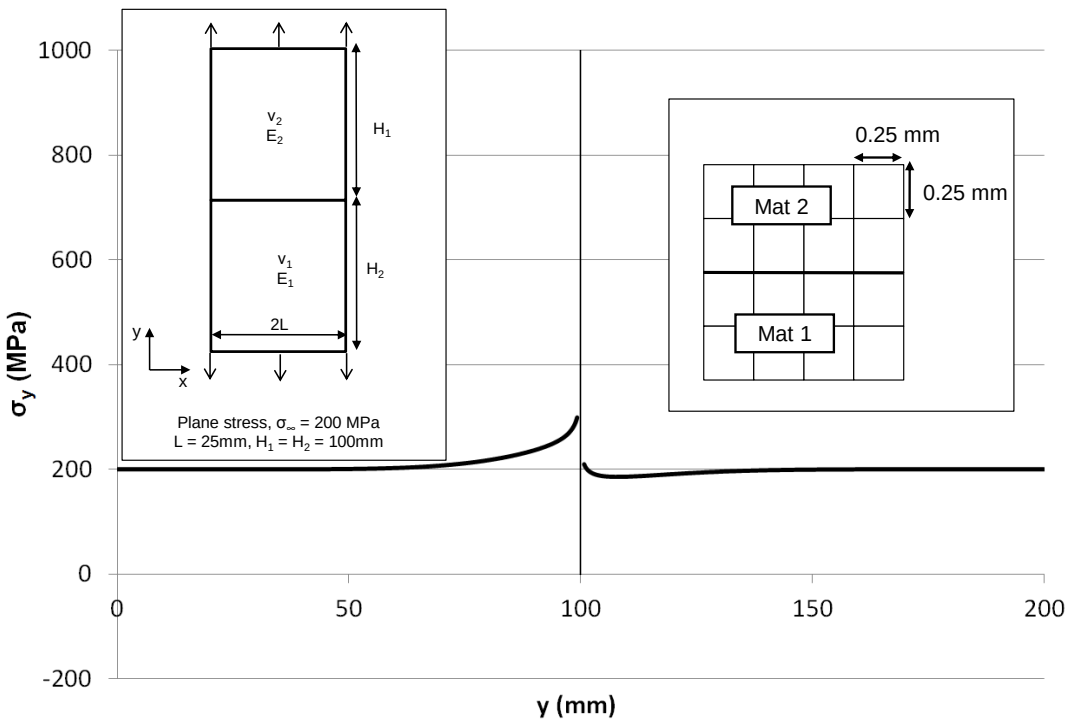

Figure 3-10 – Free edge stress perpendicular to the interface for case 1 under mechanical loading

In the case of mechanical loading, away from the interface the stress is equal to the externally applied field stress, however as the interface is approached the presence of the local stress concentration and the analytical singularity is visible. In this particular case the local stress concentration is caused by a similar mechanism to that in the thermal loading case, i.e. it results from the constraint at the interface due to compatibility requirements and a difference in strain parallel to the interface. As material 2 is less stiff than material 1, under a uniaxial applied load σ_∞ , ε_y will be greater in material 2 and hence ε_x will be greater in material 2 as the Poisson's ratios of the materials are equal and it is this which induces the constraint. The effect of this on the local stress concentration causes a reduction about the uniaxial applied stress in material 2, and an increase in material 1. Adjacent to the interface the singularity is causing the stress to tend to positive infinity.

3.5 Effect of plasticity on mechanics of dissimilar material joints

3.5.1 Do elastic singularities exist in real dissimilar material joints?

Elastic stress singularities exist in a range of problems such as point loads, point constraints, internal re-entrant corners and abrupt changes in material properties. The presence of these analytical singularities as predicted by linear elastic theory leads to the question of whether they actually exist in real dissimilar material joints. As mentioned in the previous section for the majority of dissimilar joints between real materials, the relationship in material properties will result in a theoretical singularity at the interface. Therefore in such joints the stresses at the interface are theoretically infinite under an infinitesimally small mechanical or thermal load which should result in failure of such joints. This however, is obviously not the case as satisfactory dissimilar material joints with free edges (including ceramic – metal joints) can be found in a number of applications. Therefore in reality, the theoretical infinite stresses predicted by the elastic theory do not exist and the reasons for this are discussed in this section.

Firstly, the linear elastic theory described in the previous chapter assumes a step change in material properties. In reality, as shown in the previous chapter, this step change will never occur and there will be some form of grading across a transition region of finite width due to the process of diffusion, albeit over an extremely small scale. In the case of dissimilar material brazed joints, this will occur due to a gradual transition region containing elements of the filler. Therefore there is never a true step change in material properties i.e. it is not simply a case of one molecular structure starting and the other finishing abruptly. Therefore the theoretical singular stresses predicted by the theory and linear elastic FEA will never exist in reality. However the length scale over which this transition happens is extremely small, and even though the stresses will not be infinite due do this change, it is postulated that they will be extremely high compared to any material limit.

The second reason dissimilar material joints do not fail under an infinitesimally small load is that the theoretical infinite stresses predicted by the elastic theory do not exist at the interface of a dissimilar material joint. This is due to plasticity effects in real materials i.e yielding limits the stress magnitudes in the materials being joined. This plasticity mechanism even holds true when the joined materials are brittle in nature. In this case the reason singular stresses do not occur is analogous to the Linear Elastic Fracture Mechanics

(LEFM) explanation which describes why sharp cracks in brittle materials do not fail under an infinitesimally small applied load, only if the applied load is raised to a critical value. In LEFM it is reasoned that inelastic deformations in real materials, even those that fail in a brittle manner, make the assumption of linear elastic behaviour in the region of the crack tip highly unrealistic [93]. This was verified by a series of studies performed by Orowan [94] who, using x-rays proved the presence of extensive plastic deformation on cracked surfaces of samples which failed in a brittle manner. Hence, due to plasticity effects in real materials, even those that are known to fail in a brittle manner, the theoretical infinite stresses are predicted by elastic theory in a dissimilar material joint are limited by plastic deformation. The presence of dislocations due to plasticity at the interface of Si_3N_4 ceramic to Si_3N_4 ceramic joints brazed with Cu based filler has been proven experimentally using a TEM by Singh [95] and a significant amount of theoretical work has been done to predict the size of the plastic zone theoretically. In addition to plasticity effects blunting the theoretical singularity, inelastic behaviour due to creep will also affect joint mechanics.

3.5.2 Effect of plasticity on mechanics of dissimilar material joints

In the previous section it has been argued that the effect of plasticity, even in materials that are known to fail in a brittle manner, is one of the major reasons that the theoretical infinitely high stresses predicted by the elastic theory do not exist at a dissimilar material joint interface. This poses the question of how plasticity in a real material is likely to influence the mechanics of the joint. This section aims to illustrate what happens to the stress state in a brittle material when it is joined to a ductile elastic plastic material based on the constraint mechanism developed in section 3.2. For this, an additional set of cases have been analysed. These have been performed on an axisymmetric joint model with similar elastic properties to case 1 in section 3.4.3. An axisymmetric joint model has been used instead of a plane stress model as yielding is governed by all 3 principal stress components.

For these cases the joint has been cooled from an assumed stress free temperature of 1000°C to represent a manufacturing process such as brazing or diffusion bonding. In each of these cases material 2 has a bilinear kinematic hardening plasticity law with a yield stress of 200MPa and a varying tangent modulus as per Table 3-3. The tangent modulus varies from the elastic case to elastic–perfectly plastic. Figure 3-11 shows the free edge σ_y stress distributions for each of these cases.

Case No	E_1 (GPa)	E_2 (GPa)	ν_1	ν_2	α_1 (/°C)	α_2 (/°C)	σ_{yield2} (MPa)	E_{tan2} (GPa)
4a	400	100	0.3	0.3	4×10^{-6}	16×10^{-6}	∞	N/A
4b	400	100	0.3	0.3	4×10^{-6}	16×10^{-6}	200	50
4c	400	100	0.3	0.3	4×10^{-6}	16×10^{-6}	200	10
4d	400	100	0.3	0.3	4×10^{-6}	16×10^{-6}	200	0.01

Table 3-3 – Summary of cases analysed with plasticity

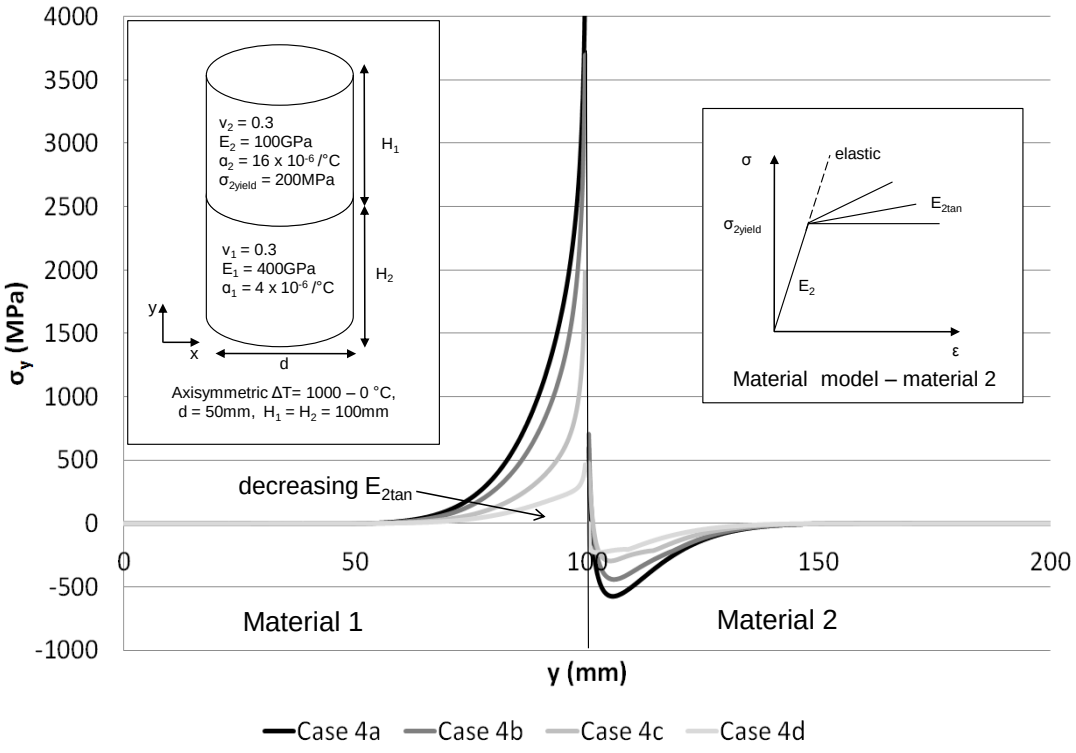

Figure 3-11 - Free edge stress perpendicular to the interface for cases 4a – 4d

Results from cases 4a-4d show that as the tangent modulus of elastic-plastic material 2 decreases, the stress in the brittle material in the region of the joint decreases. From a practical perspective this makes sense and can be explained by a reduction of the constraint due to lack of stiffness at the interface as per the mechanism described in section 3.2.

Based on this finding it should be noted that when analysing dissimilar material joints, assuming an elastic–perfectly plastic material model is non-conservative. This is because it fails to account for the strain hardening of the material after yield and the additional

constraint that this strain hardening induces. In a real material, the material will strain harden after yield and will never have a zero stiffness as assumed by an elastic-perfectly plastic material model.

To illustrate this plasticity protection further, the results from previous research on joining of ceramic to stainless steels can be explained in relation to these findings. The experimental results presented in [30] are based on a series of fabricated joints between a common ceramic and different grades of a stainless steel produced using a constant brazing process (filler and brazing process the same). One of the key findings was that a steel with a lower yield stress but higher difference in coefficient of thermal expansion was less likely to fail during joining than with a steel with the opposite trend in material properties. From an elastic perspective the higher difference in thermal expansion will increase the constraint on the ceramic at the interface and hence result in higher stresses in the region of the interface. However, the lower yield stress is obviously alleviating these higher elastic stresses and protecting the brittle ceramic by reducing the constraint at the interface.

The axial stress distributions in Figure 3-11 has consequences on the accuracy of an elastic analysis of dissimilar material joints and is best described in the context of the elastic stress distribution at a crack tip. LEFM is based on the notion that the energy from the elastic stresses out with the plastic zone that are driving failure [93] [96] and hence the stress distribution in the bulk of the medium will not differ from the purely elastic solution to any significant extent at a certain distance from the plastic zone (approximately three times the radius of the plastic zone) as shown in Figure 3-12. However, in an elastic analysis of a dissimilar material joint, the results in Figure 3-11 suggests that the elastic stress distributions vary significantly compared to the cases where plasticity is modelled. This can be attributed to the local stress concentration effect due to the constraint of the interface. This local stress concentration is not present in LEFM. Consequently if accurate stress distributions for dissimilar material joints are to be obtained, a plastic analysis should be performed. However, it should be noted, that this does not necessarily preclude the calibration of failure assessment procedures (such as hot-spot stress techniques) using the elastic stress distributions from an elastic analysis.

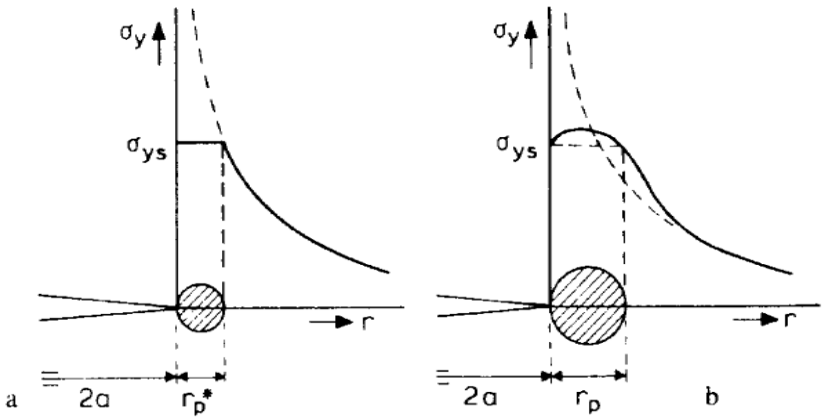

a. Assumed stress distribution; b. Approximate stress distribution

Figure 3-12 – Elastic and plastic stress distribution at crack tip [96]

3.6 Other mechanics considerations

3.6.1 Effect of thin brazed layer on dissimilar material joint mechanics

As highlighted in chapter 2, when two dissimilar materials are joined by brazing, a thin braze layer exists at the joint between the two materials as discussed. Given the constraint mechanism explained in section 3.2, it follows logic that the mechanical properties of this thin brazed layer will play a key role in the mechanics of the joint. If for example the braze filler was extremely stiff relative to the parent materials, the degree of constraint at the free edge, hence residual stresses due to joining will be large. If however the stiffness of the material was relatively very low there would be very little constraint on the materials being joined. It is therefore important to model the brazed layer if the stress state in the joint is to be accurately captured. The practice of neglecting the braze layer is effectively assuming that the braze layer and diffusion regions have exactly the same properties (mechanical and thermal) as one of the materials being brazed and will result in an over constrained model with artificially high residual stresses in the region of the joint.

Previous experimental and analytical research has shown that the key braze layer material property driving the development of high residual stresses are the yield and plasticity properties of the filler [56], [68], [97]. This is in agreement with the findings from the previous section which showed as the material properties of one material tend to elastic-perfectly plastic, the constraint at the interface due to differential thermal expansion is reduced. It follows logic that if the braze layer had zero stiffness; the residual stresses due

to joining would be zero and the stress state under a subsequent thermal load would also be zero. Hence the ideal filler from a mechanics perspective for a dissimilar material joint subjected to a purely thermal loading is zero stiffness braze filler.

Nevertheless, the stress state at the free edge of dissimilar material joint with an interlayer is dependent on both the thickness of the interlayer and the material properties of all three materials, not solely on the relationship in properties between the interlayer and the parent materials. This is highlighted in the example shown in Figure 3-13 where a dissimilar material joint with an interlayer is being joined at 800°C (in the case of a brazed joint this interlayer would be the brazing filler). In this case the interlayer (material 2) has a greater coefficient of thermal expansion than both parent materials, however material 1 as a coefficient of thermal expansion greater than material 3. During cooling to room temperature the interlayer has the greatest contraction, followed by material 1 then 3 (as highlighted in image (b) without compatibility being enforced at each interface). Based on the constraint mechanism in 3.2, both materials 1 and 3 should develop compressive axial stresses due to this joining process if it was solely the relationship in properties between the interlayer and each parent material driving the stress distribution at the free edge.

However, the final deformed shape will be a function of the stiffnesses of all 3 materials as well as the thickness of the interlayer. In this particular case, if interlayer material has sufficient stiffness (k_2) and material 3 has a much greater stiffness (k_3) (which is likely as it has a much lower coefficient of thermal expansion) the constraint on the interlayer due the large stiffness of material 3 will affect the deformed shape at the interface between the interlayer and material 1. Reducing the thickness of material 2 will also increase this effect. This could result in material 1 developing a tensile axial stress instead of a compressive axial stress which would be expected from the deformed shape between materials 1 and 2 if material 3 was neglected.

Therefore, from a practical perspective, the final stress state in the joint is a function of the relationship in properties of all three materials and not just the interlayer and the parent materials. This is especially true for brazed joints where the thickness of the interlayer that exists is relatively small (c.100μm). In addition to this simple mechanism, the elastic singularity theory described in section 3.3 also predicts the stress state at the free edge of dissimilar material joint with an interlayer is dependent on the properties of all three materials present in the joint and not solely on the relationship between the interlayer and

the parent materials [98]. Hence to accurately capture the stress state in real dissimilar material brazed joint using FEA, temperature dependent material properties of both the parent materials and the braze filler need to be included in the model.

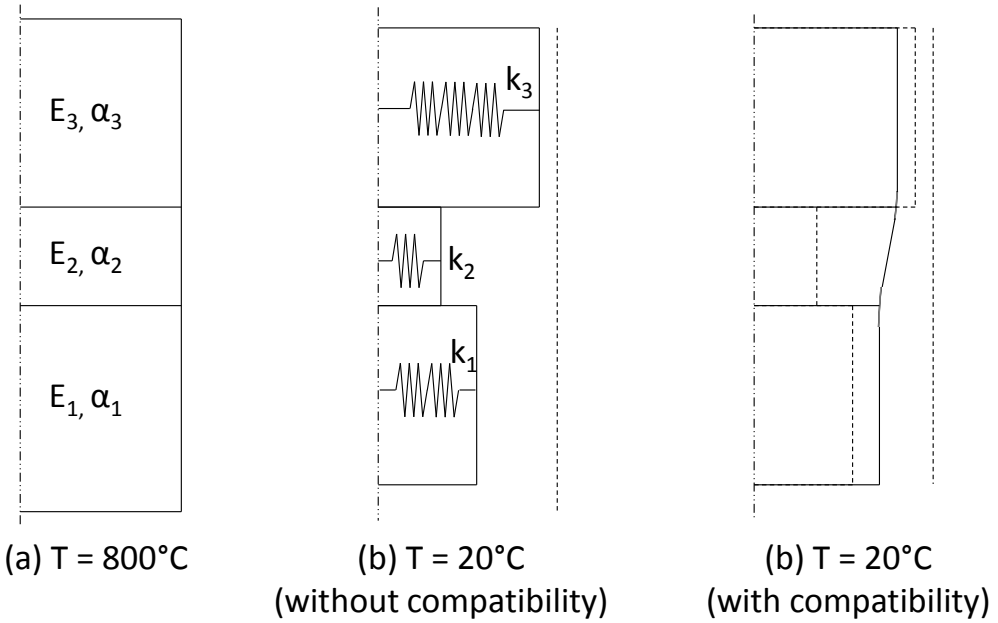

$$E_2 < E_1 < E_3 \quad , \quad \alpha_3 < \alpha_1 < \alpha_2$$

Figure 3-13 –Effect of interlayer on final deformed shape

3.6.2 Effect of joint geometry

In terms of dissimilar material joint design, the functional requirements of a structure dictate that certain material combinations are required to be joined, therefore, material selection is often a design variable which is outwith the control of the designer however this may not be the case with brazing filler material. In such instances joint geometry is a variable that can be used to improve the mechanics of the joint. Whilst a full investigation into how the geometry influences the mechanics of a dissimilar material joint is outwith the scope of this thesis, the key findings from previous research in relation to this are summarised. In addition to joint geometry, ductile interlayers and functionally graded materials have been developed to reduce the effect of a step change in properties by gradually transitioning between the two parent materials [99]–[101] .

From a theoretical perspective, Kelly [88] has shown that for material properties which give rise to singularities in 90° butt joints, analytical singularities can be removed through the use of a scarf joint as shown in left hand side of Figure 3-14. This has been investigated experimentally by Blackwell et al [33] who showed that for a series of dissimilar Cu to molybdenum brazed joints the strength of the joint increased with an increasing degree of joint edge angle. This was however up to a certain angle where failure of the joint was in the Cu away from the interface. After a certain angle the joint failed in the interface due to shearing effects because of the scarf joint geometry [33].

Xu et al [102] showed through both FEA and an experimental investigation that free edge stress singularities could be removed in dissimilar material joints through the use of a convex interface geometry as shown on the right hand side of Figure 3-14 . The effect of removing the free edge singularity resulted in an 81% increase in ultimate tensile strength of the joint for a polycarbonate to aluminium joint. Baladi et al have also shown that the stress concentration at interface can be reduced using a convex joint design [103].

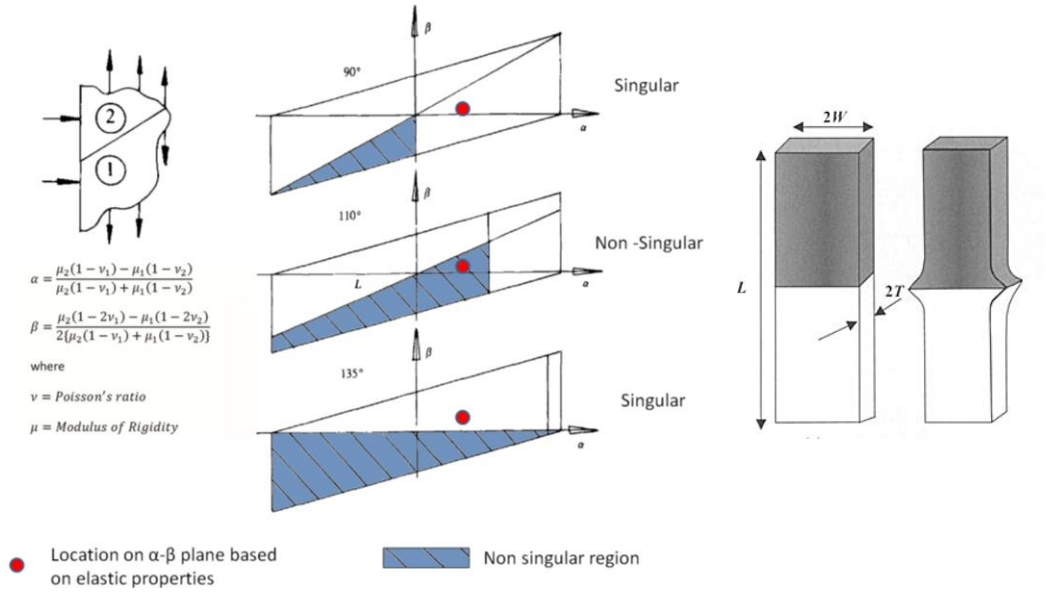

Figure 3-14 – Removing singularity through joint geometry [modified from [88], [102]]

3.7 Summary

By developing an understanding the of stress state at the abrupt interface between two dissimilar materials based on the constraint of free expansion of both materials we have shown how different relationships in material properties will affect the free edge stress distributions in the region of the joint based on the constraint due to the interface and, in most cases, the analytical singularity that exists in an elastic model. It has however been argued that such elastic singularities do not exist in practice due to the absence of an abrupt change in material properties which has been supported by the evidence presented in the metallurgical study presented in the previous chapter. It has also been argued that, in a similar fashion to linear elastic fracture mechanics, the theoretical infinite stresses predicted by the elastic theory do not exist at the interface due to plasticity effects in real materials, even those that are known to fail in a brittle manner. Furthermore, it has been shown that plasticity in one material provides a protection mechanism for the joint and limits the stresses induced in the joined material. It has also been shown in the case where an interlayer exists in a dissimilar material joint (such as a brazed layer in dissimilar material brazed joints) that the stress state at the free edge is dependent on both the size and material properties of all three materials present in the joint, not solely on the relationship between the interlayer and the parent materials.

4 Characterisation of the residual stresses in a titanium to copper brazed joint

4.1 Introduction

Due to the differences in thermal expansion coefficients and Young's modulus, high secondary discontinuity stresses can occur in the region of the joint as a result of the joining process and during operation. It has been shown in section 1.5.1 that these residual stresses can result in failure of the joint during manufacture. Clearly, these must be accounted for in any FEA model or failure assessment procedure for dissimilar material brazed joints. Consequently, the aim of this chapter is to use FEA to predict the residual stress field due to joining in the cylindrical Ti/72Ag-28Cu/Cu dissimilar material brazed joint discussed in chapter 2. The residual stresses predicted by FEA are compared with those measured using XRD.

As highlighted in section 3.6 of the previous chapter, the material properties of the braze filler will play a key role in the stress state developed in the joint, hence the thermal and mechanical properties of the 72Ag-28Cu braze filler have been measured and the brazed layer included in the FEA. Section 4.3 of this chapter summarises the material property characterization of the brazed layer. These results are then used in section 4.4 to simulate the residual stress state in the joint using FEA. Both uniform cooling and transient analyses are considered. The measurement of the residual stresses in the actual Ti/72Ag-28Cu/Cu joint is presented in section 4.5 with a comparison to those predicted by FEA. Section 4.6 summarises the findings and areas for future work in the field of predicting residual stresses due to brazing.

4.2 Brazing procedure

The parent materials and brazing filler used in this investigation are the same as those used for the metallurgical study in chapter 2. The parent materials used in this investigation were Ti grade 2 bar and OFHC Cu C110 bar. The as supplied bar of both parent materials was machined to 14mm diameter by 25mm long. The samples were brazed using 72Ag-28Cu brazing foils of 0.1mm thick. Brazing took place in a vacuum oven at 5×10^{-5} mbar and a heating rate of 10°C/min to a brazing temperature of 820°C with a dwell time of 5mins at 750°C. The samples were then allowed to cool in the vacuum furnace overnight (c.8 hours)

to a temperature of c.60°C before being removed and allowed to cool to room temperature in air. After brazing, the quality of the joints was assessed by visual inspection to confirm complete wetting and for significant defects. In addition, one sample was sectioned and inspected under a microscope. These inspections showed good and consistent wetting with no obvious large voids or inclusions as shown in section 2.3.

4.3 Material properties of the brazed filler for use in FEA

It has been shown in section 3.6 of this thesis and in previously published research [56], [58], [68], [97] that the properties of the braze filler play a key role in the development of the residual stresses generated in dissimilar material brazed joints. To characterize the material properties of the braze layer for use in FEA, a rod of 20mm diameter by 300mm length of vacuum grade 72Ag-28Cu correct to ISO 17672:2010 [104] was procured and relevant samples machined from this. In this work the material properties of the brazed layer have been characterised in the as supplied condition neglecting the diffusion of Ti into the brazed layer. Whilst chapter 2 of this thesis has shown that for this joint, due to differences in microstructure before and after brazing, the validity of this approach is questionable, it is better than ignoring its presence completely. Work is on-going to fully characterise the material properties of the brazed layer for use in FEA accounting for the changes in microstructure [60] due to the brazing process.

Both a uniform cooling thermal stress and transient thermal stress analysis of the brazing process have been considered. The starting point for each analysis is the instant the molten braze develops stiffness and it assumed that this occurs at the melting temperature of the braze filler. Consequently, all latent heat effects due to the solid-liquid phase change have been ignored. The thermal conductivity, specific heat capacity, thermal expansion coefficient and stress – strain mechanical response across the brazing temperature range have been measured on the as supplied 72Ag-28Cu. Due to the cost associated with characterising the stress – strain mechanical response, this data has only been obtained at a limited number of temperatures. The mechanical response of the filler at the intermediate temperatures is estimated based on the measured data and this process is described.

Ideally, the stress – strain response of the 72Ag-28Cu filler would be determined across a range of temperatures and included in the FEA model as a multilinear hardening or

Chaboche law for example. However due to the limited data that could be obtained, a simple bilinear kinematic hardening law, requiring only a Young's modulus, yield stress and tangent modulus, has been used to model the mechanical response of the filler.

4.3.1 Thermal conductivity and specific heat capacity

The thermal conductivity and specific heat capacity, both of which are required for the transient thermal stress analysis, have been measured using a Netszch LFA 427 laser flash on a 15.2mm diameter by 3mm thick piece of as supplied 72Ag-28Cu. The results were obtained at intervals of 50°C up to 600°C with results extrapolated up to the melting temperature of 778°C. Measurements have not been taken closer to the melting temperature of the braze filler to protect the machine. No phase changes are expected between 600°C and 778°C based on the phase diagram (Figure 2-1), hence a linear extrapolation has been used up to the braze melting temperature. Figure 4-1 and Figure 4-2 show the measured and predicted thermal conductivity and specific heat capacity of the as supplied 72Ag-28Cu respectively.

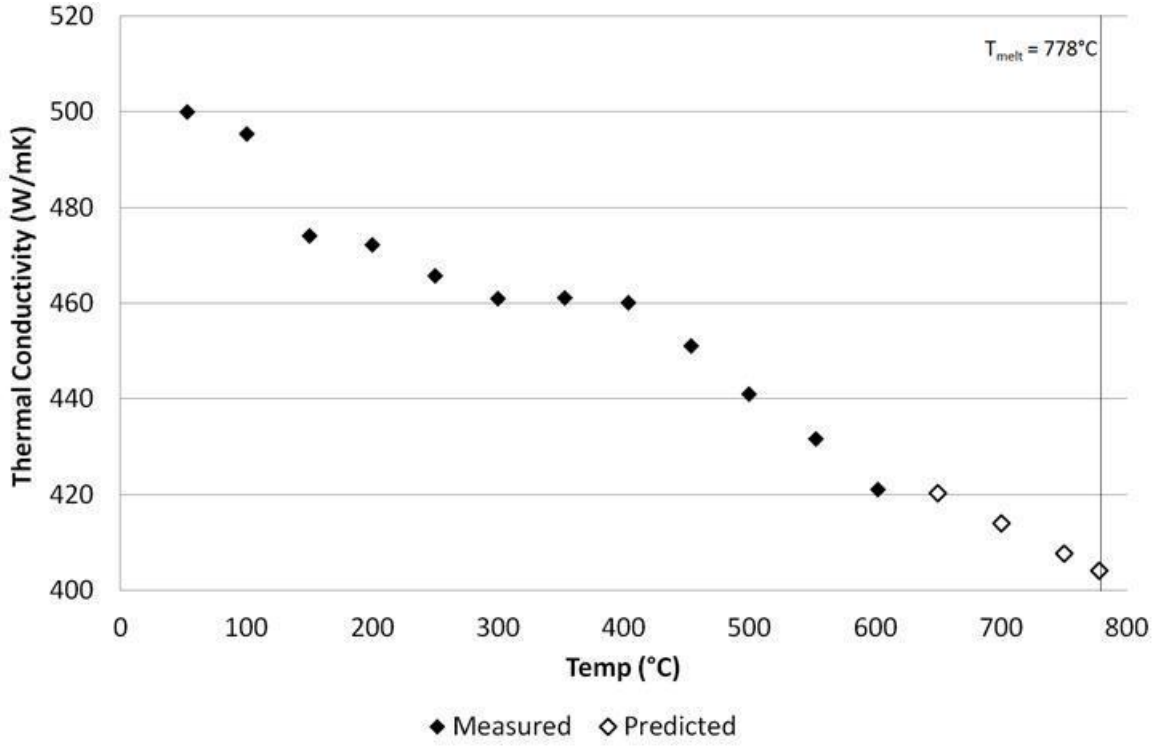

Figure 4-1 - Thermal conductivity of as supplied 72Ag-28Cu

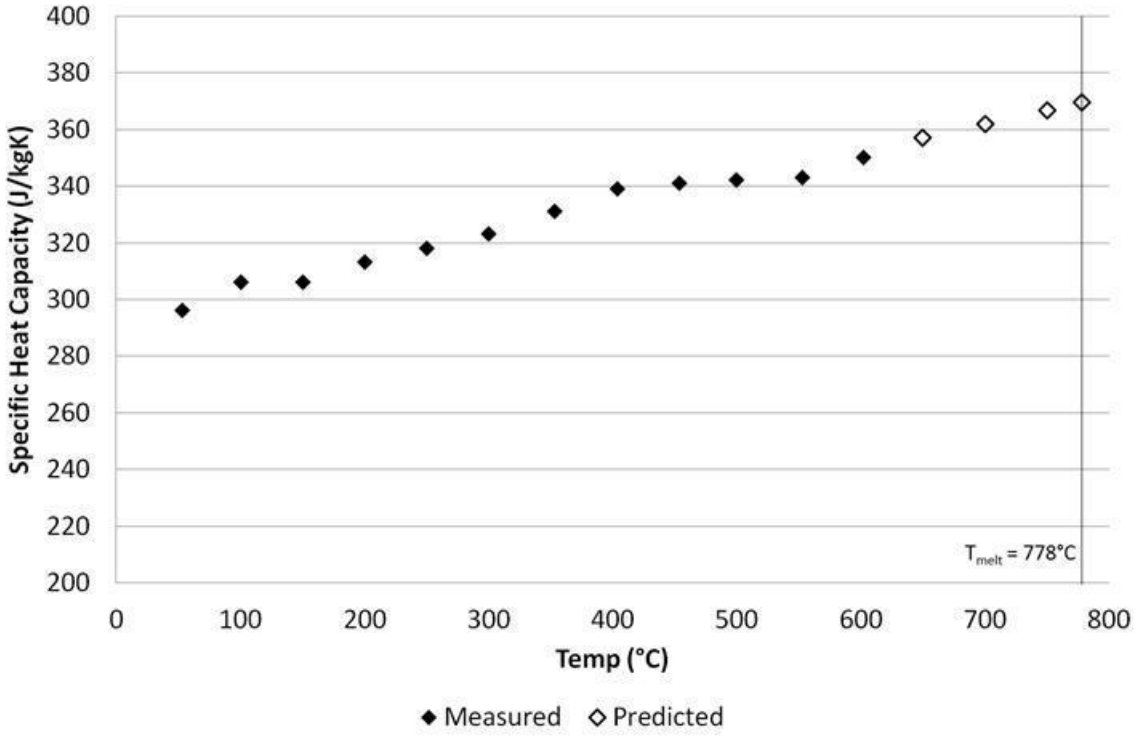

Figure 4-2 - Specific heat capacity of as supplied 72Ag-28Cu

4.3.2 Thermal expansion coefficient

The linear coefficient of thermal expansion was measured on a 15.25mm x 10mm diameter rod of the as supplied 72Ag-28Cu using a NETZSCH 402C push rod dilatometer with a heating rate of 5°C/min. The procedure used was in accordance with ASTM E228 [105] and readings were repeated until converged results were obtained as per the standard. The measurements were taken continuously over the temperature range 100°C to 600°C and results extrapolated up to 778°C. In a similar fashion to the thermal conductivity and specific heat capacity, a linear extrapolation has been used up to the melting temperature of 778°C. Measurements have not been taken closer to the melting temperature to protect the machine.

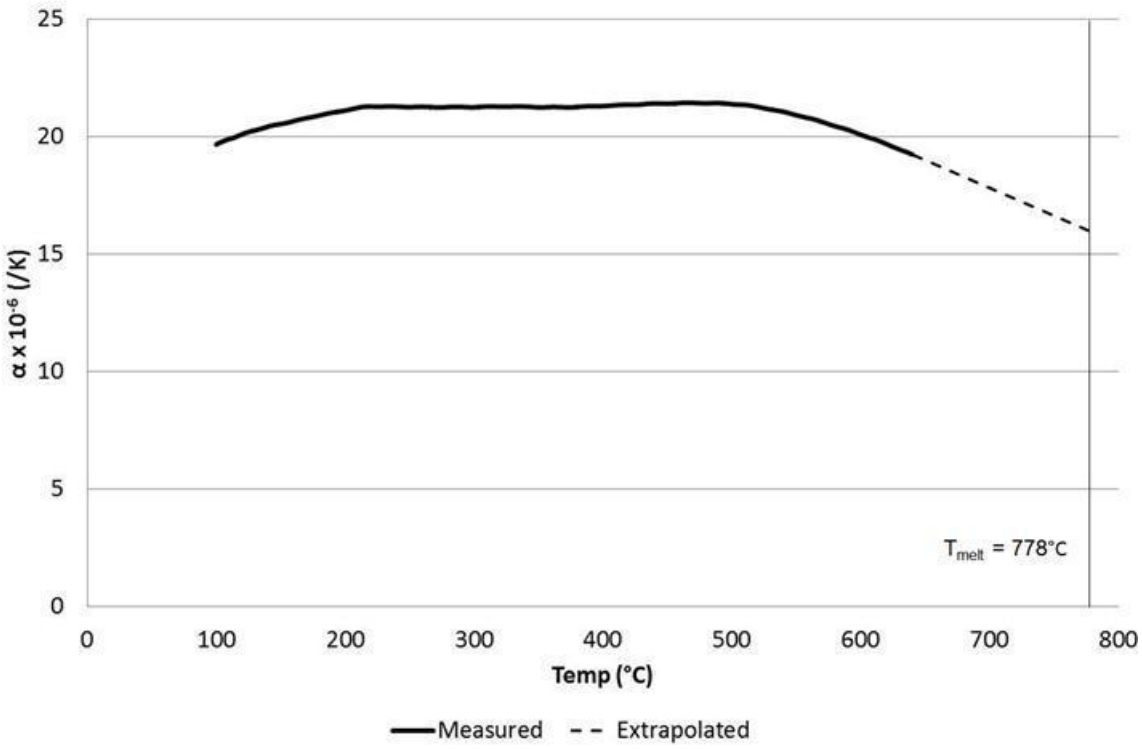

Figure 4-3 - Linear coefficient of thermal expansion of as supplied 72Ag-28Cu filler

4.3.3 Young's modulus

The Young's modulus across a range of temperatures of the as supplied 72Ag-28Cu braze filler was measured using a TA instruments Q800 Dynamic Mechanical Analyser (DMA) as opposed to using standard tensile test samples. This method of measurement allows Young's modulus to be measured across a range of temperatures using a single sample, largely reducing the amount of material and hence cost associated with obtaining the material property information. The DMA works by applying a controlled load to a sample of known geometry (in this case a beam of dimensions 50mm x 13mm x 1.5mm) in 3 point bending [106]. The deflection of the beam is measured and a stress – strain diagram can be determined using the applied load. The Young's modulus is calculated from the initial slope of the stress strain curve. The sample was subjected to a maximum load of 18N with a ramp rate of 3N/min. This corresponds to a maximum bending stress of 45MPa.

Due to limitations of the heating stage, results could only be obtained up to 500°C at intervals of 100°C, hence results been extrapolated up to the melt temperature of the filler. A linear extrapolation has been assumed from the value at 500°C to zero at the melting temperature. Previous work has been done on the mechanical characterization of weld

metal up to its melting temperature [107] which has shown a gradual decrease in stiffness up to the melting temperature. In addition, as mentioned in the previous section, no phase changes are expected between 500°C and 778°C based on the phase diagram (Figure 2-1), hence the linear extrapolation of the stiffness is likely to provide a relatively accurate representation of the mechanical response in the range 500°C to 778°C.

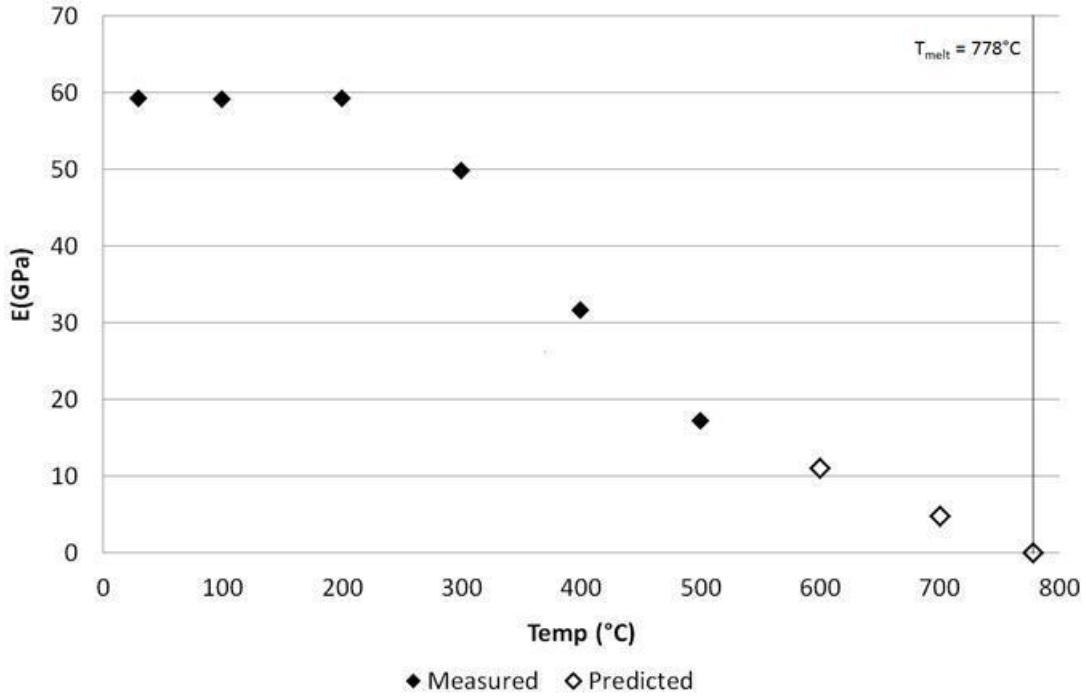

Figure 4-4 - Temperature dependent Young's modulus of as supplied 72Ag-28Cu filler

4.3.4 Yield stress and tangent modulus

Due to costs constraints, the yield stress and tangent modulus has only been obtained at room temperature and at 500°C with the results at the intermediate temperatures estimated based on the results at these two temperatures. In this instance the yield stress has been defined as the 0.1% proof stress due to the lack of a clearly defined yield point in both tests.

A single standard tensile test sample was tested in tension at room temperature using a Mayes M97194 600kN tensile test machine calibrated to BS EN ISO 7500-2:2006 [108]. The test was carried out under displacement control with an imposed displacement rate of 0.5mm/min. The specimen was instrumented with a Mayes 4183 extensometer, with a 50mm gauge length, calibrated to BS EN ISO 9513:2002 [109]. The stress – strain curve at room temperature with key parameters highlighted is shown in Figure 4-5.

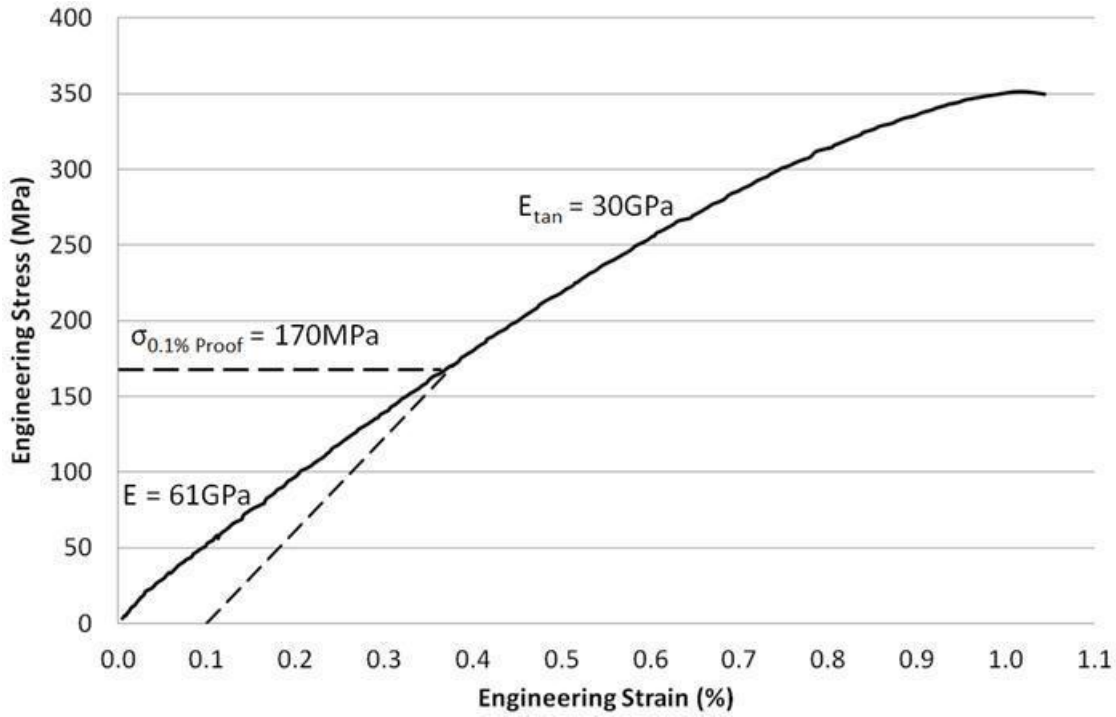

Figure 4-5 – 72Ag-28Cu Engineering stress - strain curve at room temperature

The yield stress data at 500°C was obtained from the DMA results used to measure Young's modulus. Due to the stress range which can be applied by the DMA, only the results at 500°C showed a clear change in Young's modulus over the measured stress range, hence why the yield stress and modulus can only be obtained at this temperature using this technique. The stress – strain curve from the DMA at 500°C is shown Figure 4-6 with the key parameters highlighted.

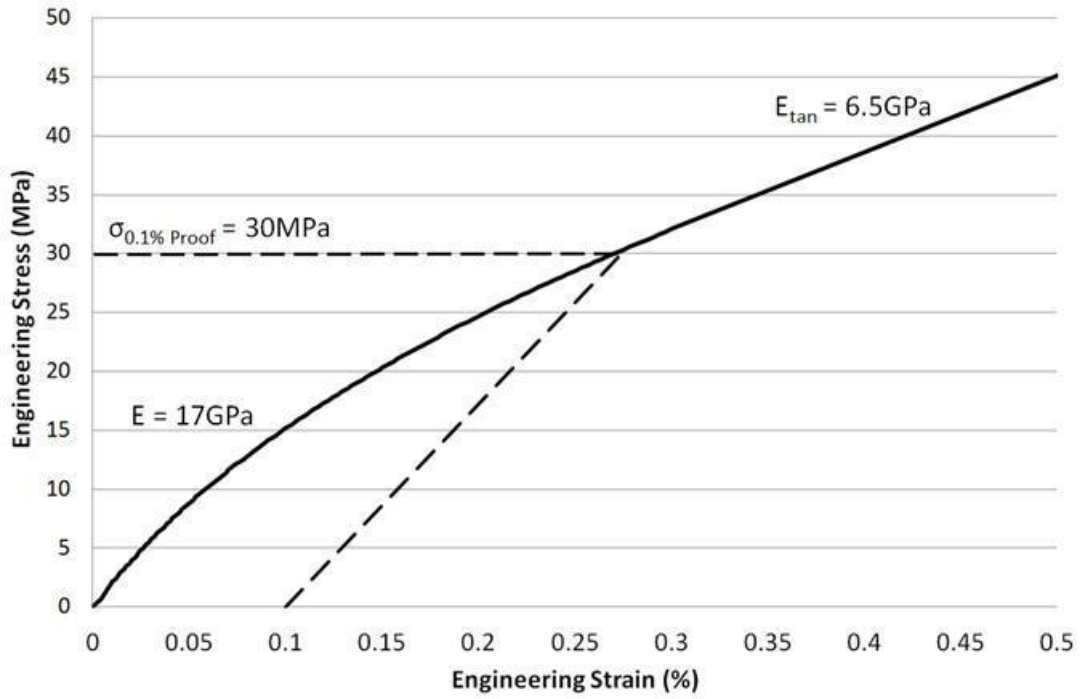

Figure 4-6 -72Ag-28Cu Engineering stress - strain curve at 500°C

The values of yield stress and tangent modulus measured at both room temperature and 500°C have been used to predict the properties at the intermediate temperatures. It has been assumed that at the melting temperature the braze filler has a yield stress and tangent modulus of zero. In a similar fashion to the Young's modulus, the work done in [107] has shown a gradual decrease in yield stress as well as stiffness all the way up to the melting temperature. In addition, as mentioned in previous sections, no phase changes are expected between 20°C and 778°C based on the phase diagram (Figure 2-1), hence the linear extrapolation of both the yield stress and tangent modulus is likely to provide a relatively accurate representation of the mechanical response. The prediction of the yield stress and tangent modulus at the intermediate temperatures are shown graphically in Figure 4-7 for yield stress and Figure 4-8 for tangent modulus. Whilst this approach has undoubtedly some uncertainty, the properties will be more representative than using a simple elastic model.

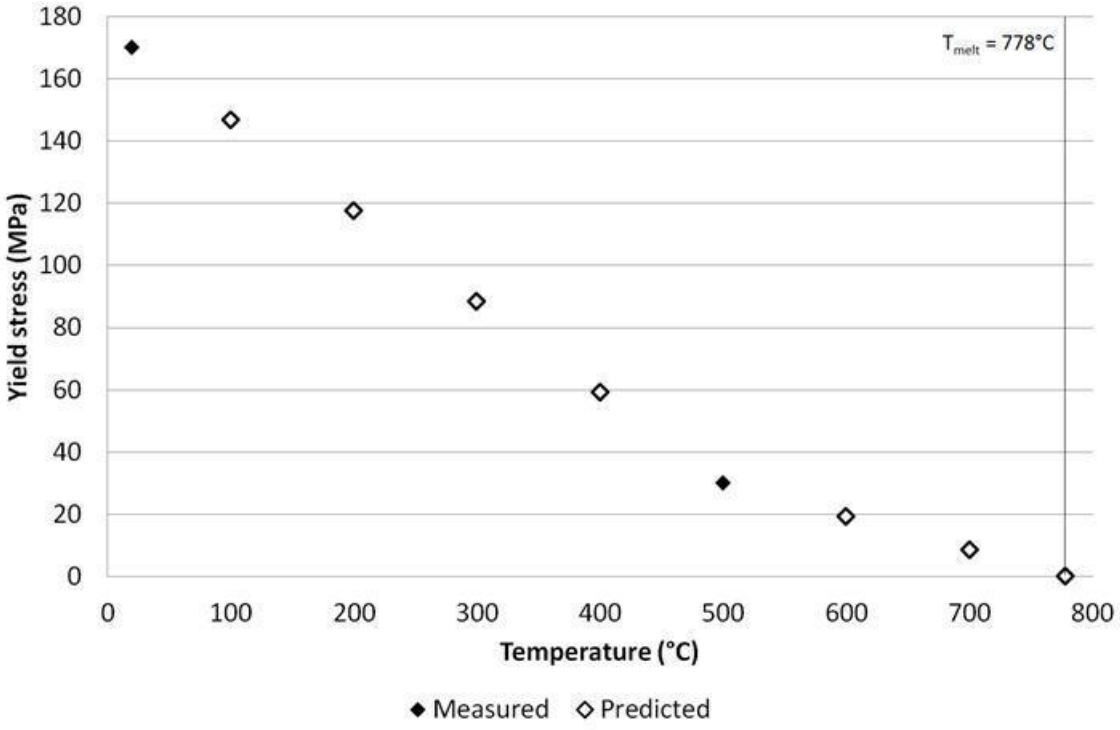

Figure 4-7 –Temperature dependent yield stress of as supplied 72Ag – 28Cu

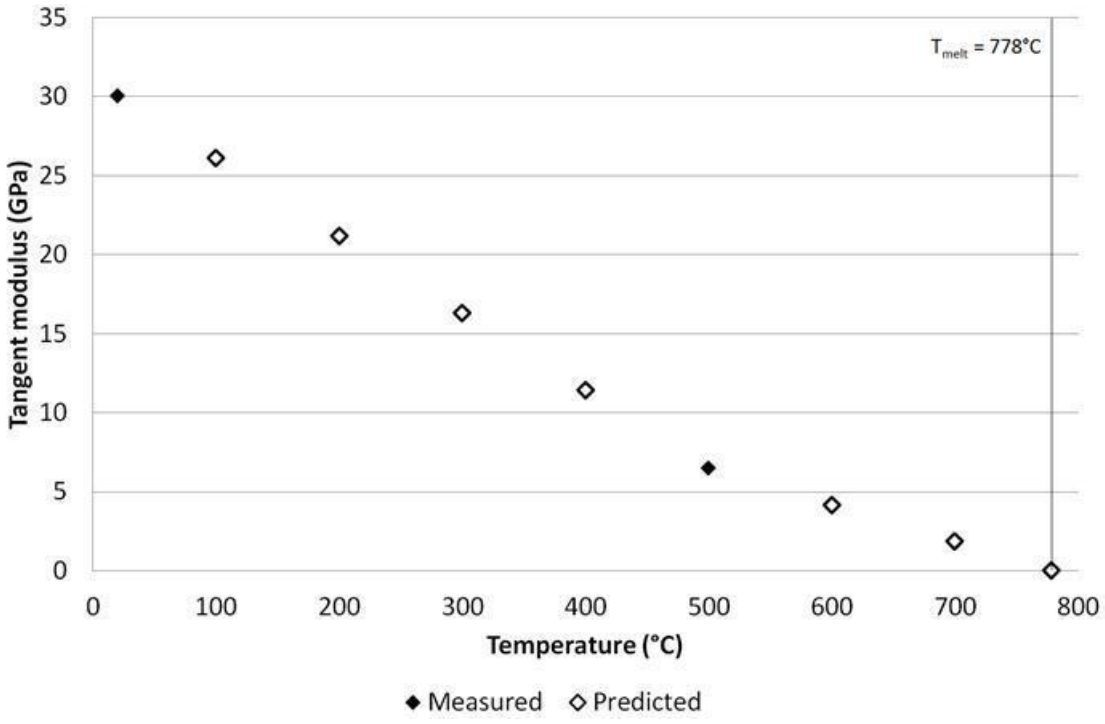

Figure 4-8 - Temperature dependent tangent modulus of as supplied 72Ag – 28Cu

4.3.5 Summary of 72Ag-28Cu temperature dependent material properties

The results from the characterization of the as supplied 72Ag – 28Cu for use in the FEA model are summarised below:

Temp (°C)	k (W/mK)	C_p (J/KgK)	α x 10^{-6} (/K)	E (GPa)	σ_{yield} (MPa)	E_{tan} (GPa)
20	493	291	15.3	59.2	170	30
100	495	306	19.7	59.2	146.7	26.1
200	472	313	21.1	59.2	117.5	21.2
300	460	323	21.3	49.9	88.3	16.3
400	459	339	21.3	31.6	59.2	11.4
500	440	342	21.4	17.2	30	6.5
600	420	350	20.1	11	19.2	4.2
700	413	362	17.8	7.8	8.4	1.8
778	404	369	16	0	0	0

Table 4-1 – Summary of 72Ag – 28Cu material properties for use in FEA

4.4 FEA of residual stresses due to joining

FEA has been used to predict the residual stresses developed in the joint during cooling from the brazing temperature to room temperature. The samples in this investigation were allowed to cool in the vacuum furnace overnight (c.8 hours) to a temperature of c.60°C before being removed from the vacuum furnace and allowed to cool to room temperature in air neglecting conduction from the base of the sample. During cooling in the vacuum oven the only mode of heat transfer from the samples is due to radiation. Given differences in the emissivity and thermal conductivity of both the Cu and Ti parent materials, there is the potential for significant temperature gradients to occur within the joint during cooling. Consequently a transient and uniform cooling thermal stress analysis has been conducted to establish if the final residual stress state is affected by nonuniform cooling. This section summarises the models used and results for both cases.

It is known that creep deformation occurs at approximately 1/3 of the melting temperature for metals [53]. This corresponds to a temperature of c. 360°C, 555°C and 260°C respectively for Cu, Ti and 72Ag-28Cu respectively. Hence it is likely that from cooling from 778°C creep will affect the development of residual stresses within the joint. This has been the topic of previous research for dissimilar material brazed joints in general [55], [110] and it has been shown that creep reduces and redistributes the residual stresses developed

during. However, creep has not been accounted for in this work and it is recommended that this forms the basis of future work in this area.

4.4.1 Parent material temperature dependent material properties

The temperature dependent material properties used for both Cu and Ti parent materials are summarised in Table 4-2 and Table 4-3 respectively. A bilinear kinematic hardening plasticity law has been used for both the parent materials in addition to the brazed layer. The material properties for both the Cu C110 and Ti grade 2 have been obtained from Material Property Database Software MPDB v7.47 (this database program contains temperature dependent material properties, obtained from various literature sources, for a range of materials. For more information please see [111]). In addition to these properties the density and emissivity of both materials are required. For the Ti a density of 4500kg/m^3 has been used across the brazing temperature range (obtained from MPDV v.7.47 [111]), a density of 9003kg/m^3 used for Cu (obtained from MPDV v.7.47 [111]), and a density of 10100kg/m^3 for 72AG-28Cu [112]. An emissivity of 0.31 has been used for Ti across the brazing temperature range [113], with a value of 0.05 used for machined Cu and 72Ag-28Cu braze [114].

Temp (°C)	k (W/mK)	C_p (J/KgK)	α x 10^{-6} (/K)	E (GPa)	σ_{yield} (MPa)	E_{tan} (GPa)
20	386	383	16.7	125	40	0.1 x E
100	385	393	17	121	32.4	0.1 x E
200	383	403	17.5	115	24.3	0.1 x E
300	380	413	17.8	109	17.6	0.1 x E
400	375	421	18.2	103	12.4	0.1 x E
500	368	429	18.6	96	8.9	0.1 x E
600	360	437	19	90	6.6	0.1 x E
700	354	446	19.3	83	5.9	0.1 x E
778	348	455	19.6	77	6.4	0.1 x E

Table 4-2 - Summary of Cu C110 material properties for use in FEA

Temp (°C)	k (W/mK)	C_p (J/KgK)	α x 10^{-6} (/K)	E (GPa)	σ_{yield} (MPa)	E_{tan} (GPa)
20	21	524	8.5	109	356	0.1 x E
100	20	542	8.8	105	246	0.1 x E
200	19	566	9	99	160	0.1 x E
300	18	589	9.1	93	111	0.1 x E
400	19	611	9.2	87	83	0.1 x E
500	19	630	9.4	81	66	0.1 x E
600	20	645	9.6	75	57	0.1 x E
700	21	666	9.8	69	53	0.1 x E
778	21	736	10	65	51	0.1 x E

Table 4-3 - Summary of Ti grade 2 material properties for use in FEA

4.4.2 Thermal stress analysis with no thermal solution

4.4.2.1 Model setup

A structural axisymmetric model of the vacuum brazing process has been created in ANSYS 12.1 and is shown schematically in Figure 4-9. The specimen is prescribed an initial temperature equal to the melting temperature of the 72Ag-28Cu braze filler (778°C) and a final temperature of 20°C. It is assumed the temperature varies uniformly to room temperature neglecting any variation in temperature through the specimen hence no thermal solution is required. The dimensions of the parent materials have been calculated at the brazing temperature based on their linear coefficients of thermal expansion to this temperature (found in Table 4-2 and Table 4-3 for Cu and Ti respectively) and the initial dimensions at room temperature (both Cu and Ti initially 14mm in diameter by 25mm long). The braze layer has been included in the model and is assumed to accommodate the differential thermal expansion of the parent materials. The braze has been approximated to be 100µm thick based on the thickness observed in Figure 2-13. Two dimensional PLANE182 4-noded structural solid quadrilateral elements have been used to mesh the

braze and parent materials in close proximity to the braze. The mesh has been graded away from the braze layer using PLANE183 triangular elements (as shown in Figure 4-9) to reduce the time taken to run the analysis. 2 elements have been used across the braze as a series of sensitivity studies [115] have shown that this is the minimum number of elements required to fully capture the constraint of the braze on the parent materials. The axisymmetry simplification assumes perfect alignment of both materials and a point constraint has been on the bottom surface to constrain the model in the y-direction as shown in Figure 4-9. A direct sparse matrix solver has been used. The ANSYS log file for this analysis can be found in appendix 4.1 at the end of this chapter.

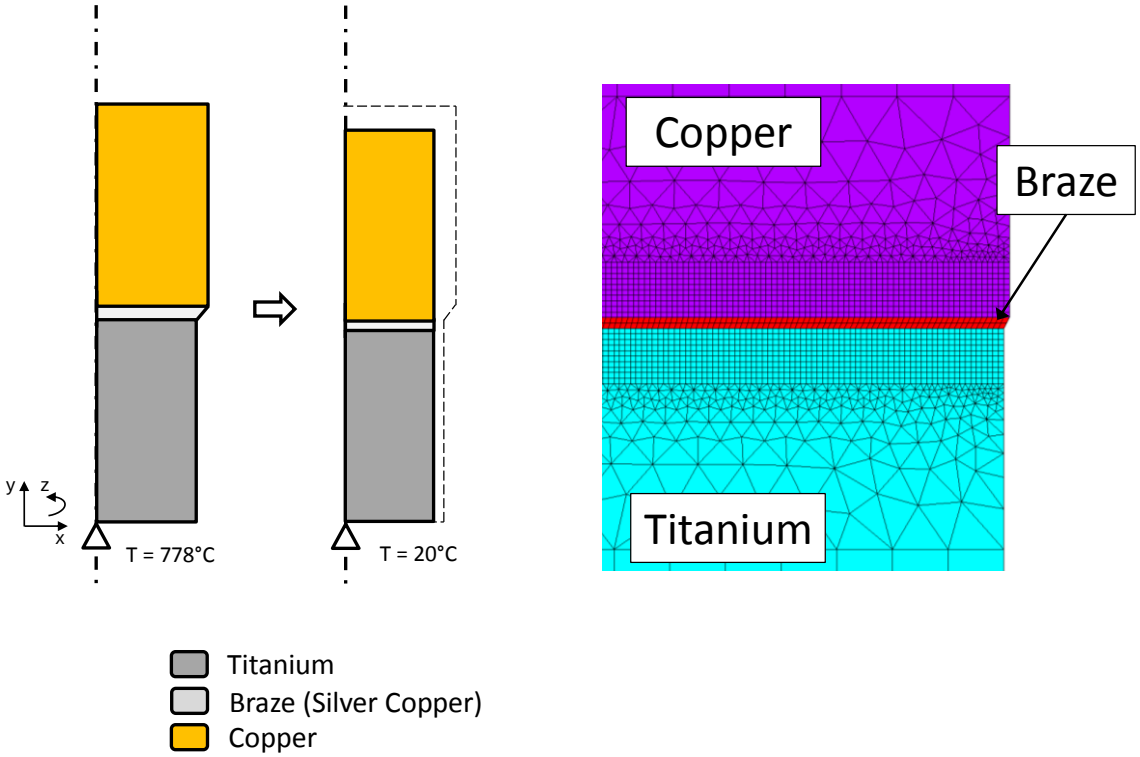

Figure 4-9 – Uniform cooling model schematic and free edge mesh

4.4.2.2 Results

Upon cooling from a stress free temperature, FEA predicts significant residual stresses will develop in the region of the joint. The free edge axial and circumferential stress distribution developed in the joint due to brazing is shown in Figure 4-10. The results from the uniform cooling FEA show that the Ti develops a tensile circumferential and axial local stress concentration, with the Cu developing a compressive circumferential and axial local stress concentration. The results also show that the largest component of stress is in the axial

direction along the free edge; however the circumferential stresses could still be significant in the initiation and propagation of cracks and cannot be neglected. The brazed interface only induces residual stresses within 10mm of the interface.

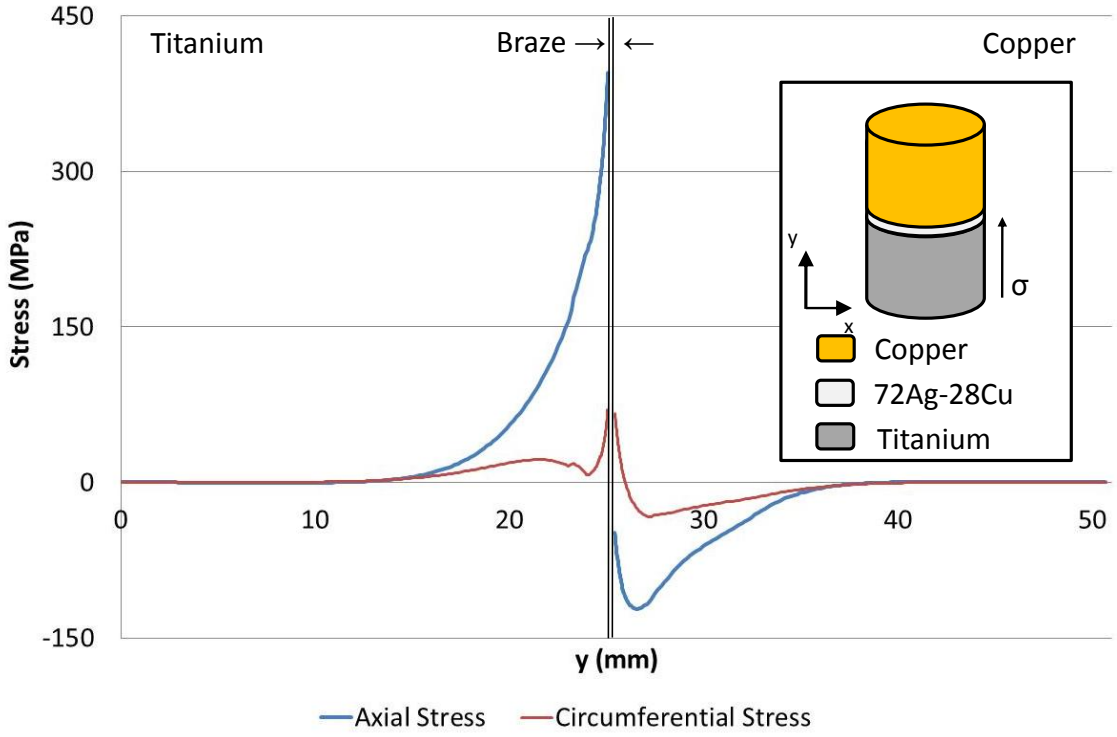

Figure 4-10 – Uniform cooling free edge residual stress distributions

Mesh refinement studies have shown (not presented in this thesis) that with these type of elements the results obtained within two elements either side of an abrupt change in material properties are non-converged (this finding is in agreement with previous research [58], [116]), hence the values at these nodes are not included in the results in the above figure. The analysis has shown that no plastic strains develop in the Ti, hence it remains elastic during the brazing cycle. However plastic strains develop in the 72Ag-28Cu and the Cu to a distance of 5mm from the interface. In terms of predicting failure in close proximity or through the interface, alternative techniques based on experimental data must be used and will form the basis of discussion in future chapters. This thermal stress analysis took c.2mins to run on a computer with a 2.4GHz Duo CPU and 4GB RAM.

4.4.3 Transient thermal stress analysis with radiation cooling

4.4.3.1 Model setup

A transient axisymmetric model of the vacuum brazing process has been created in ANSYS 12.1 and is shown schematically in Figure 4-11. In a similar fashion to the uniform cooling analysis, the specimen is initially assumed to be at a uniform temperature equal to the melting temperature of the 72Ag-28Cu braze filler (778°C), hence there is no initial variation in temperature through the specimen. The vacuum furnace temperature is assumed to be constant at 20°C throughout the analysis with the walls having an emissivity of 1. This represents a worst case in terms of heat transfer from the brazed sample to the vacuum vessel [117] as none of radiation incident on the vacuum vessel is reflected back towards the specimen. In reality the inner walls of the vacuum furnace will increase in temperature during the brazing process which would reduce the heat transfer from the sample and reduce any transient effects that may be occurring. Radiation between the sample and other samples in the furnace has been ignored. As time progresses the sample radiates heat to the vacuum furnace wall and this heat loss is conducted through the sample. As mentioned in the introduction to this chapter, the samples are only left for 8 hours in the vacuum furnace before being removed and cooled to room temperature through natural convection. It is estimated the temperature of the samples upon removal from the vacuum furnace is c.60°C. The cooling due to natural convection has not been accounted for, only the heat lost due to radiation for 8 hours in the vacuum furnace.

In a similar fashion to the uniform cooling analysis the dimensions of the parent materials have been calculated at the brazing temperature based on their linear coefficients of thermal expansion to this temperature (found in Table 4-2 and Table 4-3 for Cu and Ti respectively) and the initial dimensions at room temperature (both Cu and Ti initially 14mm in diameter by 25mm long). The braze layer has been included in the model and is assumed to accommodate the differential thermal expansion of the parent materials. The braze has been approximated to be 100µm thick based on the thickness observed in Figure 2-13. Two dimensional PLANE223 8-noded coupled field quadrilateral solid elements have been used across the braze and in close proximity to the braze, with the triangular option used to grade the mesh away from the braze layer as shown in Figure 4-11. 2 elements have been used across the braze as a series of sensitivity studies [115] have shown that this is the

minimum number of elements required to fully capture the constraint of the braze on the parent materials.

The radiosity solver method within ANSYS has been used to model the radiation heat transfer from sample to the surrounding vacuum chamber. The model is constrained in the axial direction by constraining the node on centreline of the Ti along the bottom surface as shown in Figure 4-11 below.

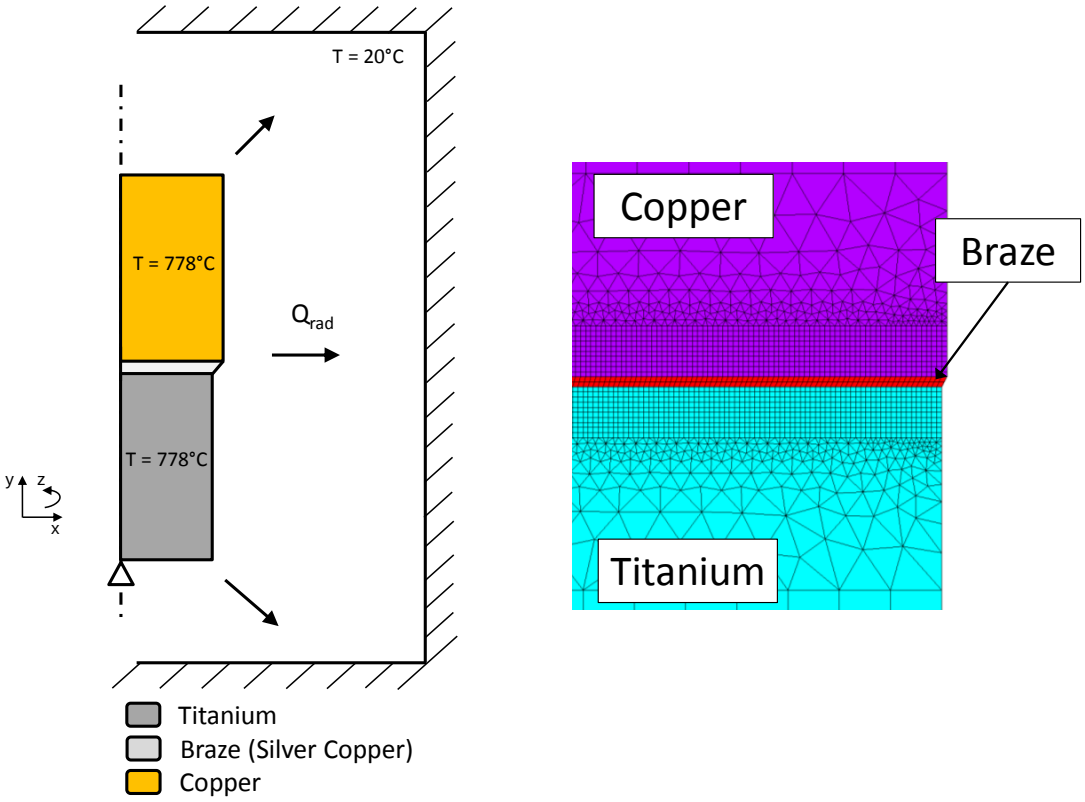

Figure 4-11 – Transient model schematic and free edge mesh

The rate of heat transfer from the outer surface of the specimen will be greatest at the start of the analysis, hence small time steps of 0.25s have been manually prescribed for the first 36s of the analysis to fully capture the development of the initial thermal gradients through the specimen (the automatic time stepping function in ANSYS fails to accurately capture the development of the initial temperature gradients in the sample and is therefore controlled manually). Larger time steps are subsequently used when the temperature distribution through the sample has been developed and the rate of radiation heat loss from the surface reduces. The transient analysis has been run for 8 hours which equals the

time the sample spends in the vacuum furnace. The ANSYS log file for this analysis can be found in appendix 4.2 at the end of this chapter.

4.4.3.2 Results

Given the emissivity of the Ti compared to the Cu (0.31 compared to 0.05) the rate of heat transfer from the Ti to the vacuum furnace is greater than that from the Cu, hence the Ti will initially cool at a faster rate than the Cu. This will result in a temperature gradient along the axis of the joint which could lead to the residual stress distribution being different to that predicted by the uniform cooling analysis. The analysis has shown that the largest difference in temperature at the centreline between the top of the Cu and the bottom of Ti occurs after 72s of cooling and is 51°C (top of Cu temperature 724°C, bottom of Ti 673°C). The variation in temperature of the centre of both the Cu and Ti for the first 3 hours of cooling is shown in Figure 4-12. As expected the initial rate of cooling is greatest and after 3 hours both materials in the joint are at c.65°C. The analysis has also shown that after 8 hours both materials in the joint are at approximately 24°C compared to the c.60°C when the samples are removed from the vacuum furnace in practice. Hence due to the assumption of the vacuum furnace walls remaining at 20°C the cooling rate is greater in the FEA which should exaggerate any transient effect on the residual stress distribution.

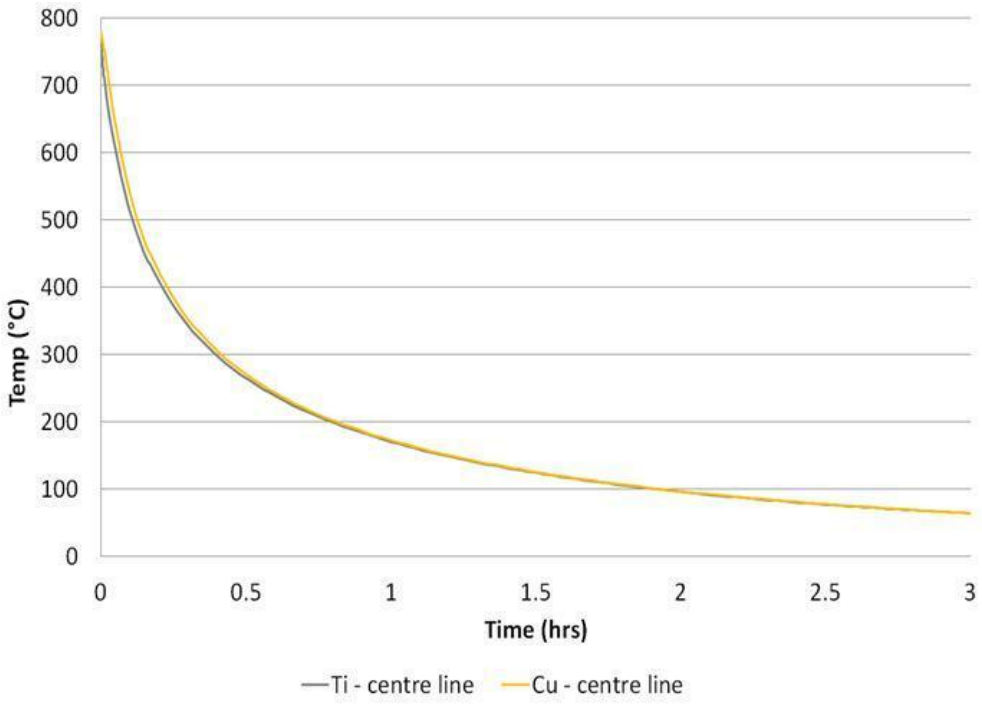

Figure 4-12 - Variation in parent material temperature due to cooling in a vacuum

The transient analysis has shown that negligible variations in temperature occur across the radius of both the parent materials and the braze. In the Cu the maximum difference in temperature between the centre of the sample and the free edge is <<1°C, and for the Ti this difference is a maximum of 3.5°C. The lack of variation in temperature across the radius of the sample can be attributed to the relatively high thermal conductivity of both the materials. Due to the lower thermal conductivity, a slightly more noticeable variation in temperatures occurs in the Ti, however this small variation is unlikely to affect the stress state developed within the joint.

The circumferential and axial stress distributions along the free edge as predicted by the transient model have been evaluated after 8 hours (simulation timescale) when both materials are at 24°C. Compared to the previous analysis, this transient thermal stress analysis took c.15mins to run on a computer with a 2.4GHz Duo CPU and 4GB RAM. The results from this analysis are shown in Figure 4-13 compared to the uniform cooling solution presented in the previous chapter.

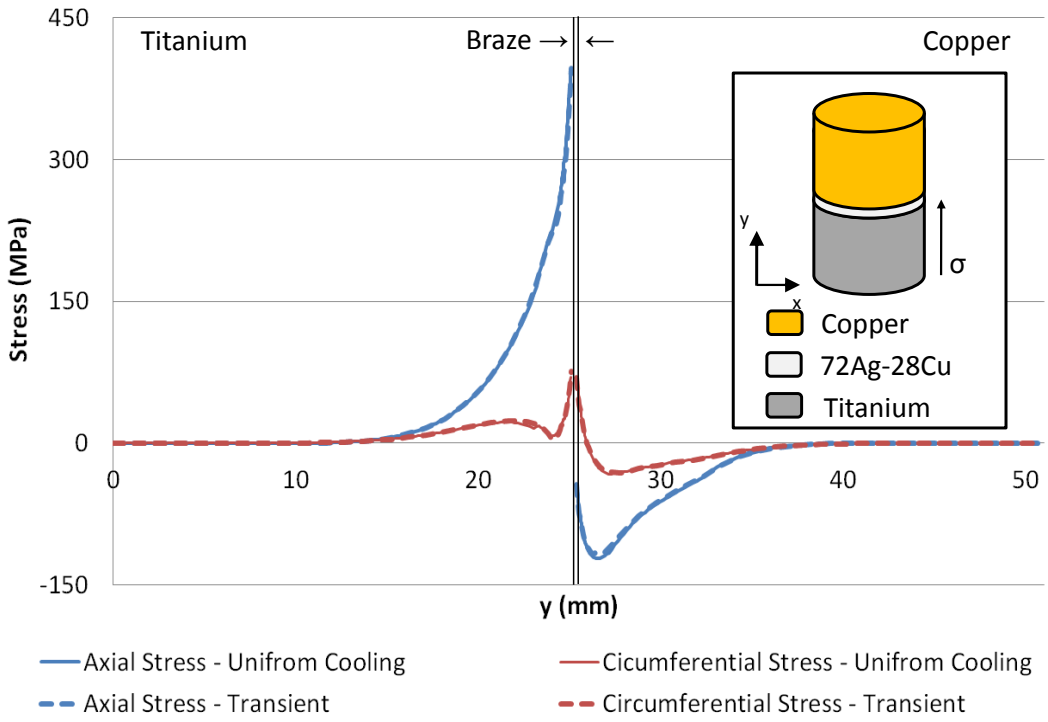

Figure 4-13 – Uniform cooling and transient free edge residual stress distributions

The transient analysis shows that there is very little difference in the residual stress state predicted by the uniform cooling analysis compared to the transient analysis. At the time the temperature gradient of 51°C occurs, due to the relatively high temperatures in the sample, the stiffness and yield stress of the braze is still very small and consequently does not have a significant effect on the final the residual stress distribution in the joint. This analysis shows that the development of residual stresses due to cooling in the vacuum furnace can be approximated to be a uniform cooling process and any thermal gradients that develop within the joint have a negligible effect on the residual stress distribution.

4.5 Measurement of residual stresses using XRD

The residual stresses due to machining then subsequent joining have been measured using XRD. The residual stresses due to machining in both the Ti and Cu parent material have been measured at three different locations. The residual stress distribution due to joining has been measured on two separate samples. On the brazed samples, measurements have only been obtained on the Ti after brazing due to texturing of the Cu during brazing [118], making it unsuitable for residual stress measurement using XRD. The residual stress measurements on each brazed sample have been obtained at various angular positions and distances away from the interface along the outer diameter of the brazed sample. Based on the recommendations given in [118], the crystallographic plane Miller indices used to obtain readings on the samples are the Ti {213} plane and the Cu {420} plane.

A summary of the XRD measurement parameters are given in Table 4-4 with a photo of the experimental setup shown in Figure 4-14. The measurements have been obtained using a collimator of 1mm diameter with a maximum measurement depth of c.5μm [118], hence the residual stress readings are average values of stress in this irradiated volume. It should be noted that the shape and size of the irradiated area changes during the measurements and is a function of both 2θ and the value of Ψ tilt with a greater change in shape occurring at higher values of both of these parameters. According to the data published in [119], for a 2θ angle of 60°, a Ψ tilt of 60° will result in an ellipse of approximately double the length of the original circular beam. Given our measured peaks are at 2θ° angles greater than double 2θ = 60° and have a maximum Ψ tilt of 50°, the change in shape in of the beam in these measurements will be less than a factor 2 for all measurements. However, it is worth bearing in mind that the readings will be averaged over a slightly larger value than the 1mm diameter spot size. The sample is held in position at the correct height using a specially

designed holder as shown in Figure 4-14. For the measurements on the brazed samples, the distance from the interface is controlled correct to $\pm$0.01mm using vernier calipers to move the sample within the holder however the initial alignment of the interface has been done by eye and is estimated to be correct to $\pm$ 0.5mm. For XRD readings on cylindrical samples the beam size has to be small in relation to the curvature of the specimen. It is recommended for measurements on cylindrical samples that a maximum spot size of ¼ x sample radius is used [118]. For samples 14mm diameter, this corresponds to maximum spot size of 7mm x 0.25 = 1.75mm, hence the beam size of 1mm can be assumed to be small in relation to the curvature of the sample.

XRD parameters	Ti	Cu
System	Bruker D8 Advance	Bruker D8 Advance
Radiation source	Cu Kα	Cu Kα
Diffraction plane	Ti 2 1 3	Cu 4 2 0
2θ	139°	137°
Tube voltage	40kV	40kV
Tube current	40mA	40mA
Collimator diameter	1mm	1mm
Method	Omega tilt, iso-inclination, sin2ψ	Omega tilt, iso-inclination, sin2ψ
ψ tilt values	+ 0°, 5°, 10°, 15°, 20°, 25°, 30°, 35°, 40°,45°,50°	+ 0°, 9°, 18°, 27°,36°, 45°
Φ values	0°, 45°, 90°	0°, 45°, 90°
Stress model	Biaxial + shear	Biaxial + shear
Peak evaluation	Pearson VII	Pearson VII

Table 4-4 – Summary of residual stress measurement parameters

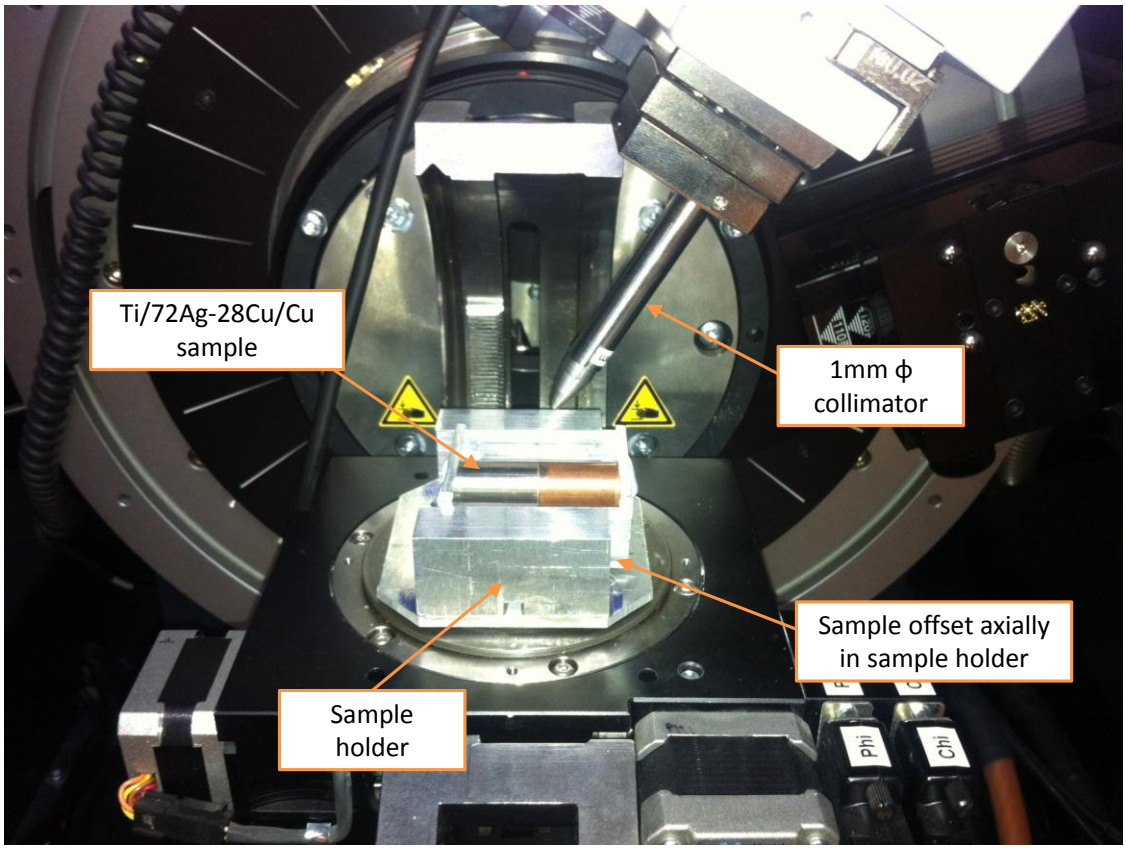

Figure 4-14 - XRD setup

The uncertainty in each residual stress measurement is described by the value that defines the range within which the value is estimated to fall with 95% confidence. This uncertainty has been calculated based on the combined uncertainty due to the calculation of the residual strain, any variation in the material Young's modulus and the repeatability of the measurements. A full description of the method used to calculate the reading uncertainties can be found in appendix A3 of [118] and is briefly summarised below.

The combined uncertainty (U) in the residual stress reading is given by the root sum square of the standard uncertainty components as described by Equation 4-1, where ($u(x_i)$) is the uncertainty in input quantity x_i, c_i is equal to the measured residual stress for the modulus error and equal to 1 for the error due to the strain calculation [118]. The quantity d_v is a divisor used to calculate the standard uncertainty based on the probability distribution of each standard uncertainty. k is defined as the coverage factor that, when multiplied by the combined standard uncertainty u_c, produces an uncertainty that is dependent on the confidence level. In this case a 95% confidence level is used, for which k = 2 [118].

In this instance there are three standard uncertainties that must be calculated: the standard uncertainty due to the strain reading, the standard uncertainty due to assumed value of Young's modulus and the standard uncertainty due to the repeatability of the measurements. The standard uncertainty due to the strain reading is provided by the post-processing software and it has been assumed the value of Young's modulus is within 10% of the real value. Both strain and Young's modulus have a rectangular probability distribution in which case d_v in Equation 4-1 is equal to √3 [118]. The standard uncertainty due to the repeatability of the measurements has based on a series of back to back measurements has been calculated to be 1.4MPa. Appendix 4.3 summarises how this value has been calculated. An example of how the combined uncertainty, based on the all three standard uncertainties, for one residual stress measurement is given in appendix 4.4.

$$U = k.u_c = k\sqrt{\sum_{i=1}^{m}\left[\frac{c_i u(x_i)}{d_v}\right]^2} \qquad \textbf{\textit{Equation 4-1}}$$

4.5.1 Measurement of residual stresses due to machining

4.5.1.1 Machining residual stresses in Ti

The residual stresses on the surface of the Ti due to machining have been measured at 3 different locations each 10mm apart on a sample which was machined to 14mm diameter in the same fashion as the samples used to create the brazed joints. A summary of the measured residual stresses at the three locations is given below (σ_y the axial component, σ_z the circumferential component as per Figure 4-11). The results show that there is both a compressive axial and circumferential stress on the surface of the machined Ti. The presence of compressive surface residual stresses in Ti due to machining has been reported elsewhere [120] [121].

Location	σ_y (MPa)	Uncertainty (MPa)	σ_z (MPa)	Uncertainty (MPa)
1	-127.4	31.1	-51.1	28
2	-91.7	28.3	-47.9	26.8
3	-117.3	32.3	-34	29.7

Table 4-5 - Machining residual stress in Ti

It has been shown that the residual stresses present in Ti can be significantly reduced by stress relieving. Sridhar et al [121], has shown that stress relieving Ti at 600°C for 1hr relieves 90% of the compressive residual stresses due to machining. This work also showed the reduction at 600°C to be bigger than at 400°C and 500°C. The depth profile of the residual stresses measured using hole drilling due to stress relief at 400°C, 500°C and 600°C compared to room temperature is shown in Figure 4-15.

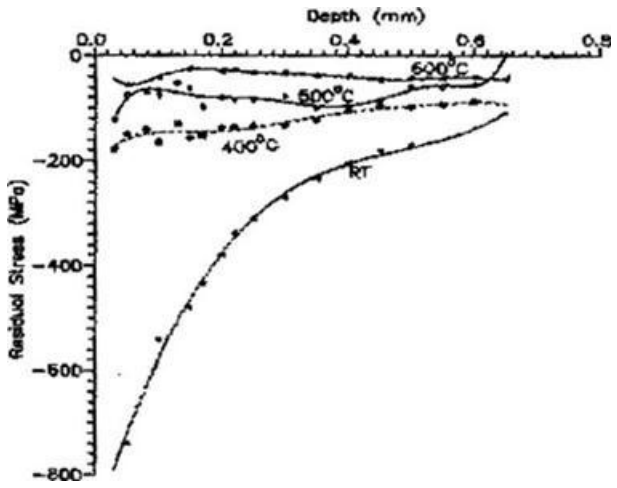

Figure 4-15 – Change in measured residual stress in Ti due to stress relief [121]

Effective stress relief of Ti has also been reported in [122] which has shown the majority of stress reduction occurs within the first 15 minutes as highlighted in Figure 4-16. This work also highlighted the improvement in stress relief with increasing temperature as expected.

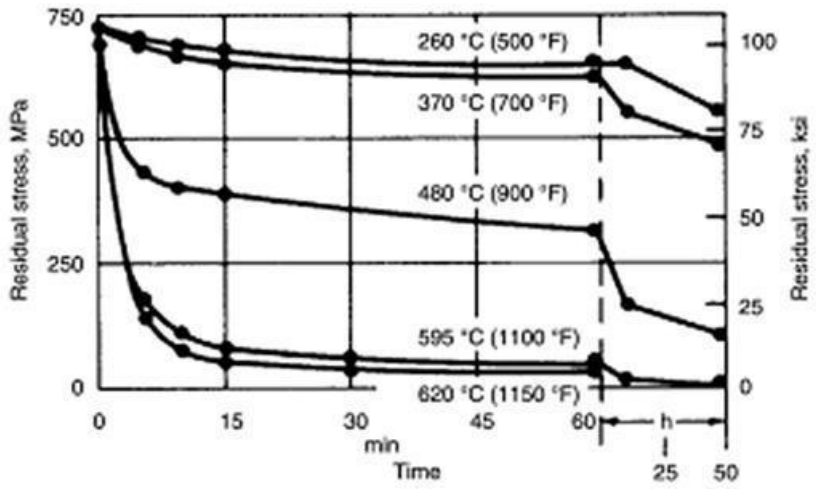

Figure 4-16 – Reduction in residual stress in Ti over time [122]

Given these findings it is assumed that the residual stresses measured due to machining will be stress relieved during heating to the brazing temperature of 820°C. This is based on the fact that at a heating rate of 10°C/minute with a dwell of 5mins at 750°C, it will take 27mins for the sample to reach 820°C from 600°C which given the findings from the [121] [122] is likely to largely reduce any residual stresses present in the material. Hence the residual stresses measured in brazed samples are assumed to come solely due to the brazing process and not from any prior machining.

4.5.1.2 Machining residual stresses in Cu

The residual stresses on the surface due to machining have been measured at 3 different locations each 10mm apart on a sample which was turned to 14mm diameter in the same fashion as the material samples used to create the brazed joints. A summary of the measured residual stresses at the three locations is given below. The results show that the residual stresses in the Cu due to machining are small. The stress relieving temperature for pure Cu is 180°C [123], hence it is likely heating to the brazing temperature of 820°C will eliminate these small residual stresses.

Location	σ_y (MPa)	Uncertainty (MPa)	σ_z (MPa)	Uncertainty (MPa)
1	-11.8	15.6	-32	15.9
2	5.7	15.1	-26.3	15.4
3	-21.9	13.7	-24.2	13.6

Table 4-6 – Machining residual stresses in Cu

4.5.2 Measurement of residual stresses due to joining

The residual stresses due to joining have been measured on two different samples along the Ti free edge at several distances from the interface and at different angular locations around the circumference. The measured axial residual stress distributions are shown in Figure 4-17 and Figure 4-18. Figure 4-17 shows the measured axial residual stress on sample 1 compared with that predicted by uniform cooling FEA. Measurements have been taken at 6 distances away from the interface on the Ti at two angular locations 90° apart. Figure 4-18 shows the measured axial residual stress on sample 2 compared with that predicted by the uniform cooling FEA. Measurements have been taken at 6 distances away from the interface on the Ti at one angular location. Measurements at the location closest to the interface have been repeated at 4 angular locations (0°, 90°, 180° and 270°) to investigate the apparent lack of axisymmetry present in sample 1. The corresponding circumferential residual stress distributions at the same locations in both samples 1 and 2 are shown in Figure 4-19 and Figure 4-20 respectively.

Each residual stress measurement is accompanied by an x and y error bar based on uncertainty calculations. The stress measured by XRD is an average over the area and depth illuminated by the x-ray beam. In this instance a diameter of 1mm by c.5µm deep at each location. The error bars in the y-direction represent the combined uncertainty in the residual stress measurement with a 95% confidence level, the calculation of which follows the process described in appendix 4.4. The error bars in the x-direction also give an indication of the surface area the results are averaged over.

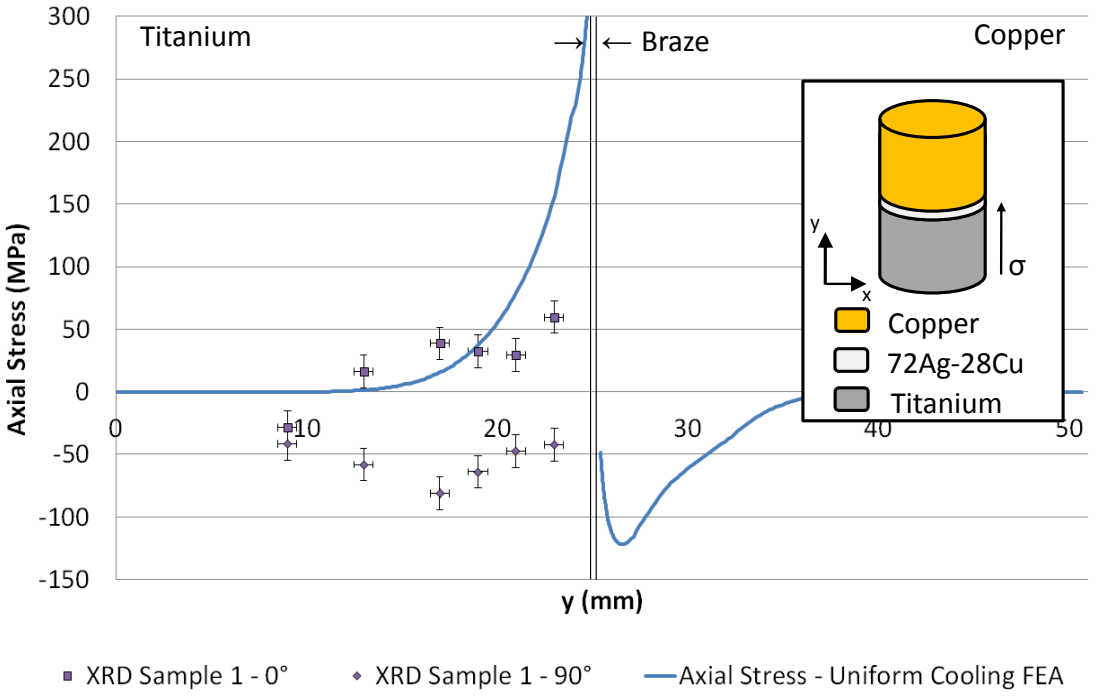

Figure 4-17 - Measured axial stress on sample 1 compared with uniform cooling FEA

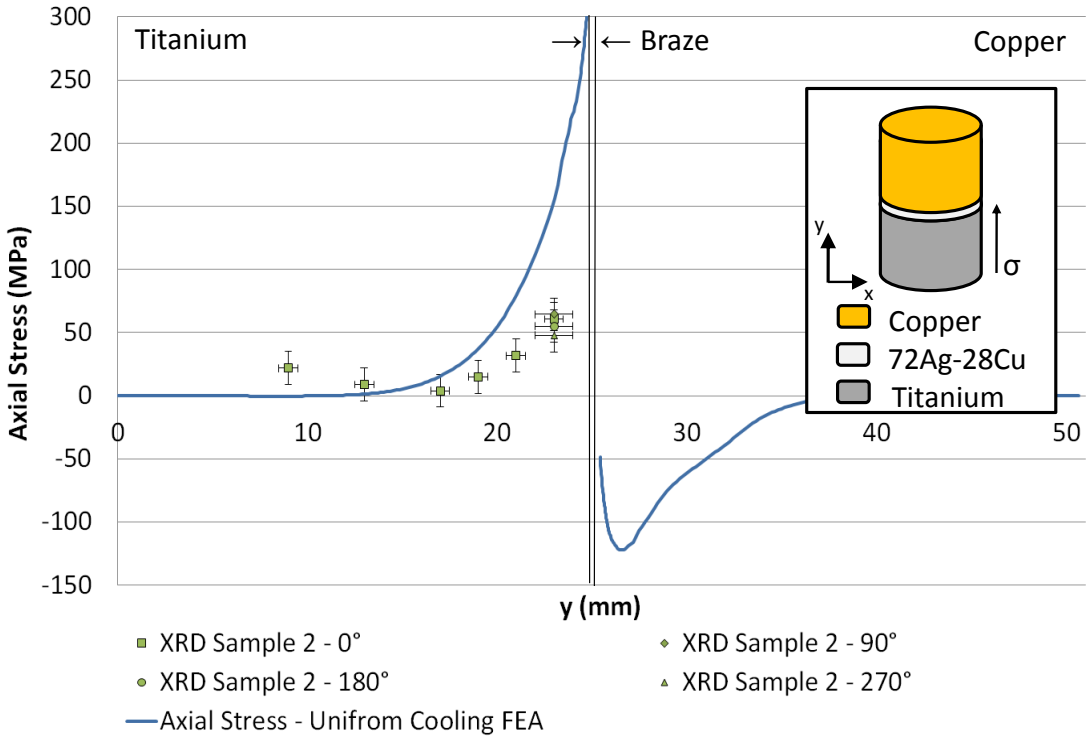

Figure 4-18 – Measured axial stress on sample 2 compared with uniform cooling FEA

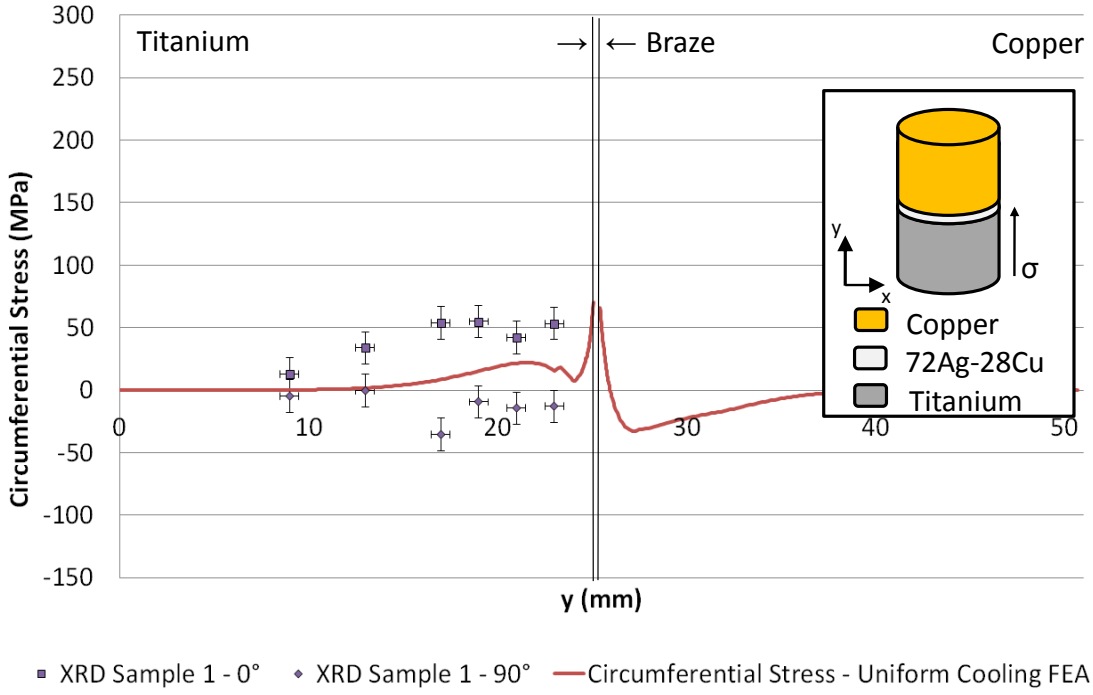

Figure 4-19 - Measured circumferential stress on sample 1 compared with uniform cooling FEA

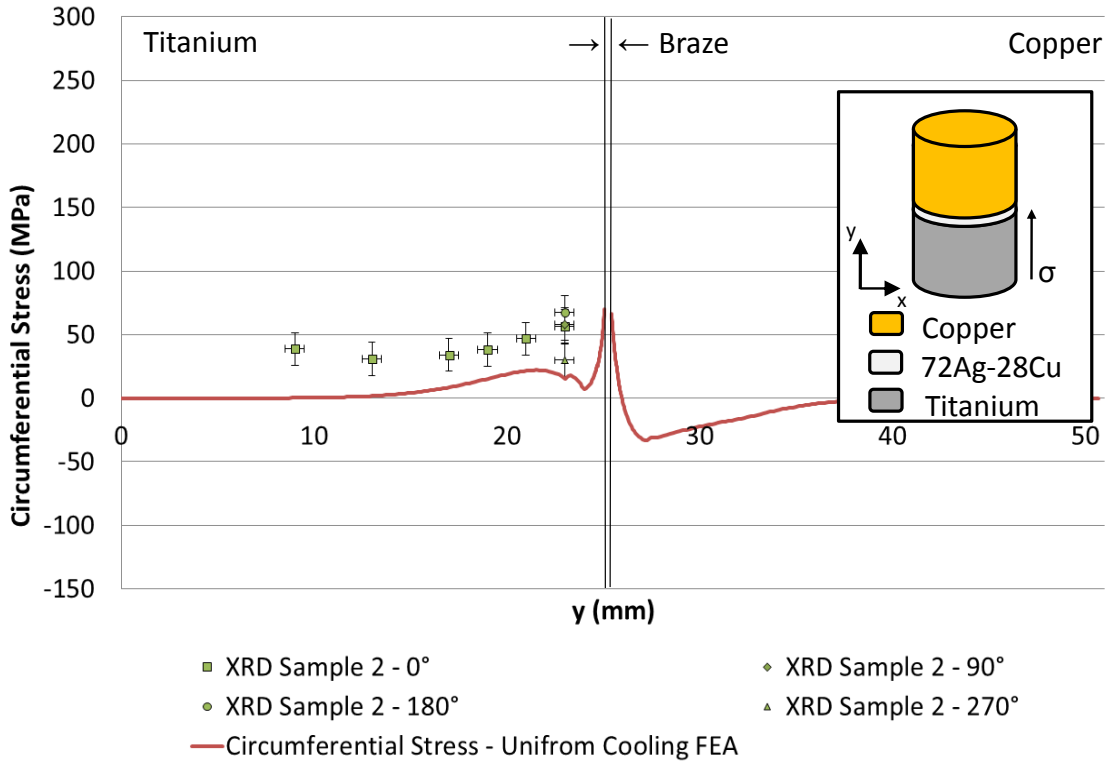

Figure 4-20 - Measured circumferential stress on sample 2 compared with uniform cooling FEA

The results taken at the 0° location on sample 1 seem to correlate reasonably well to the axial and circumferential stress predicted by FEA. Both XRD measurements and FEA predict that a tensile stress develops in the Ti in both directions and this appears to be getting more tensile as the interface is approached. At the location y = 8mm, where FEA predicts there to be a negligible stress concentration due to the interface, in both the axial and circumferential directions the effect of stress relieving the machining residual stresses can be observed. In the axial direction (Figure 4-17) the initial residual stress due to machining was measured to be between c.-91MPa and c.-117MPa (Table 4-5), hence a significant reduction is observed. A similar observation can be seen in the circumferential direction (Figure 4-19).

However the results at the 90° location on sample 1 do not match those predicted by FEA in that a compressive axial and circumferential stresses are measured. This suggests a lack of axisymmetry in the sample. The reasons for this are currently not fully understood and are postulated to be due to either axial or angular misalignment of the sample during brazing, which could be investigated using a coordinate measuring machine. The effect of mis-alignment on the measured and predicted residual stress state is currently the focus of on-going research in this area [124].

The results from sample 2 at 0° seem to reasonably match the results from the axial and circumferential stress predicted by FEA and the measured results from sample 1 at 0°. Due to the lack of axisymmetry in sample 1, measurements at the location closest to the interface have been repeated at 4 angular locations 0°, 90°, 180° and 270°. The results on this sample are repeatable at the 4 angular locations which show that this sample is exhibiting axisymmetry. The level of correlation between the measured and predicted residual stress distributions is similar to that found in previous research [58] [125] [126] [127] [128].

In general the residual stress predicted by FEA show a reasonable agreement with that measured using XRD. However in this case, the FEA over predicts the measured residual stresses. There are several possible reasons for this such as the simplified brazed layer material model is too stiff, the yield stress is too high or a combination of the pair. It is postulated that a better correlation could be obtained if a more accurate material model was used. The second possible reason is the assumption of a step change in material properties between the braze layer and the parent materials is over constraining the

model. As highlighted in chapter 2, a step change in material properties does not exist in reality.

The constraint mechanism described in section 3.2 can be used to describe the development of the tensile axial residual stresses in the Ti as shown in the free body diagram in Figure 4-21. Ignoring the presence of the thin brazed layer, assuming both materials are initially of equal widths and stress free at the braze temperature of 778°C, when the joint is cooled to room temperature, the Cu will contract more than the Ti due to its larger coefficient of thermal expansion. The compatibility constraint of the interface results in stresses being developed perpendicular to the interface as discussed in section 3.2 and, given the free body diagram for this case shown in Figure 4-21, it is expected that the Ti develops a tensile stress perpendicular to the interface due to this differential thermal contraction. This is in agreement with both the results from FEA and XRD residual stress measurements.

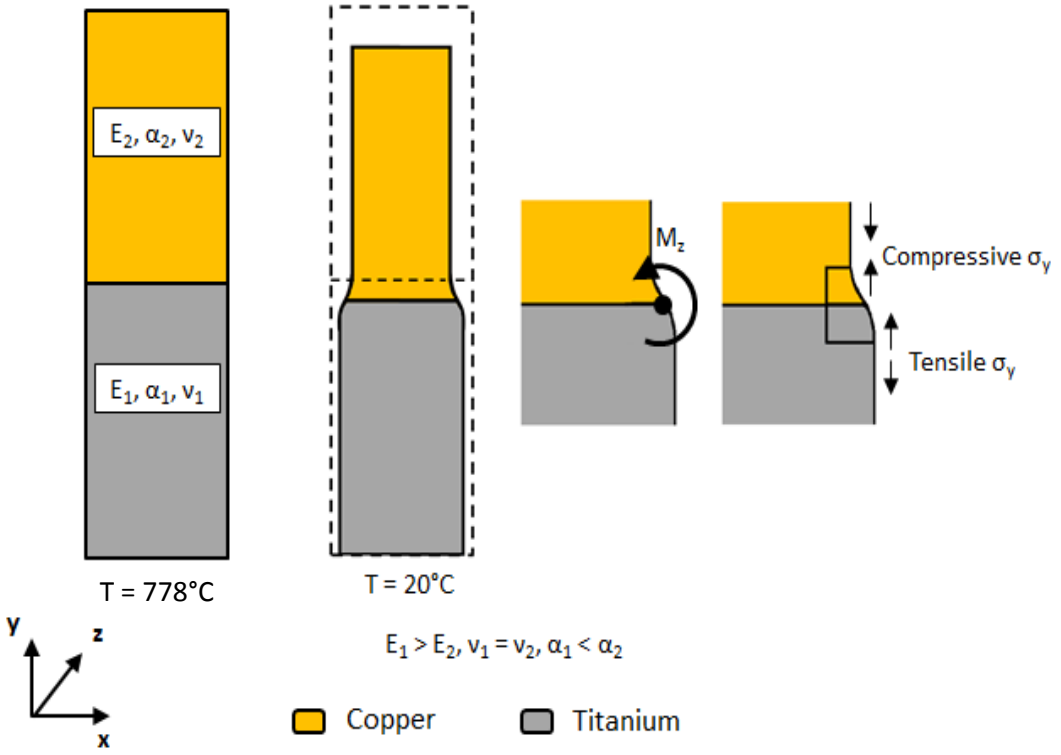

Figure 4-21 – Cu to Ti constraint mechanism

In this particular case, the constraint mechanism taking the braze layer into account, also predicts the development of tensile axial residual stresses in the Ti and compressive axial residual stresses in the Cu and this is briefly described. Over the brazing temperature range,

the Cu has a greatest coefficient of thermal expansion of the 3 materials in the joint (α_{Cu} = 19.6 x 10^{-6}), compared to both the braze layer ($\alpha_{72Ag\text{-}28Cu}$ = 16 x 10^{-6}), and the Ti (α_{Ti} = 10 x 10^{-6}). Considering the initial shape of the joint at the braze temperature of 778°C, when the joint is cooled to room temperature, at the Cu/72Ag-28Cu interface, the Cu will contract more than the 72Ag-28Cu due to its larger coefficient of thermal expansion. The compatibility constraint of the interface results in a deformed shape which will result in compressive stresses being developed in the Cu perpendicular to the interface based on the deformed shape. A similar argument can be used at Ti/72Ag-28Cu interface. In this instance the 72Ag-28Cu will contract more than the Ti due to its larger coefficient of thermal expansion resulting in tensile axial stress being developed in the Ti.

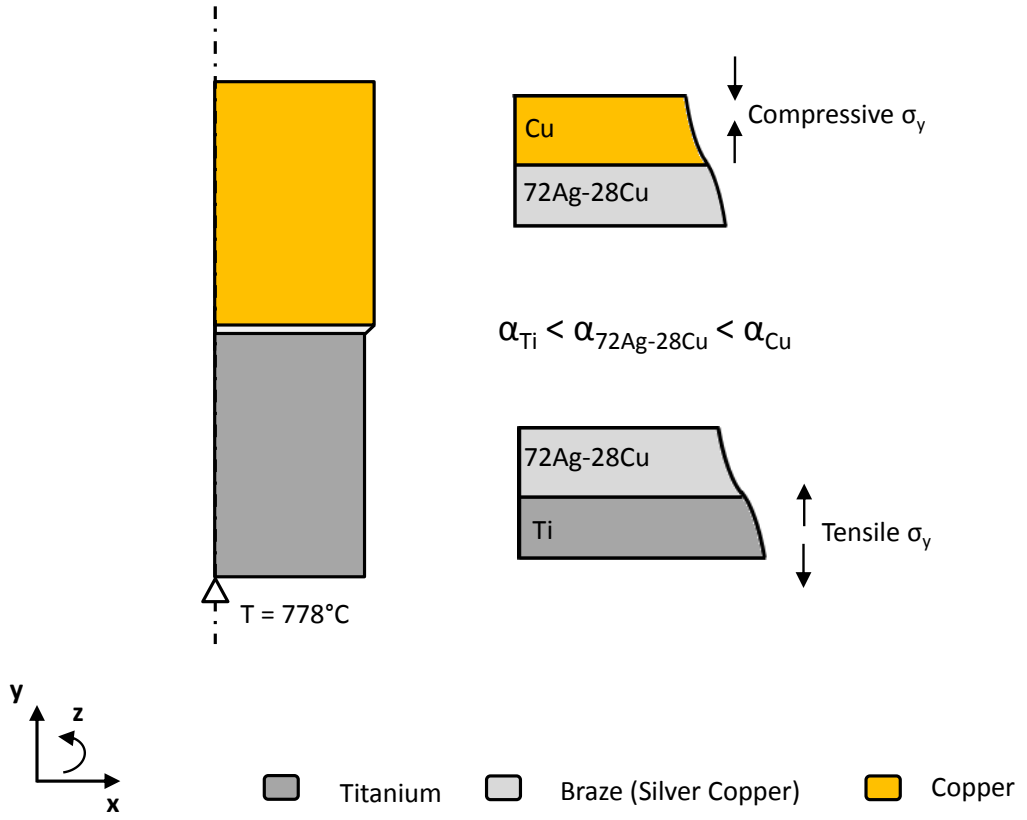

Figure 4-22 Ti/72Ag-28Cu/Cu constraint mechanism

As described in 3.6.1, the final stress distribution is a function of the properties of all three materials and not just the brazed layer and the parent materials.However in this case it is not obvious whether the relationship between the Cu and the Ti, or the parent materials and the 72Ag-28Cu braze layer which is dominating the final stress distribution.

However, measured residual stresses in dissimilar material brazed joints from previous research suggests that it is the relationship between the parent materials, and not between the parent materials and the braze, that dominates the final stress distribution and this is briefly summarised. Suganuma et al [128] measured the residual stress on the free edge of sintered silicon nitride (Si_3N_4) to Invar super alloy cylindrical and rectangular joints brazed with an aluminium braze filler. In this instance, the Al has a far greater coefficient of thermal expansion than both the Si_3N_4 and Invar. Based on the constraint mechanism presented in 3.2 between the braze and the parent materials, both parent materials should develop tensile axial residual stresses. However, based on the constraint between the Si_3N_4 and the Invar, it is expected that a tensile axial residual stress state is developed in the Si_3N_4 and a compressive stress state in the Invar super alloy (the Si_3N_4 has a lower coefficient of thermal expansion than the Invar super alloy across the brazing temperature range). The measured residual stress state along the free edge is shown below in Figure 4-23 and is in agreement with the stress state predicted by the constraint mechanism between the Si_3N_4 and the Invar and not the Al braze and the parent materials. Similar findings which show the final residual stress distribution is based on the relationships in coefficient of thermal expansion of the parent materials have been reported in various other experimental and analytical investigations [30], [125], [127], [129].

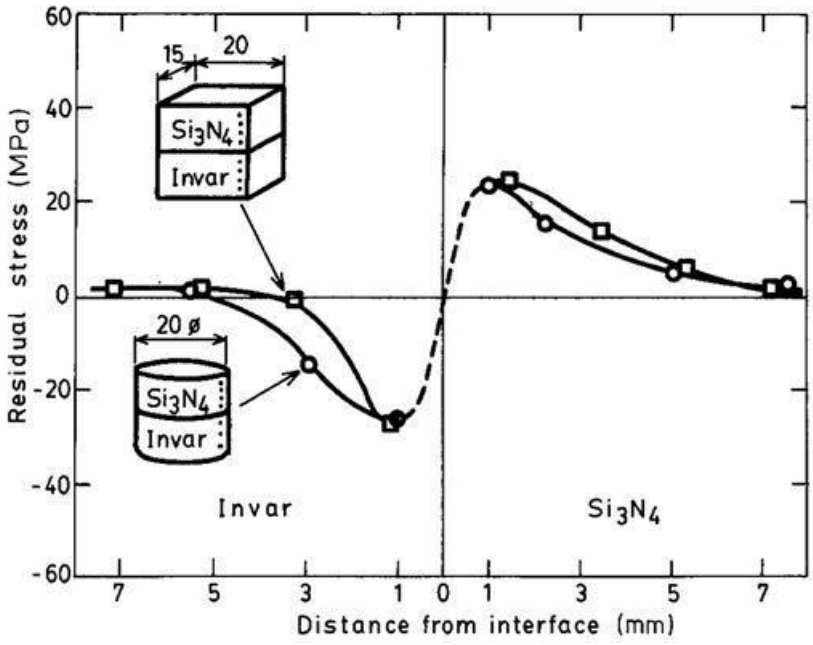

Figure 4-23 - Measured residual stresses on a silicon nitride to Invar super alloy brazed joint [128]

The failure of the joints away from the interface can also be explained by the development of damaging tensile residual stresses due to the relationship in thermal expansion coefficients between the parent materials. There are several examples from research into ceramic to steel joining as summarised in section 1.5.2. The Welding Institute [30] found that upon brazing a series of SiC/Alloy600 steel and SiC/304 steel samples failure occurred, either in the ceramic away from or through the interface. Similarly, Rohde et al [31], found cracks present in the ceramic close to the interface during cooling in ceramic to steel brazed joints. In both these cases the ceramic has a lower coefficient of thermal expansion than the adjoined grade of steel. Based on the constraint mechanism between the parent materials the ceramic should develop tensile residual stresses, and in these cases the stresses developed due to joining caused failure in the joint. This also explains the failure of the W in a W to steel brazed joint presented by Kalin [12].

These residual stresses due to joining can play a major role in determining the strength of brazed joints. This is especially true for ceramic-metal joints where the ceramic fails in a brittle manner as opposed to ductile manner, hence the presence of tensile residual stresses in the ceramic will reduce the strength of the joints and this has been shown in [32] [129] [34] [130]. However despite ceramics being brittle in nature, the mechanics of how these residual stresses develop (i.e the constraint on free thermal expansion and contraction) is the same. In addition these tensile residual stresses are also likely to reduce the fatigue performance of the joint. Due to the nature of these residual stresses they cannot be removed by stress relief. The next chapter of this thesis looks at a novel method of reducing these damaging tensile stresses based on post joining process, namely thermal autofrettage.

4.6 Summary

The work presented in this chapter shows that the residual stresses predicted by FEA in a cylindrical Ti/72Ag-28Cu/Cu brazed joint are in reasonable agreement with those measured using XRD. In this work the brazed layer has been included in the FEA, the material properties of which have been characterised in the as supplied condition neglecting any change in microstructure which occurs due to brazing. Work is ongoing to fully characterise the material properties of the brazed layer for use in FEA accounting for the changes in microstructure due to the brazing process [60].

The residual stresses measured by XRD at one angular location on sample 1 do not agree with FEA suggesting a lack of axisymmetry in this sample. It is postulated that this is due to either angular or axial misalignment of the particular sample. Future work in this area is focusing on developing an understanding of how misalignment will affect the residual stress distribution [124]. Additionally creep will also have an effect on the stresses developed in a dissimilar material joint however this has not been accounted for in this work and it is recommended that this be the topic for future research in this area. For this particular Ti/72Ag-28Cu/Cu brazed joint, a transient thermal stress analysis has shown that vacuum brazing process can simplify to a uniform cooling process.

Both FEA and XRD show the development of tensile residual stresses in the Ti. This can be explained by the relationship in material properties between the parent materials based on the constraint on free thermal contraction introduced in the previous chapter. Previous research has shown that for dissimilar material brazed joints with a similar relationship in material properties (such as ceramic or W brazed to stainless steel) that tensile residual stresses develop in the ceramic or W which can reduce the tensile and fatigue strength of such joints [32], [34], [129], [130]. The next chapter of this thesis looks at a novel method of reducing these damaging tensile stresses based on a post brazing process.

4.7 Appendix 4.1 - ANSYS log file for uniform cooling analysis

```
FINISH
/CLEAR,START
/GO
/Prep7

! Define Parameters in SI units (m/kg/s)
! Note initial dimensions at brazing temp

! Ti

h1=25.1895/1000
w1=7.05306/1000

! Cu

h2=25.37142/1000
w2=7.104/1000

! Aluminium Braze

h3=0.1/1000

x=5*h3
y=20*h3
n=2    ! Elements through braze

Tbraze=778
T1=20

! Create Geometry

k,,w1,
k,,,
k,,w2,h3
k,,,h3
a,1,2,4,3

k,,w1,-x
k,,,-x
a,5,6,2,1

k,,w1,-y
k,,,-y
a,5,6,8,7

k,,w1,-h1
k,,,-h1,
a,9,10,8,7

k,,w2,h3+x
k,,,h3+x
a,3,4,12,11

k,,w2,h3+y
k,,,h3+y
a,11,12,14,13

k,,w2,h2+h3
k,,,h2+h3
a,13,14,16,15

! Create Mesh

et,1,plane182
keyopt,1,3,1

et,2,plane183
keyopt,2,3,1

! Mesh Braze

lesize,2,,,n
lesize,4,,,n
lesize,1,,,w2*n/h3
lesize,3,,,w2*n/h3

mat,3
meshkey,1
mshape,0,
amesh,1

! Mesh Ti with Quads

Mat,1
lesize,5,,,w2*n/h3
lesize,6,,,x*n/h3
lesize,7,,,x*n/h3
meshkey,1
mshape,0,
amesh,2
lesize,9,,,w2*0.1*n/h3
lesize,11,,,w2*0.1*n/h3
lesize,12,,,(h1-y)*0.1*n/h3
lesize,13,,,(h1-y)*0.1*n/h3
meshkey,1
mshape,0
amesh,4

! Mesh Cu with Quads

Mat,2
lesize,15,,,w2*n/h3
lesize,14,,,x*n/h3
lesize,16,,,x*n/h3
meshkey,1
mshape,0,
amesh,5
lesize,18,,,w2*0.1*n/h3
lesize,21,,,w2*0.1*n/h3
lesize,20,,,(h2-y)*0.1*n/h3
lesize,22,,,(h2-y)*0.1*n/h3
meshkey,1
mshape,0
amesh,7

! Mesh Ti with Tris

type,2
mat,1
lesize,8,,,0.5*n/h3/1000,10
lesize,10,,,0.5*n/h3/1000,0.1
meshkey,1
mshape,1
amesh,3

! Mesh Cu with Tris

type,2
mat,2
lesize,19,,,0.5*n/h3/1000,0.1
lesize,17,,,0.5*n/h3/1000,10
```

```
meshkey,1
mshape,1
amesh,6

! Mat Properties

! Ti (Bottom)

MPTEMP,1,20,100,300,500,700,778
MPDATA,KXX,1,1,21,20,18,19,21,21
MPDATA,Dens,1,1,4500,4500,4500,4500,4500,4500
MPDATA,c,1,1,524,542,589,630,666,736
MPDATA,EX,1,1,109e9,105e9,93e9,81e9,69e9,65e9
MPDATA,PRXY,1,1,0.3,0.3,0.3,0.3,0.3,0.3
MPDATA,ALPX,1,1,8.5e-6,8.8e-6,9.1e-6,9.4e-6,9.8e-
6,10e-6
TB,BKIN,1,6,2,1
TBTEMP,20
TBDATA,,356e6,10.9e9,,
TBTEMP,100
TBDATA,,246e6,10.5e9,,
TBTEMP,300
TBDATA,,111e6,9.3e9,,
TBTEMP,500
TBDATA,,66e6,8.1e9,,
TBTEMP,700
TBDATA,,53e6,6.9e9,,
TBTEMP,778
TBDATA,,51e6,6.5e9,,

! Cu (Top)

MPTEMP,1,20,100,300,500,700,778
MPDATA,EX,2,1,125e9,121e9,109e9,96e9,83e9,77e9
MPDATA,KXX,2,1,386,385,380,368,354,348
MPDATA,Dens,2,1,9003,9003,9003,9003,9003,9003
MPDATA,c,2,1,383,393,413,429,446,455
MPDATA,PRXY,2,1,0.3,0.3,0.3,0.3,0.3
MPDATA,ALPX,2,1,16.7e-6,17e-6,17.8e-6,18.6e-6,19.3e-
6,19.6e-6
TB,BKIN,2,6,2,1
TBTEMP,20
TBDATA,,40e6,12.5e9,,
TBTEMP,100
TBDATA,,32.4e6,12.1e9,,
TBTEMP,300
TBDATA,,17.6e6,10.9e9,,
TBTEMP,500
TBDATA,,8.9e6,9.6e9,,,
TBTEMP,700
TBDATA,,5.9e6,8.3e9,,
TBTEMP,778
TBDATA,,6.4e6,7.7e9,,

! AgCu Braze

MPTEMP,1,20,100,300,500,700,778
MPDATA,EX,3,1,59.2e9,59.2e9,49.9e9,17.2e9,7.8e9,1e6
MPDATA,PRXY,3,1,0.3,0.3,0.3,0.3,0.3,0.3
MPDATA,KXX,3,1,493,495,460,440,413,404
MPDATA,Dens,3,1,10100,10100,10100,10100,10100,101
00
MPDATA,c,3,1,291,306,323,342,362,369
MPDATA,ALPX,3,1,15.3e-6,19.7e-6,21.3e-6,21.4e-
6,17.8e-6,16e-6
TB,BKIN,3,6,2,1
TBTEMP,20
TBDATA,,170e6,30e9,,
TBTEMP,100
TBDATA,,146.7e6,26.1e9,,
TBTEMP,300
TBDATA,,88.3e6,16.3e9,,
TBTEMP,500
TBDATA,,30e6,6.5e9,,
TBTEMP,700
TBDATA,,8.4e6,1.8e9,,
TBTEMP,778
TBDATA,,1e3,0.1e6,

! Set Ref temp and modify CTEs

tref,Tbraze
MPAMOD,1,20
MPAMOD,2,20
MPAMOD,3,20

! Apply Constraints

dk,10,UY,0

! Loads steps

/solu

OUTRES,ERASE
OUTRES,ALL,ALL
nlgeom,on

time,1
BFA,1,TEMP,T1
BFA,2,TEMP,T1
BFA,3,TEMP,T1
BFA,4,TEMP,T1
BFA,5,TEMP,T1
BFA,6,TEMP,T1
BFA,7,TEMP,T1
autots,on
DELTIM,0.1,1e-4,0.1
Solve
```

4.8 Appendix 4.2 - ANSYS log file for transient cooling analysis

```
FINISH
/CLEAR,START
/GO
/Prep7

! Define Parameters in SI units (m/kg/s)
! Note initial dimensions at brazing temp

! Ti

h1=25.1895/1000
w1=7.05306/1000

! Cu

h2=25.37142/1000
w2=7.104/1000

! Aluminium Braze

h3=0.1/1000

x=5*h3
y=20*h3
n=2 ! Elements through braze

Tbraze=778
T1=20

stefbolt=5.699*10**(-8)
t=0.1
nhour=8

! Create Geometry

k,,w1,
k,,,
k,,w2,h3
k,,,h3
a,1,2,4,3

k,,w1,-x
k,,,-x
a,5,6,2,1

k,,w1,-y
k,,,-y
a,5,6,8,7

k,,w1,-h1
k,,,-h1,
a,9,10,8,7

k,,w2,h3+x
k,,,h3+x
a,3,4,12,11

k,,w2,h3+y
k,,,h3+y
a,11,12,14,13

k,,w2,h2+h3
k,,,h2+h3
a,13,14,16,15

k,,,-0.5
k,,,
k,,1,-0.5,
k,,1,0.5
k,,,0.5
k,,,-0.5-t
k,,,
k,,1+t,-0.5-t,
k,,1+t,0.5+t
k,,,0.5+t

a,17,22,24,25,26,21,20,19,17

! Create Mesh

et,1,PLANE223
KEYOPT,1,1,11
KEYOPT,1,2,0
KEYOPT,1,3,1
KEYOPT,1,4,0

! Mesh Braze

lesize,2,,,n
lesize,4,,,n
lesize,1,,,w2*n/h3
lesize,3,,,w2*n/h3

mat,3
meshkey,1
mshape,0,
amesh,1

! Mesh Ti with Quads

Mat,1
lesize,5,,,w2*n/h3
lesize,6,,,x*n/h3
lesize,7,,,x*n/h3
meshkey,1
mshape,0,
amesh,2
lesize,9,,,w2*0.1*n/h3
lesize,11,,,w2*0.1*n/h3
lesize,12,,,(h1-y)*0.1*n/h3
lesize,13,,,(h1-y)*0.1*n/h3
meshkey,1
mshape,0
amesh,4

! Mesh Cu with Quads

Mat,2
lesize,15,,,w2*n/h3
lesize,14,,,x*n/h3
lesize,16,,,x*n/h3
meshkey,1
mshape,0,
amesh,5
lesize,18,,,w2*0.1*n/h3
lesize,21,,,w2*0.1*n/h3
lesize,20,,,(h2-y)*0.1*n/h3
lesize,22,,,(h2-y)*0.1*n/h3
meshkey,1
mshape,0
```

```
amesh,7

! Mesh Ti with Tris

mat,1
lesize,8,,,0.5*n/h3/1000,10
lesize,10,,,0.5*n/h3/1000,0.1
meshkey,1
mshape,1
amesh,3

! Mesh Cu with Tris

mat,2
lesize,19,,,0.5*n/h3/1000,0.1
lesize,17,,,0.5*n/h3/1000,10
meshkey,1
mshape,1
amesh,6

! Mesh Vacuum Vessel

Mat,4
esize,0.1
meshkey,1
mshape,0
amesh,8

! Mat Props

! Ti (Bottom)

MPTEMP,1,20,100,300,500,700,778
MPDATA,KXX,1,1,21,20,18,19,21,21
MPDATA,Dens,1,1,4500,4500,4500,4500,4500,4500
MPDATA,c,1,1,524,542,589,630,666,736
MPDATA,EX,1,1,109e9,105e9,93e9,81e9,69e9,65e9
MPDATA,PRXY,1,1,0.3,0.3,0.3,0.3,0.3,0.3
MPDATA,ALPX,1,1,8.5e-6,8.8e-6,9.1e-6,9.4e-6,9.8e-
6,10e-6
TB,BKIN,1,6,2,1
TBTEMP,20
TBDATA,,356e6,10.9e9,,
TBTEMP,100
TBDATA,,246e6,10.5e9,,
TBTEMP,300
TBDATA,,111e6,9.3e9,,
TBTEMP,500
TBDATA,,66e6,8.1e9,,
TBTEMP,700
TBDATA,,53e6,6.9e9,,
TBTEMP,778
TBDATA,,51e6,6.5e9,,

! Cu (Top)

MPTEMP,1,20,100,300,500,700,778
MPDATA,EX,2,1,125e9,121e9,109e9,96e9,83e9,77e9
MPDATA,KXX,2,1,386,385,380,368,354,348
MPDATA,Dens,2,1,9003,9003,9003,9003,9003,9003
MPDATA,c,2,1,383,393,413,429,446,455
MPDATA,PRXY,2,1,0.3,0.3,0.3,0.3,0.3
MPDATA,ALPX,2,1,16.7e-6,17e-6,17.8e-6,18.6e-6,19.3e-
6,19.6e-6
TB,BKIN,2,6,2,1
TBTEMP,20
TBDATA,,40e6,12.5e9,,
TBTEMP,100
TBDATA,,32.4e6,12.1e9,,
TBTEMP,300
TBDATA,,17.6e6,10.9e9,,
TBTEMP,500
TBDATA,,8.9e6,9.6e9,,,
TBTEMP,700
TBDATA,,5.9e6,8.3e9,,
TBTEMP,778
TBDATA,,6.4e6,7.7e9,,

! AgCu Braze

MPTEMP,1,20,100,300,500,700,778
MPDATA,EX,3,1,59.2e9,59.2e9,49.9e9,17.2e9,7.8e9,1e6
MPDATA,PRXY,3,1,0.3,0.3,0.3,0.3,0.3,0.3
MPDATA,KXX,3,1,493,495,460,440,413,404
MPDATA,Dens,3,1,10100,10100,10100,10100,10100,101
00
MPDATA,c,3,1,291,306,323,342,362,369
MPDATA,ALPX,3,1,15.3e-6,19.7e-6,21.3e-6,21.4e-
6,17.8e-6,16e-6
TB,BKIN,3,6,2,1
TBTEMP,20
TBDATA,,170e6,30e9,,
TBTEMP,100
TBDATA,,146.7e6,26.1e9,,
TBTEMP,300
TBDATA,,88.3e6,16.3e9,,
TBTEMP,500
TBDATA,,30e6,6.5e9,,
TBTEMP,700
TBDATA,,8.4e6,1.8e9,,
TBTEMP,778
TBDATA,,1e3,0.1e6,

! Vacuum Furnace

MPTEMP,1,20,100,300,500,700,778
MPDATA,KXX,4,1,1,1,1,1,1,1
MPDATA,EX,4,1,200e9,200e9,200e9,200e9,200e9,200e9
MPDATA,PRXY,4,1,0.3,0.3,0.3,0.3,0.3,0.3
MPDATA,ALPX,4,1,0,0,0,0,0,0

/ Solu

! Defining the Radiating Surfaces

SFL,21,RDSF,0.05, ,1,
SFL,22,RDSF,0.05, ,1,
SFL,19,RDSF,0.05, ,1,
SFL,16,RDSF,0.05, ,1,
SFL,4,RDSF,0.31, ,1,
SFL,7,RDSF,0.31, ,1,
SFL,10,RDSF,0.31, ,1,
SFL,13,RDSF,0.31, ,1,
SFL,11,RDSF,0.31, ,1,
SFL,30,RDSF,1, ,1,
SFL,29,RDSF,1, ,1,
SFL,28,RDSF,1, ,1,

! Define solution Options

STEF,stefbolt        ! Stefan-Boltzmann constant
TOFFST,273           ! Offset tempertures to
absolute zero
RADOPT,,,,,,,
SPCNOD,1,460
```

```
! Defining View Factor Options

HEMIOPT,,
V2DOPT,1,,,
VFOPT,NEW,,,,

! Initial Coniditions

ANTYPE,4

tref,Tbraze
MPAMOD,1,20
MPAMOD,2,20
MPAMOD,3,20
MPAMOD,4,20
TUNIF,Tbraze
ASEL,s,area,,8
nsla,s,1
IC,all,temp,T1
allsel,all,all
dk,10,UY,0

! Solution controls

OUTRES,ERASE
outres,all,all
nropt,full
lumpm,0

! Initial cooling

time,36
ASEL,s,area,,8
nsla,s,1
kbc,1
D,ALL,TEMP,T1
allsel,all,all
deltim,0.5,0.5,0.5
autots,on
lswrite,1

! Remainder of cooling

time,nhour*3600
ASEL,s,area,,8
nsla,s,1
kbc,1
D,ALL,TEMP,T1
allsel,all,all
deltim,30,30,100
autots,on
lswrite,2

lssolve,1,2
```

4.9 Appendix 4.3 – Calculation of the standard uncertainty in residual stress measurements due to results repeatability

To calculate the standard uncertainty in the residual stress measurements due to the repeatability of the results, three repeat tests have been performed at the same location on one of the readings taken on the Ti/72Ag-28Cu/Cu brazed joint sample. Each measurement was taken without removing the sample between successive tests hence this gives an indication of the "instrument-only repeatability" [118] and does not account for any variability in the test set up. This approach is valid as measurements were performed on each sample without removing the sample from the machine or altering the machine set up in any way.

The result for each of the measurements and the standard deviation of the measurements are given in Table 4-7:

Result set	σ_y (MPa)	σ_z (MPa)
1	30.0	53.2
2	30.9	50.5
3	30.3	48.3
Standard deviation, s	0.5	2.5

Table 4-7 - Repeatability of residual stress measurements

The standard uncertainty in the σ_y stress reading due to the instrument only uncertainty in is therefore [118]:

$$u_{\sigma_y} = \frac{s}{\sqrt{n}} = \frac{0.5}{\sqrt{3}} = 0.3MPa$$

Where n equals the number of readings (3 in this instance). In a similar fashion the standard uncertainty in the σ_z readings is therefore:

$$u_{\sigma_z} = \frac{s}{\sqrt{n}} = \frac{2.5}{\sqrt{3}} = 1.4MPa$$

These results are of a similar order of magnitude as other reported instrument only repeatability uncertainties [118]. For all combined uncertainty calculations a value of 1.4MPa has been assumed for the instrument only repeatability which represents a worst case out of the two values calculated values.

4.10 Appendix 4.4 – Uncertainty in residual stress measurement calculation using XRD

Consider the residual stress measurement at location 1 in table 4.5. The axial residual stress value from the post processing software is -127.4MPa ± 23.6MPa.

Hence the standard uncertainty due to the strain is:

$$u = \frac{c_i u(x_i)}{d_v} = \frac{1 \times 23.6}{\sqrt{3}} = 13.6MPa$$

Assuming the Young's modulus used in the stress calculation is within 10% of the real value, the standard uncertainty due to any error in Young's modulus is:

$$u = \frac{c_i u(x_i)}{d_v} = \frac{127.4 \times 0.1}{\sqrt{3}} = 7.4MPa$$

Hence the combined standard uncertainty is the route mean square of both standard uncertainties in the strain reading, Young's modulus and results repeatability:

$$u_c = \sqrt{(13.6^2 + 7.4^2 + 1.4^2)} = 15.55MPa$$

The combined uncertainty U is given by:

$$U = k.u_c = 2 \times 15.55 = 31.1MPa$$

Hence the estimated residual stress value is -127.4 ± 31.1MPa based on a coverage factor of 2, which corresponds to a confidence level of approximately 95%.

5 Thermal autofrettage of dissimilar material joints

5.1 Introduction

As highlighted in section 1.5, the residual stresses developed in dissimilar material brazed joints due to the joining process can be large and result in failure of the joint. The previous chapter of this thesis showed that FEA can be used to predict the residual stresses in a simple cylindrical Ti/72Ag-28Cu/Cu brazed joint and that due to relationships in parent material properties, the Ti develops a tensile axial and hoop residual stress along the free edge, with the Cu developing a compressive axial and hoop stress.

In a similar fashion to the Ti/72Ag-28Cu/Cu joint, due to a similar relationship in material properties, for a range of brazed joints between a brittle material and a ductile material (such as W to EP-450 ferritic/martensitic steel [12], SiC ceramic to 304 or Alloy 600 steel [30] and Si_3N_4 ceramic to Invar or Kovar [128]) the W / ceramic develops tensile axial and hoop residual stresses, with the stainless steel developing compressive axial and hoop residual stresses. The presence of these tensile residual stresses in a brittle material is undesirable and could reduce both the fatigue and ultimate strength of the joint. Due to the difference in material properties, stress relieving of these residual stresses in unlikely to be effective.

The aim of this chapter is to investigate a post-joining process, namely thermal autofrettage, to reduce the potentially damaging tensile residual stresses that exist in a dissimilar material brazed joint due to the joining process. This involves cooling the joint after brazing to utilise elastic unloading to reduce the tensile residual stresses developed during joining. A detailed literature and patent search has not highlighted any research in this area before, hence this idea is new and provides an original contribution to knowledge for dissimilar material joints.

The mechanism of thermal autofrettage is described in relation to the mechanical autofrettage process used to increase the durability of pressure vessels. FEA of the thermal autofrettage process has been conducted on both an idealised dissimilar material brazed joint without a brazed layer between an idealised ductile and brittle material and also in a real dissimilar material joint, namely the simple Ti/72Ag-28Cu/Cu joint which formed the basis of the investigation in residual stresses in the previous section. The effect of thermal

autofrettage on the residual stresses measured on the Ti/72Ag-28Cu/Cu brazed joint is also investigated.

It should be noted that the thermal autofrettage process is not limited to brazing as a process of joining dissimilar materials. The mechanism described is likely to work for other methods of joining dissimilar materials such as diffusion bonding, HIPing, electron beam welding and explosion welding. However the simple cylindrical Ti/72Ag-28Cu/Cu dissimilar material brazed joint used in chapters 2 and 4 of this thesis has been the focus of this investigation in this thesis.

5.2 Thermal autofrettage of dissimilar material joints

Autofrettage is a process that is used to increase the load carrying capability and fatigue resistance of gun barrels and pressure vessels by loading the structure beyond yield. One of the things that autofrettage does is induce beneficial residual stresses which can improve fatigue and enhance the yield stress. The process of inducing compressive residual stresses by exceeding yield is highlighted in the following example [131] and a description of how this mechanism can be applied to dissimilar material joints is presented.

Considering an elastic-perfectly plastic rectangular cross-section beam loaded by a pure moment, M. Yield occurs in the outer fibres of the beam when the applied moment M, equals the yield moment, M_{yield}, which using engineers theory of bending results in a stress on the out fibre of σ_{yield}. This moment is then increased to 1.5 x M_{yield} plastic strains developing on the outer fibre of the beam through the thickness. (Note: an applied moment of 1.5 x M_{yield} corresponds to the limit load for a rectangular beam. In reality the autofrettage loads are generally far less than the limit load of the material). If this applied moment is then removed, local elastic unloading occurs parallel to the original elastic loading line as shown in Figure 5-1. Using the theory of beam bending the stress on the outer fibre does not return to zero when a moment of 1.5 x M_{yield} is removed, but a residual stress of -0.5 x σ_{yield} develops in the outer fibres. The graphs of applied moment and local stress on the extreme tensile fibre throughout this process are shown in Figure 5-1.

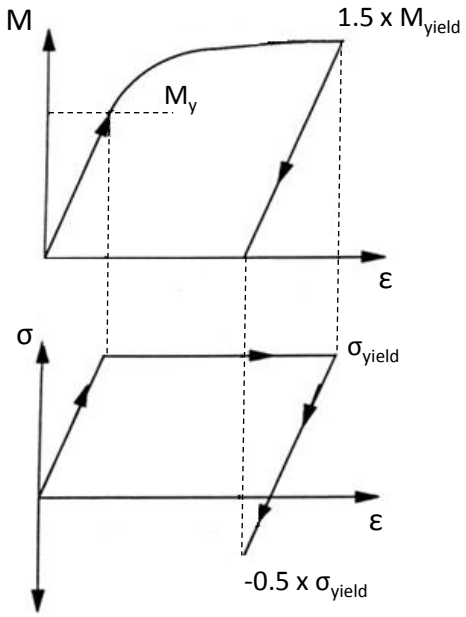

Figure 5-1 – Moment and stress on outer fibre of elastic perfectly plastic beam in bending with an applied moment of 1.5 x M_{yield} [131]

Due to the linear unloading, the stress distribution across section at limit load can be taken as the starting point to superimpose the unloading stresses to calculate the residual stress state as shown below in Figure 5-2.

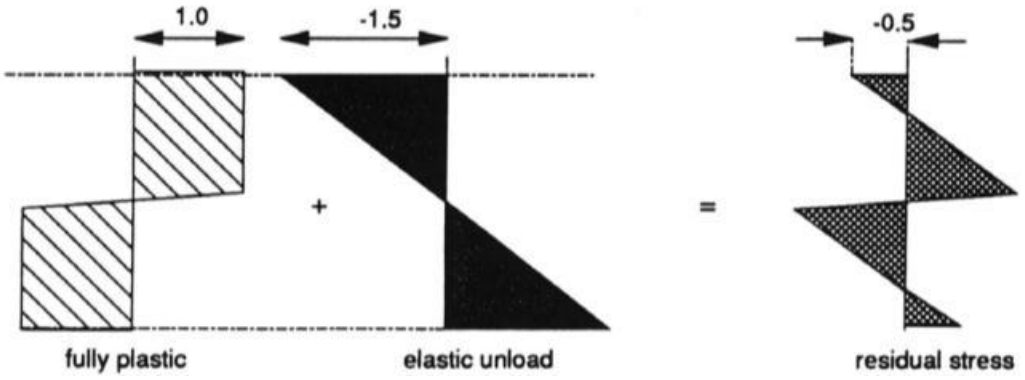

Figure 5-2 – Stress distribution across of beam in bending with an applied moment of 1.5 x M_{yield} [131]

The effect of this self-equilibrating residual stress distribution is to extend the elastic range by 50% and induce beneficial compressive residual stresses on the surface of the beam. This surface compressive residual stress will result in improved fatigue performance as upon application of a subsequent applied moment the mean stress will be reduced.

This principle of over loading a structure to induce a beneficial compressive residual stress distribution can be used to reduce the tensile residual stresses that can be found in dissimilar material joints due to the joining process. This can be achieved by continuing to cool the joint after brazing by storing the brazed sample in either a cryogenic freezer or liquid nitrogen once it has cooled to room temperature. Consider the example shown in Figure 5-3 which highlights the thermal autofrettage of a dissimilar material brazed joint. In this example, an elastic material 2 (i.e. is assumed not to yield for the purpose of this illustration) is being brazed to an elastic-perfectly plastic material 1. Material 1 is assumed to have a greater coefficient of thermal expansion than material 1 and hence a lower Young's modulus based on the relationship described in Figure 2-11. Without using specific values this relationship in material properties is representative of a brittle material such as ceramic or W (material 2) being brazed to a ductile material such as stainless steel or Cu (material 1). Figure 5-4 shows the development of the axial stress state in the region of the joint for both material 1 and material 2.

Initially, both materials are at a stress free state at the brazing temperature of 800°C (a). During cooling from the brazing temperature of 800°C to room temperature (b), the constraint of the interface due to the differential thermal expansion as described in the section 3.2 causes a compressive axial residual stress to develop in material 1, with a tensile residual stress developing in material 2. During cooling to room temperature, plasticity develops in material 2 in close proximity to the interface. When an elastic–perfectly plastic material model is assumed for material 1, upon yielding the stiffness of material 1 reduces to zero, hence no additional constraint can be applied to the joined material 2. This yielding effectively caps the stress in both materials.

After cooling to room temperature the sample is then slowly cooled in liquid nitrogen to -196°C (c). During this process, further plasticity develops in material 1, however no additional constraint is applied to material 2 due to the zero stiffness of material 1. Hence the stress in material 2 during this process remains constant. The joint is then heated back up to room temperature (d). During this process both materials unload elastically causing a change in the stresses in both materials. For real dissimilar material brazed joints such as those between ceramic and steel this will result in a reduction in tensile residual stresses in the ceramic which could improve both the fatigue and tensile strength of the joint.

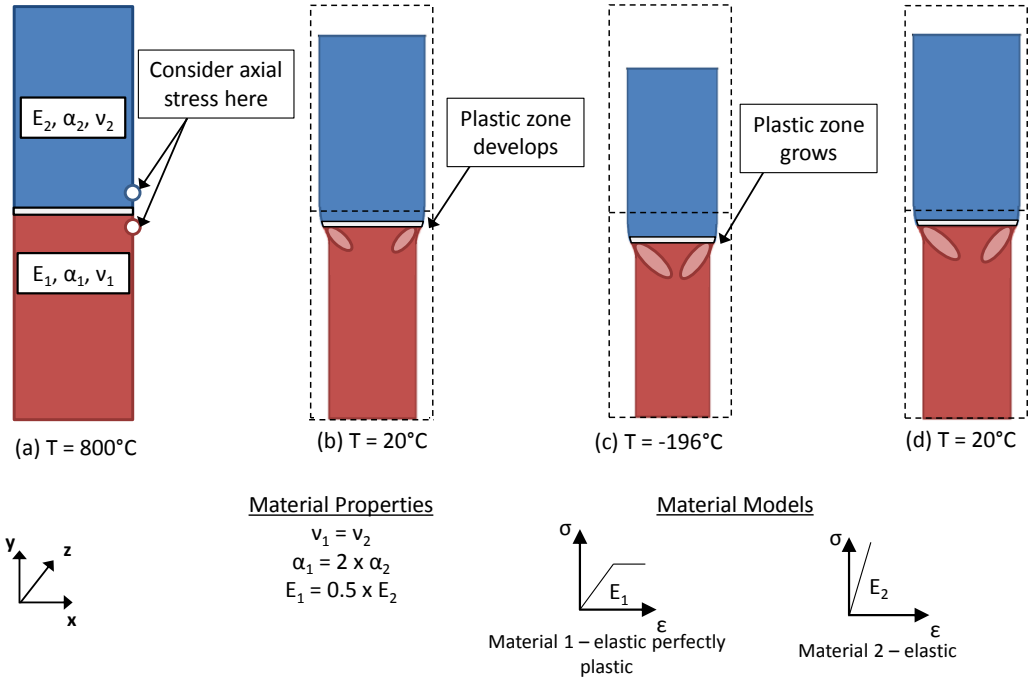

Figure 5-3 - Thermal autofrettage of a dissimilar material brazed joint

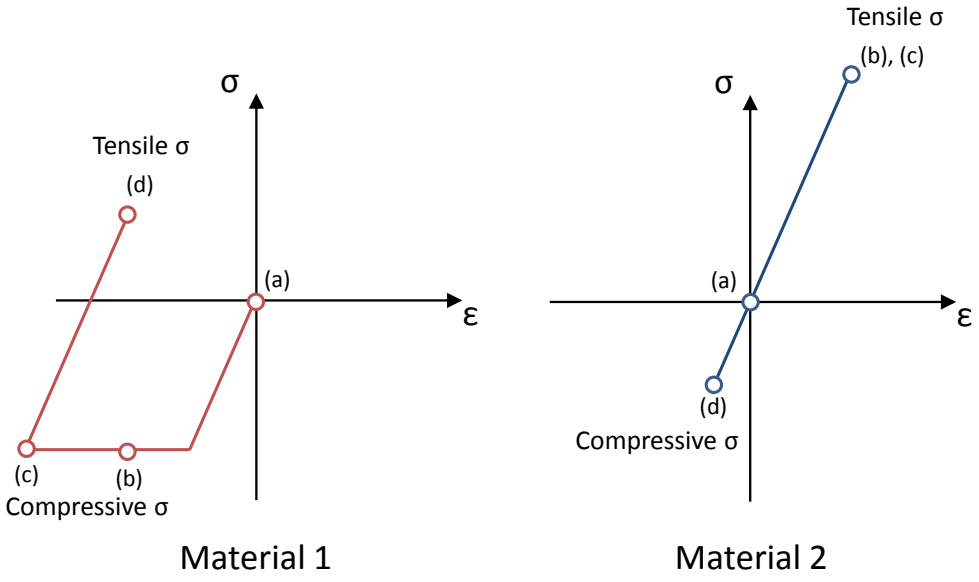

Figure 5-4 – Stress – strain response in materials 1 and 2 during thermal autofrettage

A slow cooling rate avoids quenching the sample which could result in large tensile residual stresses developing on the surface of the sample. Consequently the thermal autofrettage procedure developed for the experimental investigation in this chapter involves insulating the samples in low thermal conductivity polyethylene foam prior to storage in liquid nitrogen. The insulated samples are then wrapped in cling film to avoid the liquid nitrogen saturating the foam hence the only mode of heat transfer from the sample is due to conduction. One of the insulated samples prior to thermal autofrettage is shown below in Figure 5-5:

Figure 5-5 - Insulated sample for thermal autofrettage to -196°C in liquid nitrogen

5.3 FEA of thermal autofrettage of dissimilar material joints

The thermal autofrettage process has been investigated for two separate cases using FEA. One of these cases is of a simple plane stress 90° dissimilar material butt joint neglecting the presence of the brazed layer and any temperature variation in material properties. The other case analysed is of the real Ti/72Ag-28Cu/Cu cylindrical brazed joint with the brazed layer included which formed the basis of the investigation in the previous chapter. The results for both of these cases are presented below.

5.3.1 FEA of thermal autofrettage of an idealised dissimilar material joint

FEA has been used to establish the effect of thermal autofrettage on the idealised dissimilar material joint between an elastic material and elastic-perfectly plastic material shown in

Figure 5-6. The analysis has been performed using ANSYS 12.1, using two dimensional PLANE182 4-noded structural solid elements and the direct sparse matrix solver. The mesh is refined to an element size of 0.25mm at the interface and the model is constrained in the vertical direction by constraining the bottom surface to have zero vertical displacement. Plane stress conditions are assumed.

In this simple case, the properties of both materials remain constant for all temperatures. The material properties have been chosen to represent a relationship similar to those found in a range of applications (e.g ceramic to steel, W to steel, W to Cu). This idealised joint, which neglects the presence of the brazed layer, is initially at a stress free temperature of 800°C and is uniformly cooled to 20°C. The sample is then uniformly thermally autofrettaged to -196°C (representing cooling in liquid nitrogen) and finally returned to room temperature.

The change in axial stress at each location in the thermal cycle is shown in Figure 5-7. Upon cooling from the brazing temperature of 800°C to 20°C, the brittle material 2 develops a high tensile axial residual stress, with elastic-perfectly plastic material 1 developing a compressive axial residual stress which is as expected based on the constraint mechanism described in section 3.2 of this thesis. The effect of the elastic-perfectly plastic material model for material 1 can clearly be seen as the compressive stress is capped in material 1; close to the interface at -200MPa. During the cooling to -196°C the plastic zone in material 1 grows slightly, however no additional constraint is applied to the material 2 hence the axial residual stress distributions are almost identical at these two temperatures. However during subsequent heating back to 20°C from -196°C there is a clear reduction in the residual stresses in both materials. The largest reduction occurs in the brittle material 1 however in this instance the level of thermal autofrettage is not large enough to induce a compressive residual stress in this material. Such a reduction in tensile residual stress could be very beneficial however.

This simple model of an idealised plane stress dissimilar material joint is clearly showing that the process of thermal autofrettage reduces the residual stresses in both materials due to joining which could improve both the fatigue life and strength of the joint. This simulation however fails to account for the presence of the brazed layer, temperature dependent material properties of all 3 materials and any three dimensional effects which could occur in a real dissimilar material brazed joint.

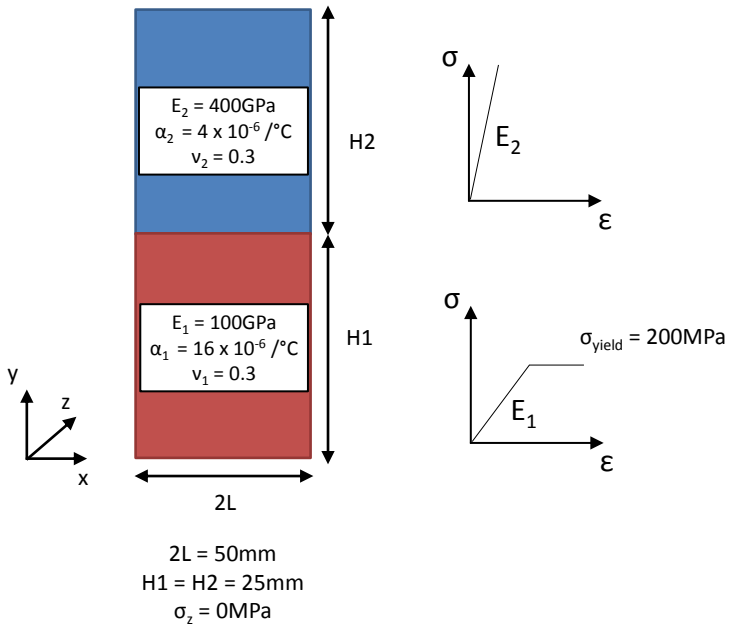

Figure 5-6 – Idealised dissimilar material joint for thermal autofrettage

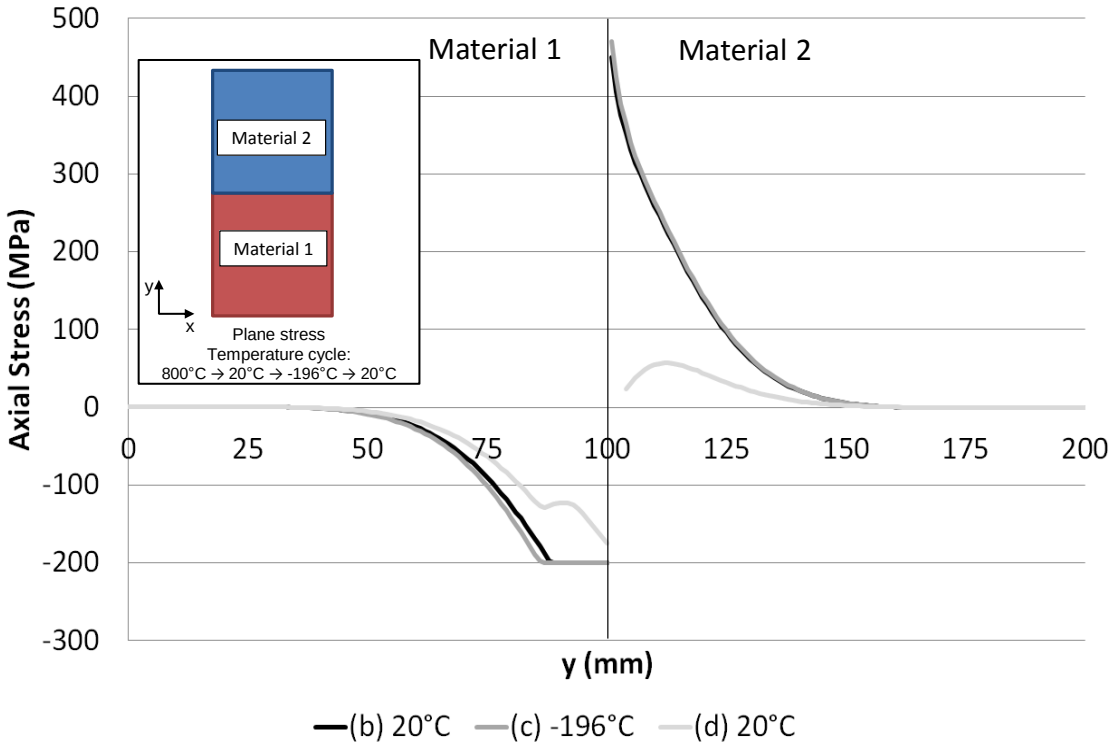

Figure 5-7 – Axial stress distributions during thermal autofrettage cycle

5.3.2 FEA of thermal autofrettage of a real dissimilar material brazed joint

The analysis in 5.3.1 has shown the thermal autofrettage process works for an idealised plane stress dissimilar material joint between an elastic material and elastic-perfectly plastic material. This analysis has not taken into account the presence the brazed layer, strain hardening and temperature dependent material properties of all materials and any 3D effects that could occur in a real structure. Consequently, the process of thermal autofrettage has been investigated on the Ti/72Ag-28Cu/Cu joint used in the previous chapter. The previous chapter of this thesis has shown that the residual stresses predicted by FEA are in reasonable agreement with those measured using XRD and that any transient effects due to differences in emissivity and thermal conductivity are negligible. Hence the FEA model used in chapter 4 to predict the residual stress distribution in the cylindrical Ti/72Ag-28Cu/Cu brazed joint has been modified to include the thermal autofrettage process as shown schematically in Figure 5-8.

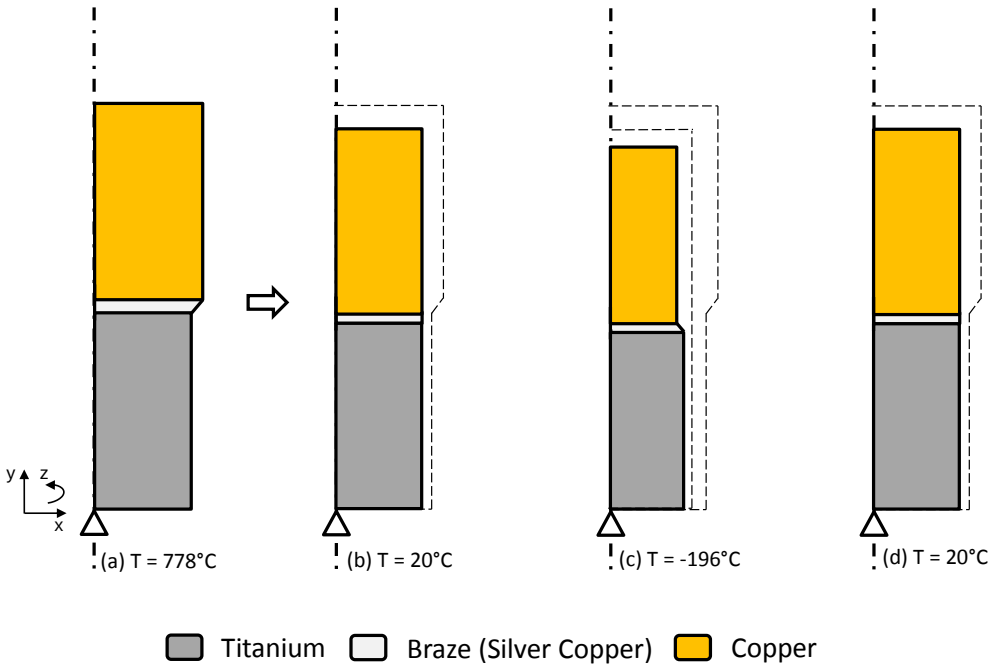

Figure 5-8 - Thermal autofrettage of Ti/72Cu-28Ag/Cu dissimilar material brazed joint

A transient thermal analysis of the thermal autofrettage process of the insulated sample starting at room temperature (not presented in this thesis) has shown that the sample takes c. 1 hour to reach a uniform temperature of -196°C with a max cooling rate of -12°C/min. This cooling rate is based on the heat transfer coefficient between the

polyethylene foam and liquid nitrogen being evaluated at film temperature of -196°C. In terms of predicting the cooling rate this represents a worst case scenario as it neglects any air pockets in the cling film and over predicts the heat transfer coefficient. This maximum cooling rate of -12°C is considerably less than the initial cooling rate of the brazing process of c.-150C/min (calculated from initial slope of Figure 4-12), hence it assumed that any transient effects during the thermal autofrettage process can be ignored. Consequently a simplified thermal stress analysis has been adopted where the temperature varies uniformly during the brazing and thermal autofrettage process, neglecting any variation in temperature.

If a small air gap of 1mm between the cling film and polyethylene foam is assumed and the heat transfer is evaluated at an average film temperature of -87.5°C, the time taken to reach a uniform temperature of -196°C increases to c.8 hours. In reality the time required to reach -196°C will be less than this. Hence, to ensure steady state thermal conditions are reached during the thermal autofrettage, the samples were stored in liquid nitrogen for c.8hours and this will ensure steady state conditions are established.

To model the thermal autofrettage in liquid nitrogen to -196°C the material properties of the Cu, Ti and 72Ag-28Cu have been included in the model in addition to the properties listed in tables 4-1, 4-2 and 4-3. The properties of the Cu and Ti at this temperature have been obtained from various literature sources [111], the properties of the 72Ag-28Cu have been linearly interpreted in a similar fashion to the other assumed properties as described in section 4.3 based on there being no phase changes within this temperature range. The properties of all materials at –196°C for use in FEA are summarised in Table 5-1. Note: the log file for this analysis is identical to that in appendix 4.1 with the additional material property data at -196°C and load steps for the thermal autofrettage process included.

Material	$\alpha \times 10^{-6}$ (/K)	E (GPa)	σ_{yield} (MPa)	E_{tan} (GPa)
Ti	6.5	123	556	0.1 x E
Cu	14	136	66	0.1 x E
72Ag-28Cu	15.3	59.2	220	40

Table 5-1 – Material properties at thermal autofrettage temperature of -196°C

The axial and circumferential residual stress distributions at the various stages of the thermal autofrettage process are shown in Figure 5-9 and Figure 5-10 respectively. Upon cooling from the melting temperature of the 72Ag-28Cu (778°C) the residual stress field

developed is as described in the previous chapter (b). The change in axial stress due to cooling to -196°C (c) and then subsequent heating to back to 20°C (d) are also shown.

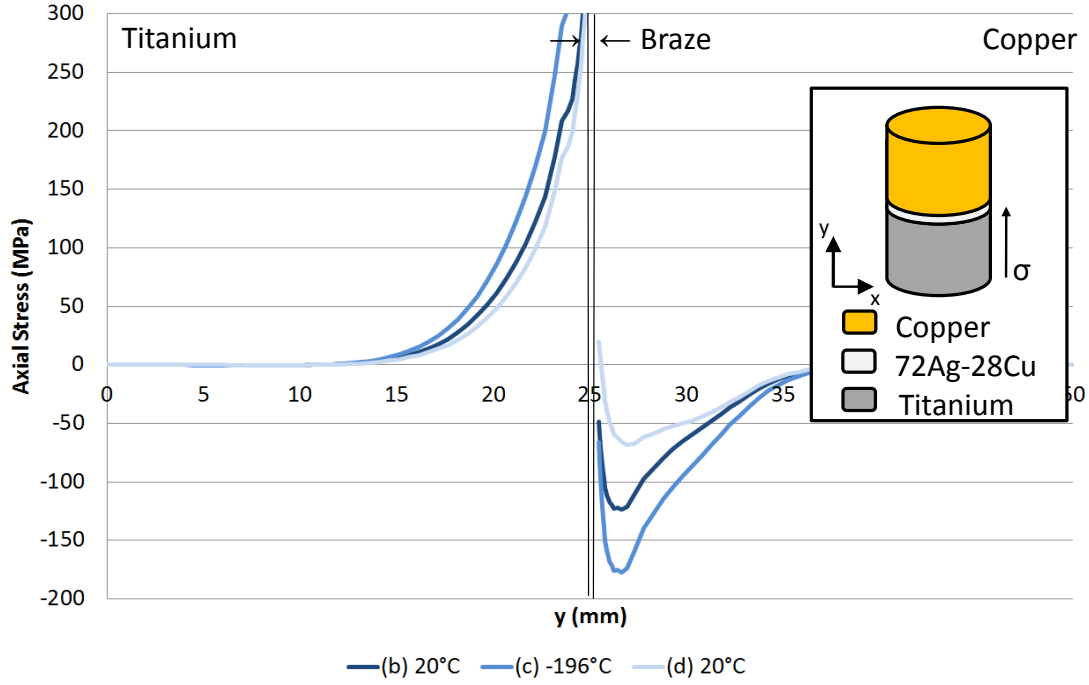

Figure 5-9 – Axial stress distributions during thermal autofrettage cycle and return to room temperature of Ti/72Ag-28Cu/Cu brazed joint

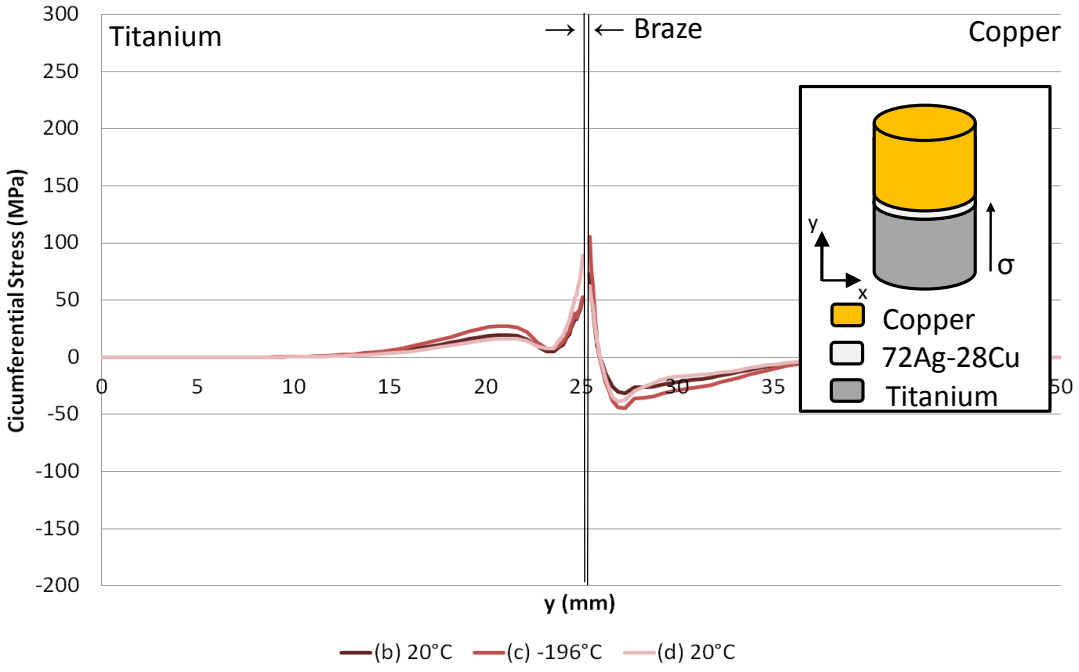

Figure 5-10 - Circumferential stress distributions during thermal autofrettage cycle and return to room temperature of Ti/72Ag-28Cu/Cu brazed joint

The results in Figure 5-9 show a small decrease in the axial tensile residual stress field in the Ti due to the thermal autofrettage and a small increase in the axial residual stress in the Cu. As described in section 3.6.1, the stress state developed during brazing and thermal autofrettage will be a function of the relationship in properties of all three materials in the joint. However, it is postulated that the thermal autofrettage process has not been successful in causing a significant reduction in the initial residual stress state in the Ti due to strain hardening in the brazed layer (as shown in the engineering stress strain curve for the braze at room temperature and -196°C in Figure 5-11). The effectiveness of autofrettage in general is dependent on the development of plastic strains (i.e if the beam in section 5.2 remained elastic, compressive residual stresses would not develop when the applied moment is removed). Hence, it is further postulated that if the 72Ag-28Cu braze filler had both a lower yield stress and behaved in an elastic-perfectly plastic fashion, the thermal autofrettage process would be more effective in changing the initial residual stress distributions in both materials. In addition to enhancing the effectiveness of the thermal autofrettage process, this change in material behaviour should also reduce the magnitude of the initial residual stress distribution. The next section investigates this case, when the 72Ag-28Cu braze material has both a lower yield stress and behaves in elastic-perfectly plastic fashion.

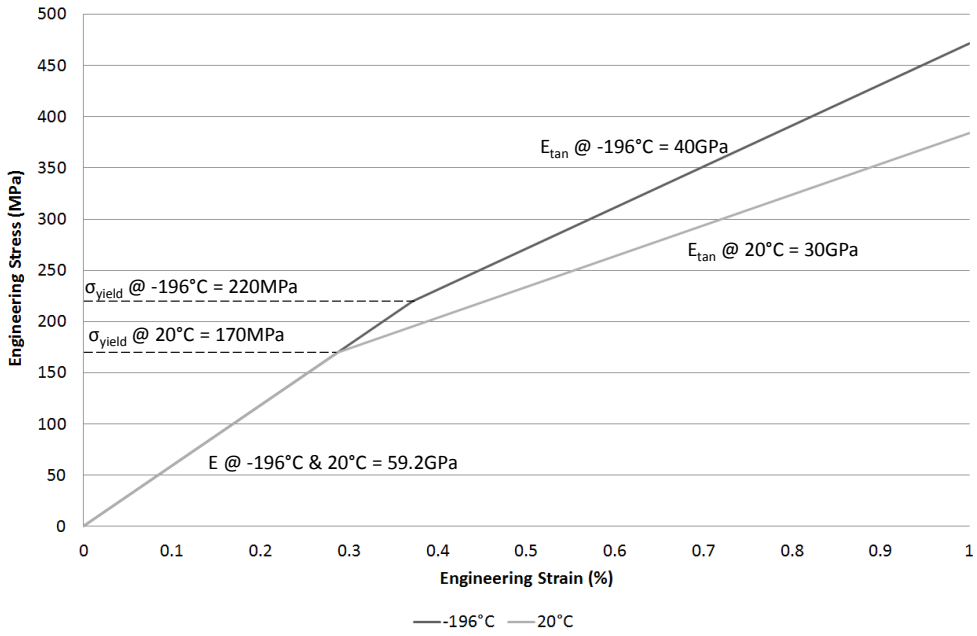

Figure 5-11 – Engineering stress strain curves for 72Ag-28Cu at -196°C and 20°C

5.3.3 FEA of thermal autofrettage of a dissimilar material brazed joint with an elastic-perfectly plastic braze

FEA of the thermal autofrettage process of a Cu-Ti dissimilar material brazed joint with an elastic-perfectly plastic braze material with a lower yield stress than the original 72Ag-28Cu has been investigated. Both the model set up and material properties for all three materials are identical to those used in the Ti/72Ag-28Cu/Cu joint used in section 5.3.2, the only difference being the yield stress and post yield stiffness of the braze filler. In this case a tangent modulus of 0.01GPa (not 0GPa to aid convergence) is used across all temperatures and the initial yield stress value for the braze in Table 4-1 and Table 5-1 have been halved. For this case the free edge axial and circumferential stress distributions are shown during the thermal autofrettage process in Figure 5-12 and Figure 5-13 respectively.

As shown in Figure 5-12, the initial axial residual stress (b) distribution with the elastic-perfectly plastic braze is similar to that with the 72Ag-28Cu braze however the magnitude of the residual stresses in both materials is less compared to the real 72Ag-28Cu braze as shown in Figure 5-9. This is due to the reduced constraint applied by the elastic-perfectly plastic braze with a lower yield stress and is in agreement with the findings discussed in paragraph 2 of section 3.6.1 . Upon thermal autofrettage to -196°C, a slight increase in this residual stress distribution is seen due to a slight increases in the yield stress of the braze, which applies an additional constraint to the Ti and the Cu. This is not apparent in the simplified case shown in Figure 5-7 as the yield stress for material 1 is assumed constant across the temperature range.

Upon heating back up to room temperature (c) the thermal autofrettage process almost completely alleviates the axial residual stresses developed in the joint due to brazing (c. 100MPa stress relief in both materials in the region of the interface). This reduction is greater than the reduction seen in Figure 5-9 which suggests an improvement in the autofrettage process due to the reduced yield stress and strain hardening of the braze. In a similar fashion to the Ti/72Ag-28Cu/Cu dissimilar material joint in Figure 5-10 there is a negligible difference in the circumferential stress distribution for this specific case.

Hence this analysis shows a reduction in both the yield stress and the post yield strain hardening is effective in reducing the residual stresses due to joining and the improving the effectiveness of the thermal autofrettage process.

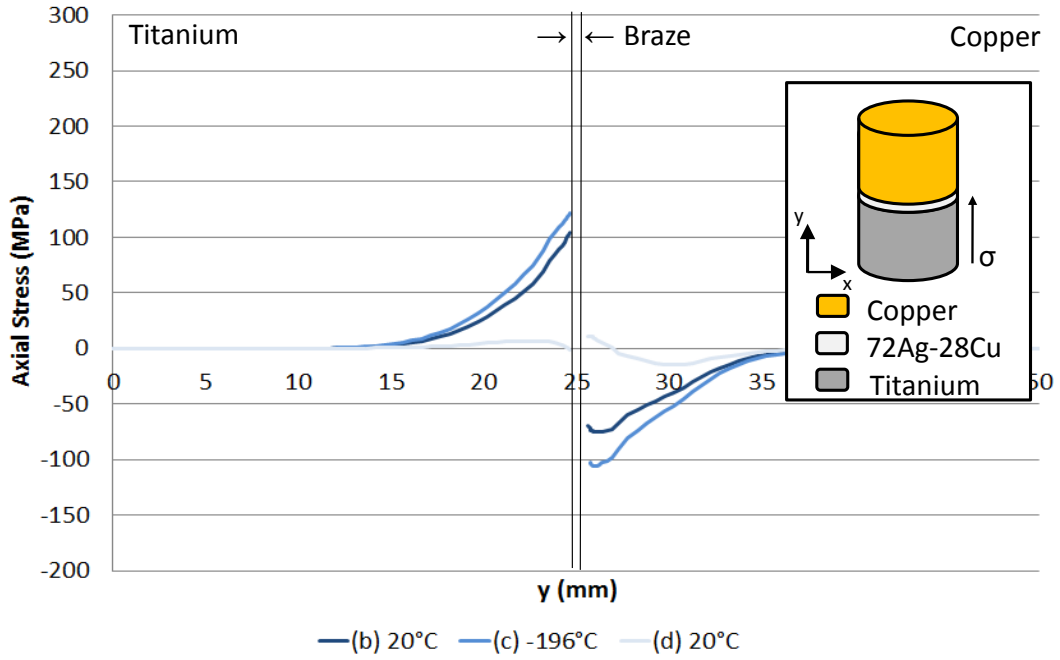

Figure 5-12 - Axial stress distributions during thermal autofrettage cycle and return to room temperature of Ti - Cu brazed joint with elastic-perfectly plastic braze

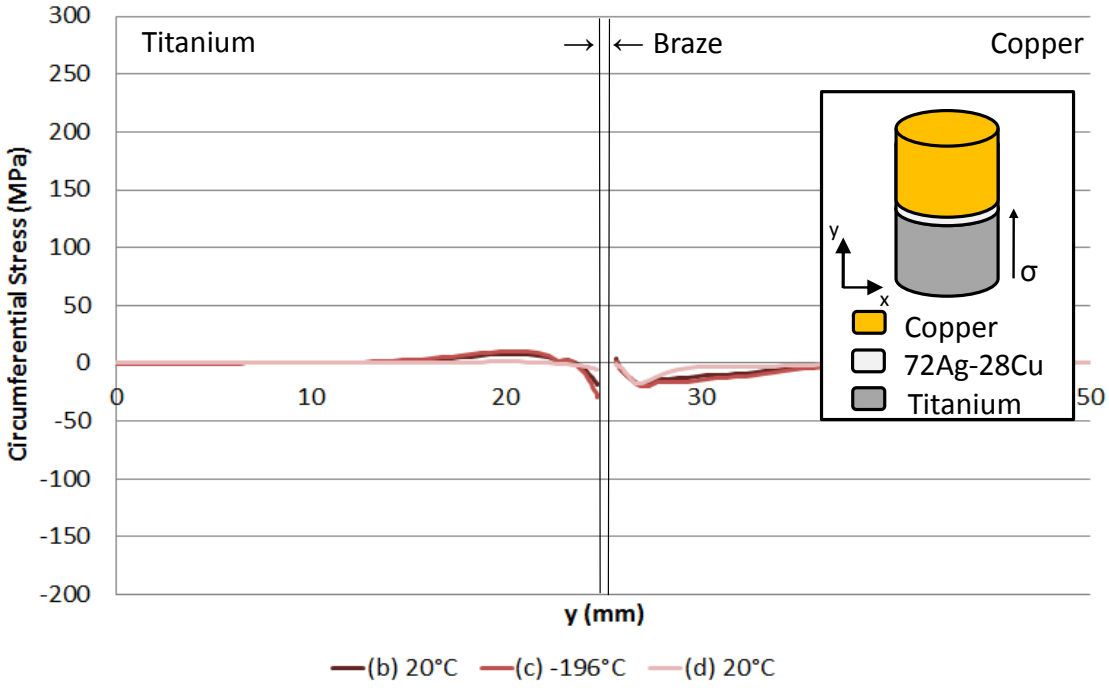

Figure 5-13 - Circumferential stress distributions during thermal autofrettage cycle and return to room temperature of Ti - Cu brazed joint with elastic-perfectly plastic braze

5.4 Measurement of residual stresses after thermal autofrettage using XRD

The change in residual stress due to the thermal autofrettage process has been measured using XRD on the axisymmetric Ti/72Ag-28Cu/Cu sample 2 which was characterised after joining in section 4.5.2. The results closest to the interface, at four angular locations 90° apart have been repeated after thermal autofrettage and compared to the original measured residual stresses and with those predicted by FEA in section 5.3.2.

The sample characterised was insulated using polyethylene foam and wrapped in cling film as shown in Figure 5-5, stored in a liquid nitrogen dewar for 8 hours before being removed and left overnight in the wrapping to return to room temperature. The XRD experimental set up, analysis parameters and uncertainty calculations are identical to those described in section 4.5 of the previous chapter. The original axial and circumferential XRD results and those measured after thermal autofrettage are shown in Figure 5-14 and Figure 5-15 respectively along with the residual stress distributions predicted by FEA.

The measured axial residual stress in Figure 5-14 shows a reduction in residual stress close to the interface at all four angular locations. The average of the four angular locations closest to the interface is 57MPa (measured values of 61$\pm$10MPa, 65$\pm$12MPa, 55$\pm$11MPa, 48$\pm$10MPa) which reduces to an average of 4MPa (measured values of -9$\pm$13MPa, 1$\pm$14MPa, 24$\pm$11MPa, -14$\pm$8MPa) after thermal autofrettage. FEA predicts a reduction of 30MPa at this location, hence the reduction in residual stress predicted by FEA is subsequently being measured in the real sample. However the absolute magnitudes of the residual stresses are larger in FEA for the reasons discussed in section 4.5.2 of the previous chapter. The measured circumferential results show a smaller reduction in residual stress. The average circumferential stress closest to the interface prior to thermal autofrettage is 53MPa (measured values of 57$\pm$10MPa, 58$\pm$11MPa, 68$\pm$12MPa, 30$\pm$9MPa) which reduces to 34MPa (measured values of 52$\pm$15MPa, 30$\pm$14MPa, 51$\pm$12MPa, 2$\pm$8MPa) after thermal autofrettage; however there is one clear outlier in the test data (reading of 2MPa.) If this is neglected the average of the results after thermal autofrettage is 44MPa which is an even smaller difference.

These results show there is a reasonable correlation to the results predicted by FEA and those measured using XRD providing confidence that the thermal autofrettage process is

having the desired effect in reducing the tensile stresses seen in the Ti, albeit a small reduction for this Ti/72Ag-28Cu/Cu joint due to the near elastic behaviour of the filler.

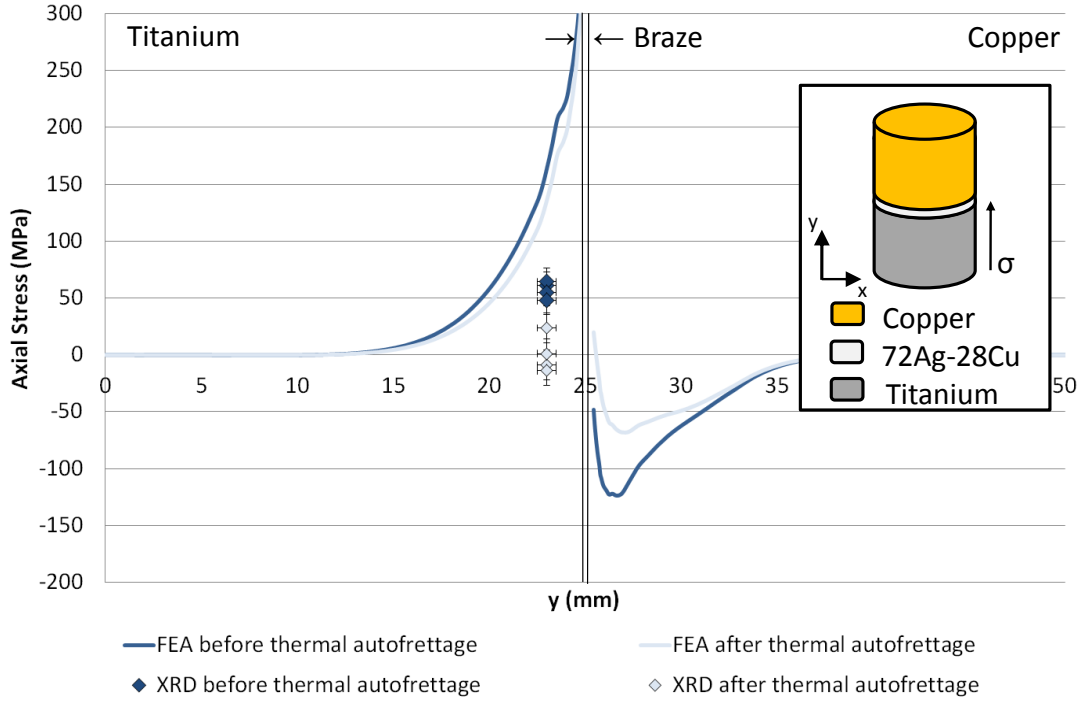

Figure 5-14 – Measured axial residual stress before and after thermal autofrettage

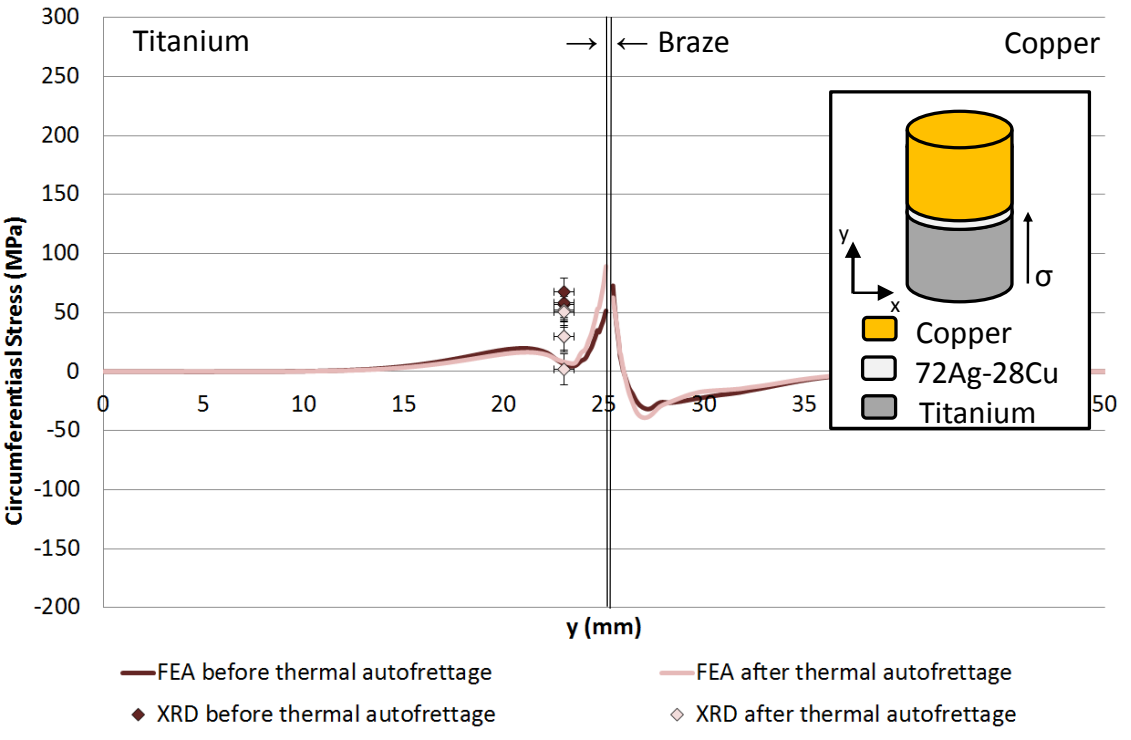

Figure 5-15 - Measured circumferential residual stress before and after thermal autofrettage

5.5 Effect of thermal autofrettage on joint performance during operation

In the previous sections of this chapter, both XRD and FEA have shown that for a Ti/72Ag-28Cu/Cu brazed joint, there is a small reduction in residual stress due to thermal autofrettage to -196°C. This small reduction has been attributed to the small change in modulus of the braze after yielding. It has subsequently been shown that if this braze layer had a lower yield stress and behaved in an elastic-perfectly plastic fashion, FEA predicts that the residual stresses developed in both materials will be less and thermal autofrettage will be effective in reducing the residual stresses due to joining.

This section uses FEA to establish the effect of thermal autofrettage on the stress state in the joint during operation, i.e. when the joint is subjected to an externally applied load with and without thermal autofrettage, and how this is likely to affect the performance of the joint in operation. In this case only two simple operational load cases are considered: uniaxial tension and bulk temperature heating. In reality other loading scenarios such as bending, torsion and differential heating could be present but only uniaxial tension and bulk temperature heating are considered in this instance. A more detailed discussion on how residual stresses in brazed joints in general affect various failure mechanisms can be found in 5.6.3.

The model for this analysis is the elastic-perfectly plastic material model used in 5.3.3 with additional operation loads applied.

5.5.1 Uniaxial tensile load of 35MPa

A uniaxial load of 35MPa has been applied to the Ti – Cu dissimilar material joint investigated in 5.3.3 (with elastic-perfectly plastic braze with lower yield stress) after thermal autofrettage to -196°C as shown in step (e) in Figure 5-16. This is compared to the case where an externally applied load is applied without thermal autofrettage after the initial brazing procedure (b).

The load applied in both cases is 35MPa which is just below the yield of the parent Cu at room temperature (40MPa). This is a relatively low applied uniaxial tension but ensures the parent Cu field stress remains elastic and does not reach limit load. In reality it is unlikely Cu would be used as load carrying structural material, however this will still be informative of

how a dissimilar material brazed joint will behave under subsequent mechanical loading. The stress distributions before and after thermal autofrettage with a subsequent uniaxial tensile load of 35MPa are shown in Figure 5-17.

For the no thermal autofrettage case, the subsequent uniaxial tensile loading of 35MPa is imposed on the initial residual stress distribution. For the case with thermal autofrettage, the subsequent uniaxial tensile load of 35MPa is imposed on the initial residual stress distribution in the Ti, however this is not the case in Cu due to the initial tensile residual stress close to the interface after thermal autofrettage. Subsequent mechanical loading of 35MPa results in plasticity developing in the Cu and load is shed away from the free edge.

The change in residual stress distribution due to thermal autofrettage when combined with operational loads will affect various failure mechanisms. In terms of failure in the Ti, the change in residual stress due to thermal autofrettage is likely to improve the fatigue performance as the mean stress is less tensile due to the change in residual stress. If the effect of the thermal autofrettage process could be improved, by for example altering the plasticity properties of the filler used for joining, it could be possible that the Ti could cycle fully in compression close to the interface. In addition, if the interface is strong relative to the parent materials, the reduction in tensile residual stress would improve the tensile strength if the Ti fails in a brittle manner.

However, the change in residual stress distribution in the Cu results in the combined mean stress being more tensile after thermal autofrettage which would decrease fatigue performance. The increase in residual stress would only reduce the limit load if the Cu was brittle in nature as the residual stresses are self-equilibrating and will not affect the limit load of a ductile material such as Cu.

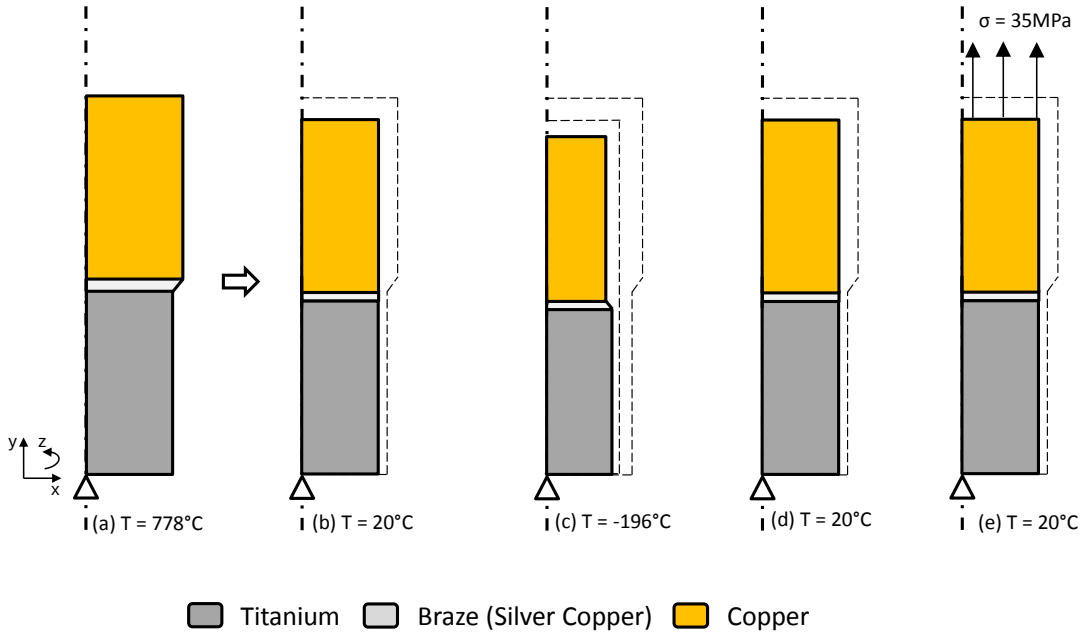

Figure 5-16 – Uniaxial applied tension after thermal autofrettage

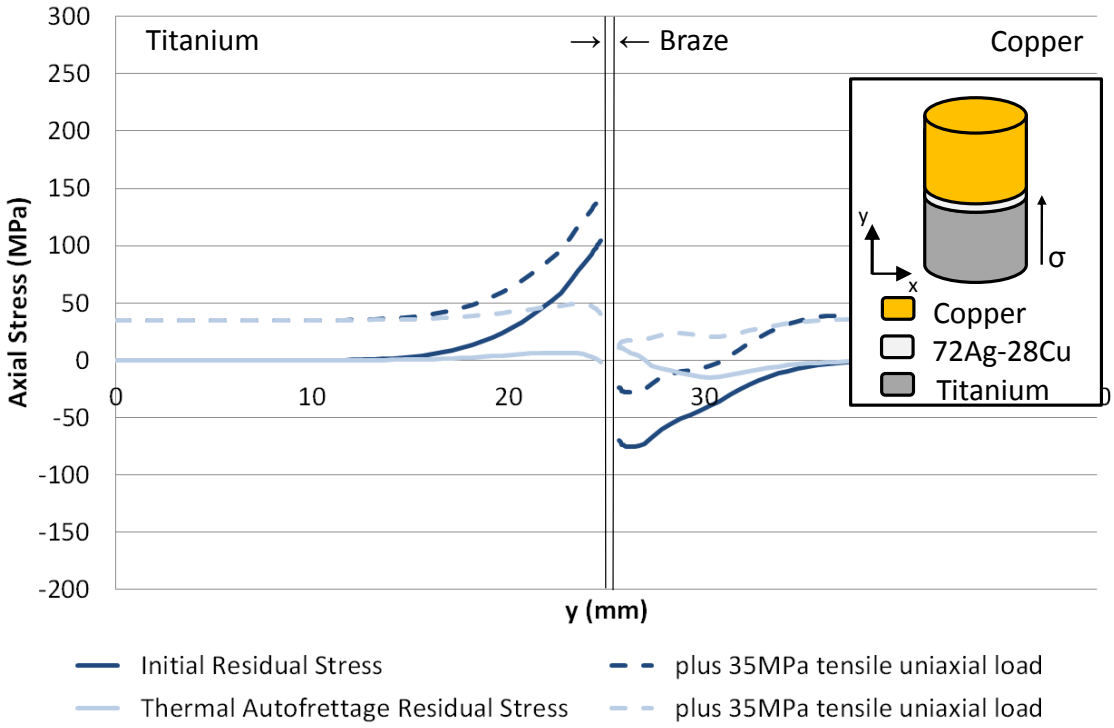

Figure 5-17 – Stress state in joint due to uniaxial tension with and without thermal autofrettage

5.5.2 Bulk temperature heating to 200°C

A bulk temperature load of 200°C has been applied to the Ti – Cu dissimilar material joint investigated in 5.3.3 (with elastic-perfectly plastic braze with lower yield stress) after thermal autofrettage to -196°C as shown in step (e) in Figure 5-18. This is compared to the case where the same bulk temperature is applied without thermal autofrettage after the initial brazing procedure (b). Any transient effects due to the subsequent heating to 200°C have been neglected. While this temperature value has been chosen arbitrarily however it will be informative as to how the joint behaves under subsequent thermal loading. The residual stress distributions before and after thermal autofrettage with a subsequent bulk thermal loading of 200°C are shown in Figure 5-19.

For the no thermal autofrettage case, the subsequent thermal load of 200°C causes a reduction of the stresses in both materials as the joint temperature increases towards initial stress free temperature of 778°C. For the case with thermal autofrettage, the subsequent thermal load causes the stresses in the joint to continue to change in a similar fashion to the initial reduction during the heating from -196°C to 20°C. In this example, under cyclic thermal loading the thermal autofrettage process results in the Ti cycling almost fully in compression whereas without thermal autofrettage the Ti cycles in tension. Hence in terms of thermal fatigue performance of the Ti, the thermal autofrettage process should result in an improved life. However, conversely the Cu is now cycling about a higher mean stress with a smaller stress range due to the thermal autofrettage process. Hence depending on the fatigue strength of both materials, the thermal autofrettage could be developed to control the material which has the cyclic tensile stress and hence used to optimise fatigue performance of the joint.

However, if in operation the joint was under steady state conditions for a long period of time such that creep as opposed to fatigue was the failure criteria of concern, the stress state in the joint at the operating temperature of 200°C without thermal autofrettage would appear to be beneficial as there is virtually zero stress in the joint under these conditions. In this specific example the operating temperature of 200°C is below the likely creep temperatures of Ti and Cu (c.555°C for Ti and c.360°C for Cu based on the 1/3 of the melting temperature of both materials), however it is postulated that the thermal autofrettage process and the braze filler plasticity properties could be used to beneficially influence the operational stresses in dissimilar material brazed joints.

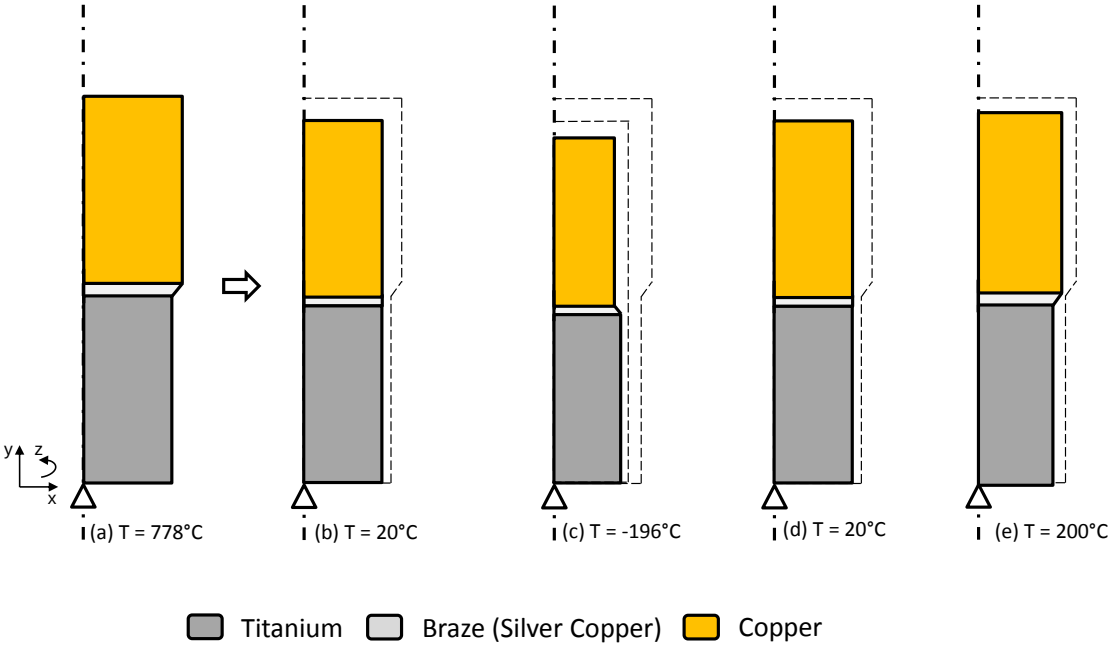

Figure 5-18 - Bulk temperature heating to 200°C after thermal autofrettage

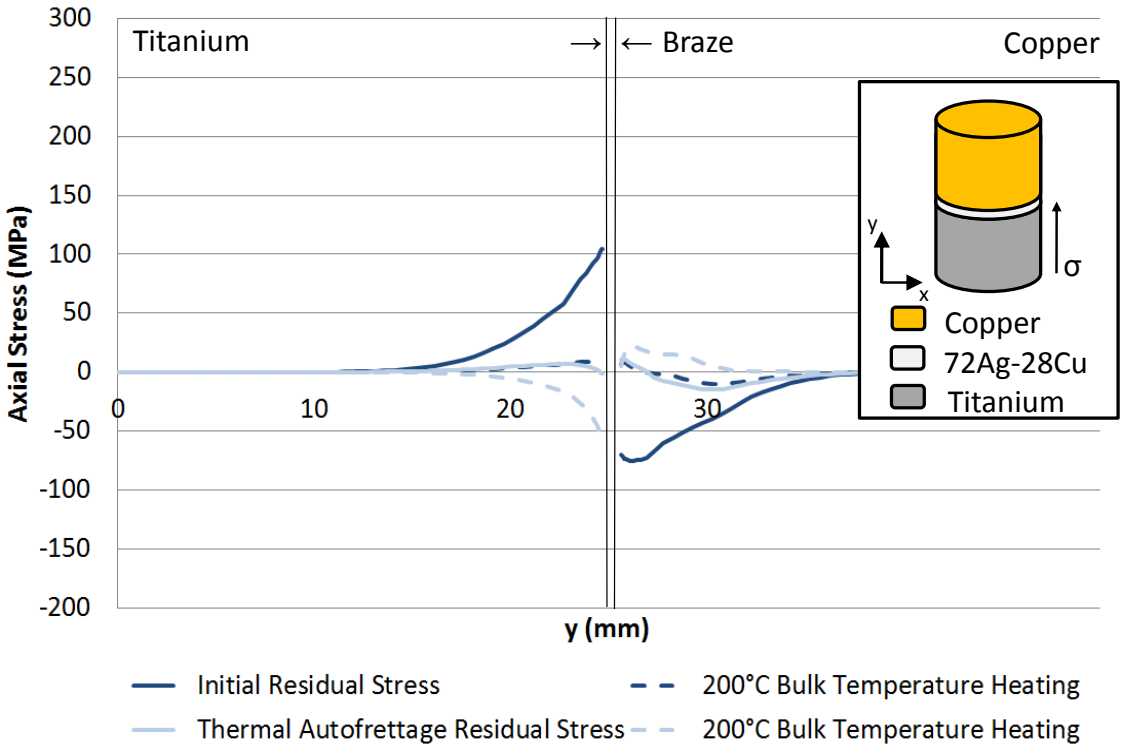

Figure 5-19 - Stress state in joint due to bulk temperature heating to 200°C with and without thermal autofrettage

5.6 Discussion and future work

The process of thermal autofrettage has been introduced as a method of altering the residual stress field in dissimilar material joints to improve joint performance in operation. A discussion into the practical issues surrounding the thermal autofrettage process is presented in addition to recommendations for future experimental verification work and how any changes in the residual stress field are likely to influence the various failure mechanisms (not just tensile strength and fatigue mentioned previously).

5.6.1 Practical issues of performing thermal autofrettage

The process of thermal autofrettage is limited by the temperature which the joint can be exposed to. The limit on this is absolute zero (-273°C), however this may not be practical in reality. For smaller components such as the Ti/72Ag-28Cu/Cu joints used in this work storage in liquid nitrogen is straightforward if the component is sufficiently well insulated to prevent micro cracking due to thermal shock or quenching of the component. Cryogenic freezers which can cool to -80°C are commonplace and could be used to thermally autofrettage larger components, however the change in residual stress will be dependent on the reduction in temperature. It is recommended that some form of NDT is used before and after thermal autofrettage to ensure the cooling process does not induce microcracking in the brazed interlayer. The sample which has undergone thermal autofrettage to -196°C for this investigation has been assessed for microcracking using dye penetrant testing and an optical assessment of the braze cross section after the residual stress measurements. As shown in Figure 5-20, both dye penetrant testing (a) and the optical inspection showed no signs of microcracking before (b) and after (c) thermal autofrettage.

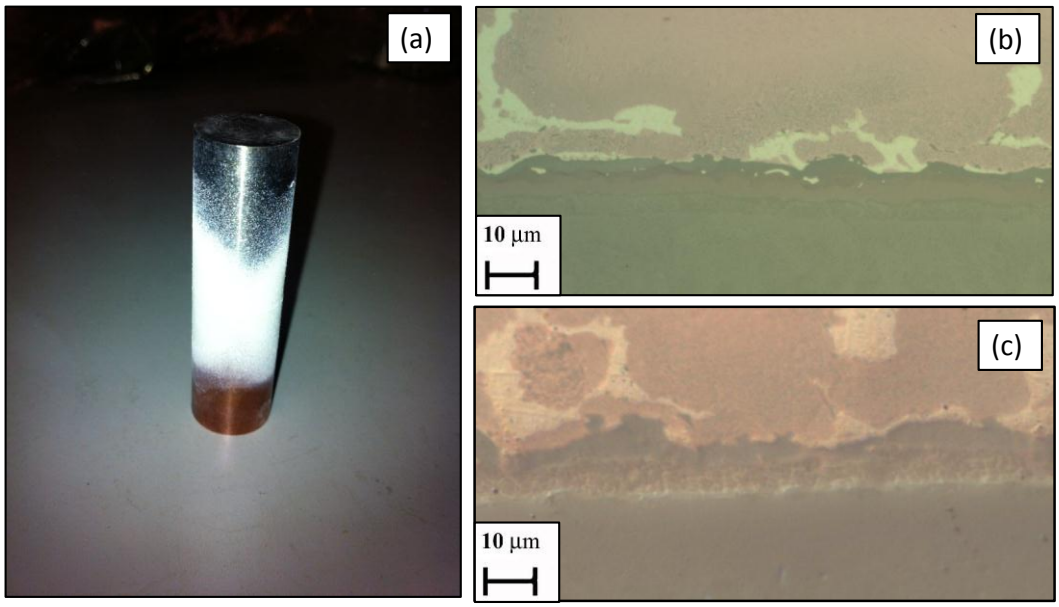

Figure 5-20 - Microcracking investigation: (a) dye penetrant testing (b) optical inspection of braze before thermal autofrettage and (c) after thermal autofrettage.

In addition to thermal autofrettage there also exists the opportunity to develop mechanical autofrettage for dissimilar material joints. This could be done by applying a compressive load perpendicular to the interface. Initial FEA of this case looks promising [115] and it is recommended that this process is the topic of future research.

Another practical consideration is the development of any further residual stresses during the thermal autofrettage procedure. In section 5.3.2, the material model used for the braze filler at room temperature and at -196°C had a significant post yield stiffness which resulted in additional residual stresses being developed in the joint during the thermal autofrettage procedure. If this is the case care needs to be taken to ensure that this does not cause failure in the joint during the thermal autofrettage process. There also exists the possibility that the materials have a ductile to brittle transition in the thermal autofrettage temperature range which could result in failure of the joint.

In addition, a dissimilar material joint in a real structure is likely to be between components of more complex geometry than cylindrical butt joints and could be subjected to a combination of mechanical and thermal loading. Obviously these must be taken into consideration if a thermal autofrettage procedure is being developed for a real structure.

5.6.2 Experimental verification

It is recommended that FEA and XRD verification of the thermal autofrettage process is conducted on different combination of materials and brazing fillers. Due to the expense associated with characterising the braze filler and fabrication of the brazed joints, only Ti/72Ag-28Cu/Cu brazed joints have been used in this work. Ideally one of the fillers used in future should behave close to elastic-perfectly plastic which should result in large changes in the residual stress field.

In addition any change in the residual stress field due to thermal autofrettage needs to be correlated to an improvement in either joint strength or mechanical and thermal fatigue performance. Hence it is recommended that any future experimental verification of the thermal autofrettage process include a series of tests to prove an improvement or otherwise.

5.6.3 Effect of residual stresses on failure mechanisms

The stresses developed in the joint due to joining and subsequent operational loads will relate to the performance of the joint in operation. The relevance of the residual stresses due to joining on any failure mechanism will be dependent on the whether the parent materials present in the joint are brittle or ductile in nature and whether failure occurs in the parent materials or at the interface. The significance of these residual stresses on various failure mechanisms is briefly discussed and whether thermal autofrettage is likely to affect the failure mechanism.

5.6.3.1 Brittle failure away from interface

Tensile residual stresses will influence failure in brittle materials. Tensile residual stresses could cause the joint to fail during manufacturing or combine with operation loads to cause failure. Thermal autofrettage could be used to reduce damaging tensile residual stresses found in dissimilar material joints due to joining, however care must be taken to ensure the thermal autofrettage process itself does not cause failure of the joint.

5.6.3.2 Brittle failure at the interface

Tensile residual stresses due to joint manufacture will influence brittle failure at the interface. As indicated, thermal autofrettage could be used to reduce these damaging

tensile residual stresses found at the interface of dissimilar material joints; however care must be taken to ensure the thermal autofrettage process does not cause interfacial failure of the joint during cooling.

5.6.3.3 Plastic collapse

Plastic collapse only occurs under a primary load and cannot generally occur due to a static secondary thermal loading alone. Residual stresses in dissimilar material joints are self-equilibrating through the thickness of the joint. Due to this self-equilibrating nature, they are unlikely to influence an applied load which would cause plastic collapse hence it is unlikely that altering the initial residual stress field using thermal autofrettage will influence the plastic collapse load of a joint between dissimilar ductile materials. However it is possible that residual stresses could influence other failure mechanisms such which in turn leads to plastic collapse.

5.6.3.4 Fatigue

Tensile residual stresses due to joining are generally detrimental to fatigue life. Conversely compressive residual stresses in the surface layers are usually beneficial and can improve fatigue life. Fatigue failure could occur in either the parent materials or the interface between the braze and the parent materials. Thermal autofrettage could be used to control the initial residual stress field to improve the fatigue performance of the joint.

5.6.3.5 Ratcheting

A ratcheting failure analysis usually requires initial plastic straining at stress concentrations to be modelled. The initial plastic straining and subsequent accumulation will be influenced by residual stresses.

5.6.3.6 Buckling

Buckling instability is a function of the stress state existing in a body and it will be affected by the initial residual stress distribution. For example, if the brazing process resulted in a global residual field stress being induced in an assembly and this would have to be accounted for in any buckling assessment. Hence thermal autofrettage could be used to control the buckling performance of dissimilar material joints.

5.7 Summary

The process of thermal autofrettage has been presented as a method of altering the residual stress field due to joining in dissimilar material brazed joints and in doing so reducing the damaging tensile residual stresses that are present after the joining process. It could also be used to beneficially influence the operational stresses in dissimilar material joints. FEA of the change in residual stress in a real Ti/72Ag-28Cu/Cu dissimilar material brazed joint due to thermal autofrettage is in reasonable agreement with the change measured using XRD. It is postulated that due to the stress – strain response of the 72Ag-28Cu filler, the change in residual stress due to thermal autofrettage is small, however FEA has shown if the braze filler has both a lower yield stress and tends towards behaving in an elastic-perfectly plastic fashion, the thermal autofrettage process is more effective in reducing the residual stresses due to joining. In addition, the initial residual stresses developed in the joint are will be less due to the reduced constraint on both materials. This could result in the thermal autofrettage process being used to improve the performance of dissimilar material joints for failure mechanisms where residual stresses contribute to failure such as brittle failure and fatigue.

The thermal autofrettage process is not limited to dissimilar material brazed joints and is likely to work for other methods of joining such as diffusion bonding, HIPing, electron beam welding and explosion welding. It is recommended that future work focuses on verifying the change in residual stress field due to thermal autofrettage process on joints of different relationships in material properties and through mechanical (or thermal) testing to establish the effect of thermal autofrettage on the performance of the joint in operation. A detailed literature and patent search has not highlighted any research in this area before, hence this idea is new and provides an original contribution to knowledge.

6 Conclusions and future work

6.1 Summary of key findings and observations

The findings from the work presented in this thesis are summarised in the following bullet points:

- Residual stresses exist in dissimilar material brazed joints due to joining and must be taken in consideration when modelling or assessing failure in such joints. These residual stresses can be large enough to cause failure in the joint during the joining process.
- The compatibility constraint on free contraction and expansion of the parent materials can be used to explain the stress state developed in dissimilar material joints. In general it has been shown that the material with the lowest coefficient of thermal expansion will develop axial tensile residual stresses.
- In the case where both materials are elastic, linear elastic theory predicts a singularity at the interface for most combinations of real materials. In addition to the elastic theory, the results from FEA can be used to calculate the strength of the singularity which exists at a dissimilar material interface.
- Plasticity provides a protection mechanism for the joint by blunting the analytical singularity and also reduces the constraint due to the interface.
- The mechanical properties of the braze layer plays a key role in the development of residual stresses and failure in dissimilar material brazed joints. However obtaining the relevant material property data for use in FEA and general assessment is non-trivial due to changes in the microstructure during brazing.
- In terms of joint design for an application which is subjected to thermal loading only, a low modulus braze will reduce the constraint on both materials due to joining and subsequent thermal operational loads. In the ideal case, a zero stiffness braze will not induce any stresses in the joint during joining and operation.
- The residual stresses predicted by FEA in a real cylindrical Ti/72Ag-28Cu/Cu brazed joint are in reasonable agreement with those measured using XRD. FEA has shown that there are no significant transient effects on the stress state developed during brazing due to significant transient thermal events (i.e large temperature gradients in the joint).

- Thermal autofrettage can be used as a method of altering the residual stress field due to joining to reduce damaging tensile residual stresses that are present after the joining process. This could result in an improvement in performance of dissimilar material joints.
- FEA has shown that thermal autofrettage could significantly change the initial residual stress distribution due to joining depending on the plastic properties of braze filler.
- Thermal autofrettage could also be used to beneficially influence the operational stresses in dissimilar material joints.
- The work presented throughout this thesis is not only relevant to dissimilar material brazed joints but also dissimilar material joints manufactured by other processes.

6.2 Discussion of key findings

The work presented in this thesis introduces the concept of thermal autofrettage to alter the residual stress field generated during the brazing process to remove potentially damaging tensile residual stresses. It could also be used to beneficially influence the operational stresses in dissimilar material joints. This process has been developed through gaining an understanding of the mechanics and development of residual stresses in dissimilar material brazed joints in general. It has been shown in section 1.5 that the residual stresses due to joining can be large enough to cause failure of the joint, hence the residual stresses due to joining must be taken into consideration when modelling and assessing failure in such joints.

In terms of using FEA to predict the stresses developed in dissimilar material brazed joints, it follows logic that the mechanical properties of the braze layer will play a key role in the mechanics of the joint and must be included in any FEA model if the stress state due to joining is to be accurately captured. In this work the properties of the brazed layer have been characterised in the as supplied condition neglecting the diffusion of elements to and from the brazed layer. However, a metallurgical investigation into the braze microstructure before and after brazing presented in chapter 2 has shown the microstructure of the brazed layer is considerably different to that in the as cast condition. This has been attributed to diffusion of elements into the braze from the parent materials during the brazing process.

Due to these differences in microstructure before and after brazing, the validity of assuming the material properties are the same before and after brazing is questionable, however, it is more representative than ignoring its presence completely. Nano-indentation has also shown that there are variations in properties in the different phases present in the braze after joining. Metallurgical studies have shown the presence of brittle intermetallics in some cases.

However in general, due to the diffusion mechanism occurring, step changes in material compositions between the different phases within the braze and the braze and parent materials will not occur, instead there will be gradual transition between the individual phases, albeit over a small distance. There are several barriers to accurately capturing the stress state in the region of the joint and across the brazed layer, as highlighted by the findings of the metallurgical investigation in chapter 2 of this thesis. At the heart of any procedure to assess failure at the interface, an experimentally derived failure criterion is required which inherently accounts for the complex metallurgy of the braze. However this does not preclude using a simplified braze layer with representative material properties in joint design and assessment of failure away from the interface. This is discussed in detail in section 2.8 .

Residual stresses are developed in the joint due to the constraint on free thermal contraction from the brazing temperature, the mechanics of which have formed an investigation in chapter 3. By developing an understanding of the stress state at the abrupt interface between two dissimilar materials it is has been shown that different relationships in material properties will affect the free edge stress distributions in the region of the joint based on the constraint due to the interface and the analytical singularity that exists in an elastic model. The stress component perpendicular to the interface is larger in magnitude than other stress components, however the other stress components cannot be ignored in any failure assessment procedure. The mechanism for the development of large stresses perpendicular to the interface is discussed in section 3.2. It has however been argued in section 3.5.1 that such elastic singularities do not exist in practice due to the absence of an abrupt change in material properties which has been supported by the evidence presented in the metallurgical study in chapter 2. It has also been argued that, in a similar fashion to linear elastic fracture mechanics, the theoretical infinite stresses predicted by the elastic theory do not exist at the interface due to plasticity effects in real materials, even those

that are known to fail in a brittle manner. Furthermore, it has also been shown in section 3.5.2 that plasticity in one material provides a protection mechanism for the joint and limits the stresses induced in the joined material. This protection mechanism forms the basis of the thermal autofrettage process developed in chapter 5 to alter the initial residual stress field due to joining.

In chapter 4, FEA has been used to predict residual stresses due to joining in a Ti/72Ag-28Cu/Cu cylindrical brazed joint assuming the braze layer to be a separate homogenous material. A transient thermal stress analysis of the brazing process of a Ti/72Ag-28Cu/Cu joint has shown that the vacuum brazing process can simplify to a uniform cooling process i.e there are no significant transient effects on the stress state developed during brazing due to large temperature gradients in the joint. The residual stresses predicted by FEA in a cylindrical Ti/72Ag-28Cu/Cu brazed joint are in reasonable agreement with those measured using XRD. Both FEA and XRD show the development of tensile residual stresses in the Ti. This can be explained by the relationship in material properties and an understanding of the mechanics of the joint.

Thermal autofrettage has been presented in chapter 5 as a method of altering the initial residual stress field due to joining in dissimilar material brazed joints to reduce damaging tensile residual stresses that are present after the joining process. This process is based on cooling the joint after brazing to reduce the tensile residual stresses developed during joining. A detailed literature and patent search has not highlighted any previous research in the area of thermal autofrettage of dissimilar material brazed joints, hence this idea is new and provides an original contribution to knowledge for dissimilar material joints. FEA of the change in residual stress in a real Ti/72Ag-28Cu/Cu dissimilar material brazed joint due to thermal autofrettage is in reasonable agreement with the change measured using XRD It is postulated that due to the stress – strain response of the 72Ag-28Cu filler, the change in residual stress due to thermal autofrettage is small, however FEA has shown if the braze filler has both a lower yield stress and tends towards behaving in an elastic-perfectly plastic fashion, the thermal autofrettage process is more effective in reducing the residual stresses due to joining. In addition, the initial residual stresses developed in the joint are will be less due to the reduced constraint on both materials. This could result in the thermal autofrettage process being used to improve the performance of dissimilar material joints for failure mechanisms where residual stresses contribute to failure such as brittle failure

and fatigue. Thermal autofrettage could also be used to beneficially influence the operational stresses in dissimilar material joints.

6.3 Future work

The work presented in this thesis has opened several avenues for future work and these are summarised in the following discussion.

One major area for future work surrounds obtaining representative temperature dependent material property data for the braze layer accounting for microstructural changes due to the brazing operation. There are several avenues which could be pursued to achieve this. One way is to cast macro scale samples of the braze layer with a microstructure similar to that found within the braze after joining [58]. An additional approach is to use techniques such as nanoindentation to characterise the mechanical and thermal properties of the brazed layer after brazing and scale these properties up to those commensurate with the scale of the finite element model. Another approach is to use homogenization software such as DIGIMAT-FE [61] to generate representative material properties for complex material microstructures based on the constituents of the individual phases. This technology has predominantly been developed for use in the composites industry, however this approach could possibly be adapted for brazing applications. These techniques are currently the subject of current research to fully characterise the material properties of the brazed layer for use in FEA and are summarised in [60].

Compared to other joining techniques such as welding, there is a lack of defined and agreed procedures and data for assessing failure in dissimilar material brazed joints. There exists the opportunity to develop procedures to assess failure in dissimilar material brazed joints both at the interface and away from the interface. In terms of fatigue and failure at the interface techniques such as interfacial fracture mechanics [62]–[67], [78], structural hot-spot stress techniques [69]–[72] and cohesive zone modelling [73]–[77], [79] could be developed to assess interfacial failure. All of these strategies suggested require experimentally derived failure criterion which account for the complex metallurgy of the brazed layer as discussed in chapter 2 of this thesis. This experimental data will only be valid for the materials being joined, the braze filler adopted and the joining process used. In instances where failure occurs away from the interface, it may not be necessary to fully capture what is happening across the interface. In cases such as this, procedures could be

developed which include a brazed layer with representative macroscopic properties, similar to the procedure used in chapter 4 to predict the residual stress state, to assess various failure mechanisms away from the interface. Experimental validation will also be required.

The functional requirements of a structure often dictate that certain material combinations are required to be joined, therefore parent material selection is often a design variable which is outwith the control of the designer. In such instances there exists the opportunity for the designer to select the braze filler based on its mechanical properties and subsequent effect on the stresses in the joint. Other joint designs are being developed to improve the performance of dissimilar material joints in operation, as summarised in simplified form in Figure 6-1, and could be applied to more complex components. The thickness of the brazed layer is a joint variable which could be used to reduce the development of large stresses in the joint during operation (a). In this case, from a theoretical perspective, analytical singularities will still exist at the interface of the braze layer and parent materials and the strength of these singularities will not be reduced by an increase in braze thickness. In addition, low moduli braze fillers could be developed to stop the development of large residual stresses and operational stresses under thermal loading. There will still however be a local stress concentration in practice as described in section 3.4.1 and it is this that may be reduced by increasing braze thickness. Other joint designs such ductile interlayers (b) [132]–[135] and functionally graded materials with either a series of interlayers of varying properties (c) [136], [137] or a gradual transition [138], [139] have also been developed to reduce the effect of a step change in properties. In cases (b) and (c) the strength of the theoretical singularities at each interface between materials will be reduced and in the limit will be eliminated in case (d). In case (d) the magnitude of the local stress concentration will be reduced with increase in the width of the transition region.

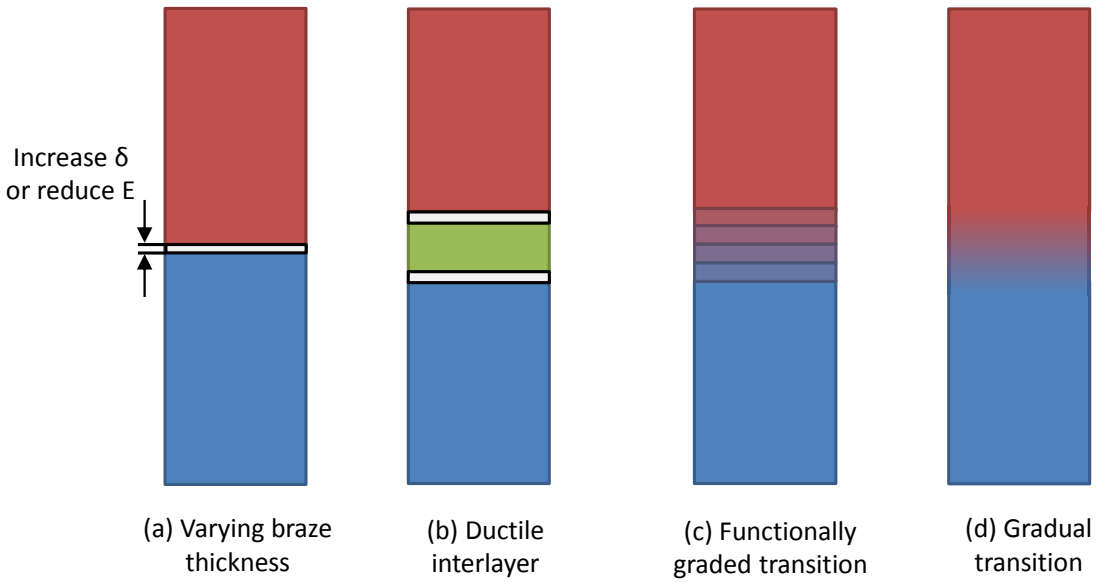

Figure 6-1 – Various dissimilar material joint designs

In chapter 4 of this thesis the residual stresses measured by XRD on one of Ti/72Ag-28Cu/Cu samples are not in agreement with FEA suggesting a lack of axisymmetry in this sample. It is postulated that this is due to either angular or axial misalignment of the particular sample. Future work in this area is focusing on developing an understanding of how misalignment will affect the residual stress distribution [124] and subsequently failure in dissimilar material brazed joints. Creep will also have an effect on the stresses developed in a dissimilar material joint and during joining and in operation where thermal loading is present. Creep as a failure mechanism, and its interaction with other failure mechanisms such fatigue, will be of increasing importance in fusion devices which favour steady state operation as opposed to pulsed operation. Creep of both the parent materials and the braze filler has not been accounted for in this work and it is recommended that this be the topic of future research.

There also exists the opportunity to set the initial size of the machined components to control the stress levels in the joint during operation. Consider the following example of a simple Cu-Ti dissimilar brazed joint brazed at 820°C and used in a steady device at a uniform operating temperature of 500°C. The initial dimensions could be selected such that there is no differential thermal expansion between the parent Cu and Ti at the operating temperature of 500°C which could result in a stress free joint at this temperature. It is likely that the properties of the brazed layer will affect the stress distribution, however FEA could

be used to perform sensitivity studies to determine the initial dimensions of the parent materials such that there is no stress in the joint for a given set of mechanical properties for the braze.

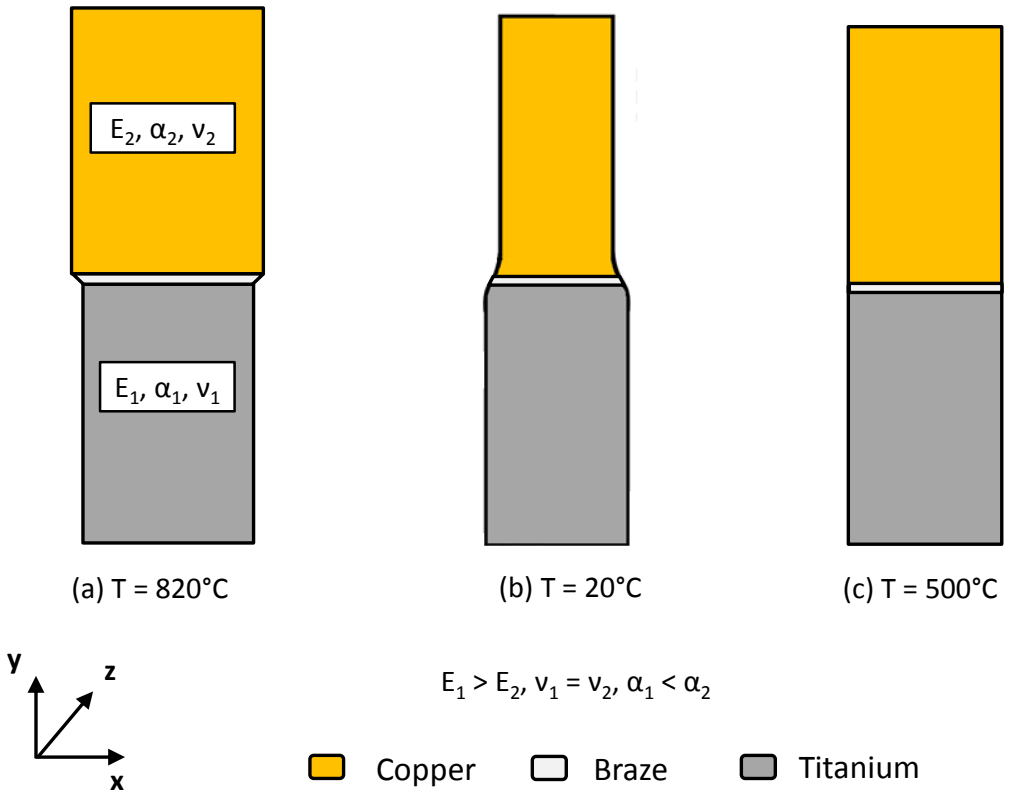

Figure 6-2 - Controlling initial diameters to control residual stress distributions

In terms of using the process of thermal autofrettage to control the residual stress state in the joint, it is recommended that future work focuses on experimentally verifying the change in residual stress field due to thermal autofrettage process on joints with different relationships in material properties and through mechanical (or thermal) fatigue testing to establish any effect of the process on joint performance. There also exists the opportunity to change the specimen design to use other methods of residual stress measurement techniques such as hole drilling [140] or the contour method [141].

The work presented in this thesis has been targeted specifically at designers and engineers from any industry who deal with the structural integrity issues of dissimilar material brazed joints, however many of the findings are applicable to dissimilar material joints fabricated using other joining methods. Consequently, the mechanics, residual stress predictions and thermal autofrettage investigation has focused on joints of simple geometry, subjected to

uniform thermal or mechanical loads, using brazing as a joining process. In terms of real fusion applications, dissimilar material brazed joints are subjected to cyclic high-heat-flux and mechanical loads and in many cases do not take the form of simple shapes as highlighted in section 1.2 of this thesis. In addition, in the fusion environment this is compounded by the use of relatively unusual materials (and hence not well characterised) which can be non-ductile in nature. There also exists the goal of overcoming the challenges in quantifying the long term effects of fusion levels of irradiation on such materials. It is recommended that future work focuses on the behaviour of brazed joints used in real applications subjected to more realistic loading cases. However, whilst these challenges exist, at the heart of any procedure for modelling and assessing the design or failure of dissimilar material brazed joints must be a basic understanding of the metallurgy, mechanics and development of residual stresses in the joint and how these will affect the joint in operation. The work presented in this thesis has been about developing this basic understanding whilst introducing a post-joining process, namely thermal autofrettage, as a method of modifying these residual stresses to improve joint performance.

7 References

[1] *AWS Brazing Handbook 4th Edition*. American Welding Society, 1991.

[2] "ITER Materials Assessment Report (MAR), ITER Doc no G 74 MA 10 W 0.3," 2004.

[3] "The roadmap to magnetic confinement fusion," 2012. [Online]. Available: http://www.dur.ac.uk/superconductivity.durham/The roadmap to magnetic confinement.pdf. [Accessed: 26-Nov-2012].

[4] "JET EFDA Homepage." [Online]. Available: http://www.jet.efda.org/jet/. [Accessed: 01-Aug-2012].

[5] "ITER Website." [Online]. Available: http://www.iter.org/mach. [Accessed: 01-Aug-2012].

[6] "ITER Divertor Design Description Document, ITER Doc no G 17 DDD 6 R 0.2," 2004.

[7] J. Reiser and M. Rieth, "Optimization and limitations of known DEMO divertor concepts," *Fusion Engineering and Design*, pp. 2–5, Mar. 2012.

[8] Y. Zhang, A. V. Ganeev, J. T. Wang, J. Q. Liu, and I. V. Alexandrov, "Observations on the ductile-to-brittle transition in ultrafine-grained tungsten of commercial purity," *Materials Science and Engineering: A*, vol. 503, no. 1–2, pp. 37–40, Mar. 2009.

[9] P. Norajitra, S. Antusch, R. Giniyatulin, V. Kuznetsov, I. Mazul, H.-J. Ritzhaupt-Kleissl, and L. Spatafora, "Progress of He-cooled divertor development for DEMO," *Fusion Engineering and Design*, vol. 86, no. 9–11, pp. 1656–1659, Oct. 2011.

[10] E. Lucon, P. Benoit, P. Jacquet, E. Diegele, R. Lässer, a. Alamo, R. Coppola, F. Gillemot, P. Jung, a. Lind, S. Messoloras, P. Novosad, R. Lindau, D. Preininger, M. Klimiankou, C. Petersen, M. Rieth, E. Materna-Morris, H.-C. Schneider, J.-W. Rensman, B. van der Schaaf, B. K. Singh, and P. Spaetig, "The European effort towards the development of a demo structural material: Irradiation behaviour of the European reference RAFM steel EUROFER," *Fusion Engineering and Design*, vol. 81, no. 8–14, pp. 917–923, Feb. 2006.

[11] B. Kalin, V. Fedotov, O. Sevrjukov, A. Kalashnikov, A. Suchkov, A. Moeslang, and M. Rohde, "Development of brazing foils to join monocrystalline tungsten alloys with ODS-EUROFER steel," *Journal of Nuclear Materials*, vol. 367–370, pp. 1218–1222, Aug. 2007.

[12] B. Kalin, V. Fedotov, O. Sevrjukov, A. Moeslang, and M. Rohde, "Development of rapidly quenched brazing foils to join tungsten alloys with ferritic steel," *Journal of Nuclear Materials*, vol. 329–333, pp. 1544–1548, Aug. 2004.

[13] A. Cardella, K. Skladnov, K. Ioki, H. Pacher, Y. Strebkov, and W. Daenner, “Design and manufacturing of the ITER limiter,” *Fusion Engineering and Design*, vol. 61–62, pp. 111–116, Nov. 2002.

[14] M. Gasparotto, L. . Boccaccini, L. Giancarli, S. Malang, and Y. Poitevin, “Demo blanket technology R&D results in EU,” *Fusion Engineering and Design*, vol. 61–62, pp. 263–271, Nov. 2002.

[15] J. Pamela, A. Bécoulet, D. Borba, J.-L. Boutard, L. Horton, and D. Maisonnier, “Efficiency and availability driven R&D issues for DEMO,” *Fusion Engineering and Design*, vol. 84, no. 2–6, pp. 194–204, Jun. 2009.

[16] F. Cismondi, S. Kecskés, P. Pereslavtsev, E. Magnani, and U. Fischer, “Preliminary thermal design and related DEMO relevancy of the EU-HCPB TBM in vertical arrangement,” *Fusion Engineering and Design*, vol. 85, no. 10–12, pp. 2040–2044, Dec. 2010.

[17] “Ion Cyclotron Resonant Heating,” 2012. [Online]. Available: http://www.efda.org/fusion/focus-on/plasma-heating-current-drive/ion-cyclotron-resonant-heating/. [Accessed: 13-Feb-2013].

[18] A. Borthwick, C. Waldon, J. Fanthome, M. Nightingale, N. Richardson, and C. Hamlyn-harris, “Engineering Design of an RF Vacuum Window for the ITER ICRH Antenna,” *Fus Eng Des*, vol. 84, no. 2, pp. 1–5, 2009.

[19] “ITER Materials Property Handbook (MPH), ITER Doc no: G 74 MA 10 W 0.3,” 2004.

[20] T. Chehtov, J. Aktaa, and O. Kraft, “Mechanical characterization and modeling of brazed EUROFER-tungsten-joints,” *Journal of Nuclear Materials*, vol. 367–370, pp. 1228–1232, Aug. 2007.

[21] F. A. Kandil, J. D. Lord, A. T. Fry, and P. V Grant, “A Review of Residual Stress Measurement Methods,” *NPL Report MATC(A)04*, 2001.

[22] M. M. Schwartz, *Brazing Second Edition*. ASM International, 2003.

[23] M. Brochu, M. Pugh, and R. Drew, “Joining silicon nitride ceramic using a composite powder as active brazing alloy,” *Materials Science and Engineering: A*, vol. 374, no. 1–2, pp. 34–42, Jun. 2004.

[24] K. Shinozaki and K. Koyama, “Development of Al/Cu Dissimilar Brazing Joint Controlled Form of Intermetallic Compound,” *Materials Science Forum*, vol. 539–543, pp. 4075–4080, 2007.

[25] Naka et al, “Ti-precoating Effect on Wetting and Joining of Cu to SiC,” *ISIJ International*, vol. 30, pp. 1108–1113, 1990.

[26] C. Kim, S. Kim, “Interfacial reaction product and its effect on the strength of of copper to alumin eutectic bonding,” *J.Material Science*, vol. 7, no. 27, pp. 2061–2066.

[27] T. Ning, X. Okamoto, “Bond strength and interfacial structure of silicon nitride joints brazed with aluminium-silicon and alumium-mangesium alloy,” *Journal of Materials Science*, vol. 26, pp. 2050–2056, 1991.

[28] M. Singh, T. P. Shpargel, and R. Asthana, “Braze oxidation behavior and joint microstructure in YSZ/steel joints made using palladium brazes for SOFC applications,” *Materials Science and Engineering: A*, vol. 485, no. 1–2, pp. 695–702, Jun. 2008.

[29] Z. Zhong, H. Jung, T. Hinoki, and A. Kohyama, “Effect of joining temperature on the microstructure and strength of tungsten/ferritic steel joints diffusion bonded with a nickel interlayer,” *Journal of Materials Processing Technology*, vol. 210, no. 13, pp. 1805–1810, Oct. 2010.

[30] P. Bastid and P. Jackson, “Predicting successful manufacture of ceramic/metal joints using Weibull modelling,” *TWI Report 852/2006*, 2006.

[31] M. Rohde, I. Südmeyer, a. Urbanek, and M. Torge, “Joining of alumina and steel by a laser supported brazing process,” *Ceramics International*, vol. 35, no. 1, pp. 333–337, Jan. 2009.

[32] G. Blugan, J. Kuebler, V. Bissig, and J. Janczak-Rusch, “Brazing of silicon nitride ceramic composite to steel using SiC-particle-reinforced active brazing alloy,” *Ceramics International*, vol. 33, no. 6, pp. 1033–1039, Aug. 2007.

[33] B. Blackwell, “A framework for derterming the mechanical properties of dissimilar material joints,” Massachusetts Institute of Technology PhD Thesis, 1992.

[34] Y. Liu, Z. R. Huang, and X. J. Liu, “Joining of sintered silicon carbide using ternary Ag–Cu–Ti active brazing alloy,” *Ceramics International*, vol. 35, no. 8, pp. 3479–3484, Dec. 2009.

[35] I. Südmeyer, T. Hettesheimer, and M. Rohde, “On the shear strength of laser brazed SiC–steel joints: Effects of braze metal fillers and surface patterning,” *Ceramics International*, vol. 36, no. 3, pp. 1083–1090, Apr. 2010.

[36] R. Shiue, S. Wu, and C. Chan, “The interfacial reactions of infrared brazing Cu and Ti with two silver-based braze alloys,” *Journal of Alloys and Compounds*, vol. 372, no. 1–2, pp. 148–157, Jun. 2004.

[37] E. Ganjeh, H. Sarkhosh, H. Khorsand, H. Sabet, E. H. Dehkordi, and M. Ghaffari, “Evaluate of braze joint strength and microstructure characterize of titanium-CP with Ag-based filler alloy,” *Materials & Design*, vol. 39, pp. 33–41, Aug. 2012.

[38] F. Brossa, P. Ghiselli, G. Tommei, G. Piatti, and P. Schiller, “Experimental tests concerning the use of the tungsten-copper couple design concept on the divertor system,” *Nuclear technology fusion*, pp. 491–496, 1982.

[39] M. I. Seki, T. I. Horie, T. Tone, K. Nagata, K. Kitamura, M. Shibui, T. Araki, and Y. Shibutani, “Fatigue strength of tungsten - copper for divertor plates duplex structures,” *Journal of Nuclear Materials*, vol. 155–157, pp. 392–397, 1988.

[40] T. Horie, M. Seki, A. Minato, and T. Tone, “Analysis and experiments on lifetime predictions for first wall and divertor plate structures in JAERI,” *Fusion Technology*, vol. 10, pp. 753–758, 1986.

[41] X. X. Yao and R. Sandstro, “Strain-controlled fatigue of a braze clad Al – Mn – Mg alloy at room temperature and at 75°C and 180°C,” *Materials Science and Engineering A*, vol. 267, pp. 1–6, 1999.

[42] H. Nishi and K. Kikuchi, “Influence of brazing conditions on the strength of brazed joints of alumina dispersion-strengthened copper to 316 stainless steel,” *Journal of Nuclear Materials*, vol. 263, pp. 281–288, 1998.

[43] B. Y. H. D. Solomon, “A Statistical Analysis of Brazed Joint Fatigue Behavior,” *Welding Research Supplement, June 2001 Edition*, pp. 148–156, 2001.

[44] W. Callister, *Fundamentals of Material Science and Engineering 5th Edition*. John Wiley & Sons, 2001, p. 293.

[45] A. Shafiei, P. Abachi, K. Dehghani, and K. Pourazarang, “On the Formation of Intermetallics during the Furnace Brazing of Pure Titanium to 304 Stainless Steel Using Ag (30–50%)–Cu Filler Metals,” *Materials and Manufacturing Processes*, vol. 25, no. 11, pp. 1333–1340, Dec. 2010.

[46] H. Okamoto, “Cu-Ti (Copper-Titanium),” *Journal of Phase Equilibria*, vol. 23, no. 6, pp. 549–550, 2002.

[47] J. Liotard, “Intermetallic compound formations in titanium-copper thin films couples,” *Journal of Applied Physics*, vol. 57, pp. 1895–1901, 1985.

[48] *ASM Handbook Volume 6: Welding Brazing and Soldering*. ASM International, 1993.

[49] N. R. Hamilton, J. Wood, A. Galloway, M. B. O. Robbie, and Y. Zhang, “The Metallurgy, Mechanics, Modelling and Assessment of Dissimilar Material Brazed Joints,” *Journal of Nuclear Materials*, vol. 423, no. 1–3, pp. 42–51, Jul. 2012.

[50] A. Fischer-Cripps, *The IBIS Handbook of Nanoindentation*. Fischer-Cripps Laboratories Pty Ltd, 2009.

[51] F. K. Mante, G. R. Baran, and B. Lucas, “Nanoindentation studies of titanium single crystals.,” *Biomaterials*, vol. 20, no. 11, pp. 1051–5, Jun. 1999.

[52] “Young’s Modulus (Tensile Modulus) for common materials,” *The Enigneering Toolbox*, 2012. [Online]. Available: http://www.engineeringtoolbox.com/young-modulus-d_417.html. [Accessed: 06-Sep-2012].

[53] M. F. Ashby, *Materials Selection in Mechanical Design Second Edition*. Butterworth Heinemann, 1999.

[54] J. You and H. Bolt, “Structural analysis of a plasma facing component reinforced with fibrous metal matrix composite laminate,” *Journal of Nuclear Materials*, vol. 329–333, pp. 702–705, Aug. 2004.

[55] R. Williamson, B. Rabin, and G. Byerly, “FEM study of the effects of interlayers and creep in reducing residual stresses and strains in ceramic-metal joints,” *Composite Engineering*, vol. 5, no. 7, pp. 851–863, 1995.

[56] P. Dadras, J. Ting, and M. L. Lake, “Brazing residual stresses in Glidcop-All2Si-Be,” *Journal of Nuclear Materials*, vol. 230, pp. 164–172, 1996.

[57] J. H. You and G. Breitbach, “Deformation of ductile braze layer in a joint element under cyclic thermal loads,” *Fusion Engineering and Design*, vol. 38, no. 3, pp. 307–317, Jan. 1998.

[58] M. Galli, J. Botsis, J. Janczak-Rusch, G. Maier, and U. Welzel, “Characterization of the Residual Stresses and Strength of Ceramic-Metal Braze Joints,” *Journal of Engineering Materials and Technology*, vol. 131, no. 2, pp. 021004–1, 2009.

[59] J. Gong, W. Jiang, Q. Fan, H. Chen, and S. T. Tu, “Finite element modelling of brazed residual stress and its influence factor analysis for stainless steel plate-fin structure,” *Journal of Materials Processing Technology*, vol. 209, no. 4, pp. 1635–1643, Feb. 2009.

[60] Y. Zhang, “Challenges towards the characterisation of brazed EUROFER97-tungsten joints using miniature test specimen design and nanoindentation,” in *27th Symposium on Fusion Technology*, 2012.

[61] “ExStream Engineering Digimat FE,” 2012. [Online]. Available: http://www.e-xstream.com/en/digimat-software/digimat-fe.html. [Accessed: 13-Feb-2013].

[62] H. Cao and A. Evans, “An experimental study of the fracture resistance of bimaterial interfaces,” *Mechanics of Materials*, vol. 7, pp. 295–304, 1989.

[63] J. Rice, “Elastic fracture mechanics concepts for interfacial cracks,” *Journal of Applied Mechanics*, vol. 110, pp. 289–324, 1988.

[64] S. Barbara, “Numerical simulations of dynamic crack growth along an interface,” pp. 289–324, 1996.

[65] Z. Suo and J. Hutchinson, “Interface crack between two elastic layers,” *International Journal of Fracture*, vol. 43, pp. 1–18, 1990.

[66] P. Charalambides, J. Lund, A. Evans, and R. McMeeking, “A test specimen for determining the fracture resistance of bimaterial interfaces,” *Journal of Applied Mechanics*, vol. 56, pp. 77–82, 1989.

[67] R. Dauskardt, M. Lane, Q. Ma, and N. Krishna, “Adhesion and debonding of multi-layer thin film structures,” *Engineering Fracture Mechanics*, vol. 61, pp. 141–162, 1998.

[68] A. Levy, “Thermal Residual Stresses in Ceramic-to-Metal Brazed Joints,” *J. Am. Ceram. Soc*, vol. 74, pp. 2141–2147.

[69] E. Niemi, W. Fricke, and S. Maddox, *Fatigue analysis of welded components: designer’s guide to the structural hot-spot stress approach*, 2nd ed. Woodhead Publishing, 2006.

[70] S. Maddox, *Fatigue strength of welded structures*, 2nd ed. Woodhead Puiblishing, 1991.

[71] I. Poutianen, “Determination of the structural hot spot stress using finite element method – a comparison of current procedures,” *IIW Report XIII 1991-03*, 1991.

[72] W. Fricke and R. Bogdan, “Determination of hot spot stress in structural members with in-plane notches using a coarse element mesh,” *International Institute of Welding*, 2001.

[73] DS Simulia, *Modelling Fracture and Failure with Abaqus - Course notes*. 2010.

[74] A. Needleman, “A continuum model for void nucleation by inclusion debonding,” *Journal of Applied Mechanics*, pp. 525–531, 1987.

[75] D. Dugdale, “Yielding of steel sheets containing slits,” *Journal of Mechanics and Physics of Solids*, vol. 8, pp. 100–104, 1960.

[76] A. Needleman, V. Tvergaard, and J. Hutchnison, *Void Growth in Plastic Solids*. Springer-Verlag, New York, 1992, pp. 145–178.

[77] O. Nguyen, E. Repetto, M. Ortiz, and R. Radovitzky, “A cohesive model of fatigue crack growth,” *International Journal of Fracture*, vol. 110, pp. 351–369, 2001.

[78] P. Jousset and M. Rachik, “Cohesive Zone Model for the Finite Element Simulation of Structural Bonded Joints: Modelisation Parameters Identification and Validation,” *NAFEMS - FEM Idealisation of Joints*, pp. 93–103, 2010.

[79] M. K. Ghovanlou, H. Jahed, and A. Khajepour, “Cohesive Zone Modeling of Ductile Tearing Process in Brazed Joints,” *Engineering Fracture Mechanics*, pp. 1–15, Dec. 2012.

[80] K. L. Roe and T. Siegmund, “An irreversible cohesive zone model for interface fatigue crack growth simulation,” *Engineering Fracture Mechanics*, vol. 70, no. 2, pp. 209–232, Jan. 2003.

[81] *2007 ASME Boiler & Pressure Vessel Code*. 2007.

[82] R. B. Pipes and N. J. Pagano, “Interlaminar Stresses in Composite Laminates Under Uniform Axial Extension,” *Journal of Composite Materials*, vol. 4, p. 538, 1970.

[83] N. J. Pagano and R. B. Pipes, “The Influence of Stacking Sequence on Laminate Strength,” *Journal of Composite Materials*, vol. 5, no. 1, pp. 50–57, Jan. 1971.

[84] N. Pagano and B. Pipes, “Some observations on the interlaminar strength of composite laminates,” *Int.J.mech.Sci*, vol. 15, no. 12, 1973.

[85] C. H. Hsueh and A. G. Evans, “Residual Stresses in Metal Ceramic Bonded Strips,” *Journal of the American Ceramic Society*, vol. 68, no. 5, pp. 241–248, 1985.

[86] D. Munz and Y. Y. Yang, “Stress Singularities at the Interface in Bonded Dissimilar Materials Under Mechanical and Thermal Loading,” *Journal of Applied Mechanics*, vol. 59, p. 857, 1992.

[87] J. Dunders, “Discussion,” *Journal of Applied Mechanics*, pp. 650–652, 1969.

[88] P. Kelly, D. Hills, and D. Nowell, “The design of joints between elastically dissimilar components,” *Journal of Strain Analysis*, vol. 27, no. 1, pp. 15–20, 1992.

[89] D. Bogy, “Two Edge-bonded Elastic Wedges of Different Materials and Wedge Angles Under Surface Tractions,” *Journal of Applied Mechanics*, p. 377, 1971.

[90] D. Bogy, “Edge-Bonded Dissimilar Orthogonal Elastic Wedges Under Normal and Shear Loading,” *Tranactions of ASME*, p. 460, 1968.

[91] D. Munz, “Stresses Near the Free Edge of the Interface in Ceramic-to-Metal Joints,” *Journal of the European Ceramic Society*, p. 453, 1993.

[92] J. H. You and H. Bolt, “Analysis of singular interface stresses in dissimilar material joints for plasma facing components,” *Journal of Nuclear Materials*, vol. 299, no. 1, pp. 1–8, Oct. 2001.

[93] F. Erdogan, “Fracture mechanics,” *International Journal of Solids and Structures*, vol. 37, no. 1–2, pp. 171–183, Jan. 2000.

[94] E. Orowan, “Fracture and strength of solids,” *Reports on Progress in Physics XII*, pp. 185–232, 1948.

[95] M. Singh, R. Asthana, F. M. Varela, and J. Martínez-Fernández, “Microstructural and mechanical evaluation of a Cu-based active braze alloy to join silicon nitride

ceramics," *Journal of the European Ceramic Society*, vol. 31, no. 7, pp. 1309–1316, Jun. 2011.

[96] S. Broek, *Elementary engineering fracture mechanics 3rd Edition*. Martinus Nijhoff Publishers, 1982.

[97] A. Levy and A. Tobin, "Residual Stress Analysis and Microstructural Observations of Ceramic-to-Metal Brazed Joints," in *Metal- Ceramic Joining; Proceedings of the Symposium, TMS Fall Meeting, Detroit, MI, October 8–9, Minerals, Metals & Materials Society*.

[98] D. Munz, M. A. Sckuhr, and Y. Yang, "Thermal Stresses in Ceramic-Metal Joints with an Interlayer," *J.Am.Ceram.Soc*, vol. 90, no. 193629, pp. 285–290, 1995.

[99] I. Shiota and Y. Miyamoto, "Functionally Graded Materials," *Engineering Fracture Materials*, vol. 56, pp. 691–710, 1997.

[100] M. Vieira and A. Ramos, "The influence of ductile interlayers on the mechanical performance of tungsten nitride coatings," *Journal of Materials Processing Technology*, vol. 92–93, pp. 156– 161, 1999.

[101] L. Yun-Han, "Fabrication and evaluation of SiC/Cu functionally graded material used for plasma facing components in a fusion reactor," *Journal of Nuclear Materials*, pp. 188–195, 2002.

[102] L. Xu, S. Kuai, and S. Sengutap, "Dissimilar Material Joints With and Without Free-edge Stress Singularities: Part 1. A Biologically Inspired Design," *Society for Experimental Mechanics*, vol. 44, pp. 608–615, 2004.

[103] A. Baladi and A. F. Arezoodar, "Dissimilar Materials Joint and Effect of Angle Junction on Stress Distribution at Interface," *Engineering and Technology*, pp. 47–50, 2011.

[104] "Brazing Filler Metals ISO 17672:2010," 2010.

[105] "ASTM E228 - 11 Standard Test Method for Linear Thermal Expansion of Solid Materials With a Push-Rod Dilatometer."

[106] "TA Instruments Dynamic Mechanical Analyzer Q800," 2012. [Online]. Available: http://www.tainstruments.com/pdf/literature/TA284.pdf. [Accessed: 13-Feb-2013].

[107] R. J. Dennis, N. A. Leggatt, M. C. Smith, and P. J. Bouchard, "R6 weld modelling guidlines - application to groove weld worked example," *Proceedings of the ASME 2010 Pressure Vessels & Piping Division*, pp. 1–14, 2010.

[108] "BS EN ISO 7500-2:2006 Metallic materials. Verification of static uniaxial testing machines. Tension creep testing machines. Verification of the applied force," 2006.

[109] "BS EN ISO 9513:2002 Metallic materials. Calibration of extensometers used in uniaxial testing," 2002.

[110] W. C. Jiang, J. M. Gong, S. D. Tu, and H. Chen, “Three-dimensional numerical simulation of brazed residual stress and its high-temperature redistribution for stainless steel plate-fin structure,” *Materials Science and Engineering: A*, vol. 499, no. 1–2, pp. 293–298, Jan. 2009.

[111] “Temperature Dependent Elastic & Thermal Properties Database.” [Online]. Available: www.jahm.com/. [Accessed: 21-Apr-2013].

[112] MatWeb, “Silver-Copper Eutectic Alloy (72Ag-28Cu; UNS P07720), 20% Cold Work,” 2012. [Online]. Available: http://www.matweb.com/search/datasheet.aspx?matguid=d8d7166fb80346a2a869f322156dfd1c&ckck=1. [Accessed: 13-Feb-2013].

[113] W. Michels and S. Wilford, “The Physical Properties of Titanium. I. Emissivity and Resistivity of the Commercial Metal,” *J. Appl. Phys*, vol. 20, p. 1223, 1949.

[114] “Emissivity of Common Materials,” 2012. [Online]. Available: http://www.omega.co.uk/literature/transactions/volume1/emissivitya.html.

[115] T. Peat, “An Investigation into the Modelling of Dissimilar Material Joints and the Application of Autofrettage to Reduce Residual Stresses,” University of Strathclyde - Department of Mechanical and Aerospace Engineering - Undergraduate Project Thesis, 2012.

[116] J. D. Whitcomb, I. S. Raju, and J. G. Goree, “Reliability of the finite element method for calculating free edge stresses in composite laminates,” *Computers & Structures*, vol. 15, no. 1, pp. 23–37, Jan. 1982.

[117] Y. Cengal and R. Turner, *Fundamentals of Thermal - Fluid Sciences International Edition*. McGraw-Hill Higher Education, 2001, p. 855.

[118] M. Fitzpatrick, A. Fry, P. Holdway, F. Kandil, J. Shackleton, and L. Souminen, “Determination of Residual Stresses by X-ray Diffraction - Issue 2,” *NPL Measurement Good Practice Guide*, no. 52, p. 10, 2005.

[119] U. Kocks, *Texture and Anisotropy - Preferred Orientations in Polycrystals and their Effect on Material Properties*. Cambridge University Press, 1998, p. 144.

[120] J. Köhler, T. Grove, O. Maiß, and B. Denkena, “Residual Stresses in Milled Titanium Parts,” *Procedia CIRP*, vol. 2, pp. 79–82, Jan. 2012.

[121] B. R. Sridhar, G. Devananda, K. Ramachandra, and R. Bhat, “Effect of machining parameters and heat treatment on the residual stress distribution in titanium alloy IMI-834,” *Journal of Materials Processing Technology*, vol. 139, no. 1–3, pp. 628–634, Aug. 2003.

[122] M. Donachie, *Titanium - A Technical Guide*, 2nd ed. ASM International, 2000, p. 56.

[123] J. R. Davis, *Copper and copper alloys - ASM Speciality Handbook*. 2001, p. 247.

[124] P. Watson, “Observations on the misalignment in dissimilar material brazed joints,” University of Strathclyde - Department of Mechanical and Aerospace Engineering - Masters Project Thesis, 2012.

[125] S. Lee and H. Kobayashi, “Fatigue strength and fracture mechanism of ceramic-metal joints under cyclic bending,” *Science*, 1995.

[126] B. Rabin and W. Williamson, “Characterization of residual stresses in graded ceramic-metal structures: a comparison of diffraction experiments and FEM calculation,” 1994.

[127] S. Y. Kweon and S. K. Choi, “Prediction of residual stress-induced cracking by finite element analysis,” *Scripta Metallurgica er Materialia*, vol. 32, no. 3, pp. 359–364, 1995.

[128] K. Suganuma, T. Okamoto, M. Koizumi, and K. Kamachi, “Influence of shape and size on residual stress in ceramic/metal joining,” *Journal of Materials Science*, vol. 22, no. 10, pp. 3561–3565, Oct. 1987.

[129] G. Blugan, J. Janczak-Rusch, and J. Kuebler, “Properties and fractography of Si3N4/TiN ceramic joined to steel with active single layer and double layer braze filler alloys,” *Acta Materialia*, vol. 52, no. 15, pp. 4579–4588, Sep. 2004.

[130] L. Martens, W. Tillrnann, E. Lugscheider, and G. Ziegler, “Strength and microstructure of brazed cemented carbide and silicon nitride joints,” *Journal of Materials Processing Technology*, vol. 58, no. 1996, 2000.

[131] R. Hamilton, D. Mackenzie, and J. Boyle, “ME401 Stuctural Integrity Course Notes,” *University of Strathclyde - Department of Mechanical and Aerospace Engineering*, 2007.

[132] P. Li, J. Li, J. Xiong, F. Zhang, and S. H. Raza, “Diffusion bonding titanium to stainless steel using Nb/Cu/Ni multi-interlayer,” *Materials Characterization*, vol. 68, pp. 82–87, Jun. 2012.

[133] G. Madhusudhan Reddy and P. Venkata Ramana, “Role of nickel as an interlayer in dissimilar metal friction welding of maraging steel to low alloy steel,” *Journal of Materials Processing Technology*, vol. 212, no. 1, pp. 66–77, Aug. 2011.

[134] Y. Shen, Z. Li, C. Hao, and J. Zhang, “A novel approach to brazing C/C composite to Ni-based superalloy using alumina interlayer,” *Journal of the European Ceramic Society*, vol. 32, no. 8, pp. 1769–1774, Jul. 2012.

[135] Y. Zhou, F. Bao, J. Ren, and T. North, “Interlayer selection and thermal stresses in brazed Si3N4 – steel joints,” *Materials Science and Technology*, vol. 7, p. 1991, 1991.

[136] J. Chapa and I. Reimanis, “Modeling of thermal stresses in a graded Cu / W joint,” *Stress: The International Journal on the Biology of Stress*, vol. 303, pp. 131–136, 2002.

[137] Z. Zhou, S. Song, J. Du, and C. Ge, “High heat flux testing of tungsten plasma facing materials,” *Journal of Nuclear Materials*, vol. 367–370, pp. 1468–1471, Aug. 2007.

[138] A. J. Goupee and S. S. Vel, “Transient multiscale thermoelastic analysis of functionally graded materials,” *Composite Structures*, vol. 92, no. 6, pp. 1372–1390, May 2010.

[139] G. Pintsuk, S. E. Brünings, J.-E. Döring, J. Linke, I. Smid, and L. Xue, “Development of W/Cu—functionally graded materials,” *Fusion Engineering and Design*, vol. 66–68, pp. 237–240, Sep. 2003.

[140] “Determining Residual Stresses by the Hole-Drilling Strain-Gage Method,” *ASTM Standard E837*, 2009.

[141] F. Hosseinzadeh and P. Bouchard, “Application of the contour method to validate residual stress predictions,” in *Second International Conference on Advances in Nuclear Materials*, 2011.

8 Previous Publications